Evaluation of Thermal Radiation Models for Fire Spread Between Objects

by

Rob Fleury

Supervised by

Dr. Michael Spearpoint and

Associate Professor Charles Fleischmann

2010

A thesis submitted in partial fulfilment of the requirements for the degree of Master of Engineering in Fire Engineering

Department of Civil and Natural Resources Engineering

University of Canterbury

Christchurch, New Zealand

ABSTRACT

Fire spread between objects within a compartment is primarily due to the impingement of thermal radiation from the fire source. In order to estimate if or when a remote object from the fire will ignite, one must be able to quantify the radiative heat flux being received by the target. There are a variety of methods presented in the literature that attempt to calculate the thermal radiation to a target; each one based on assumptions about the fire.

The performance of six of these methods, of varying complexity, is investigated in this research. This includes the common point source model, three different cylindrical models, a basic correlation and a planar model. In order to determine the performance of each method, the predictions made by the models were compared with actual measurements of radiant heat flux. This involved taking heat flux readings at numerous locations surrounding a propane gas burner. Different fire scenarios were represented by varying the burner geometry and heat release rate. Video recordings of the experiments were used to determine the mean flame heights using video image analysis software.

After comparing the measured data with predictions made by the theoretical radiation methods, the point source model was found to be the best performing method on average. This was unexpected given the relative simplicity of the model in comparison to some of its counterparts. Additionally, the point source model proved to be the most robust of the six methods investigated, being least affected by the experimental variables. The Dayan and Tien method, one of the cylindrical models, was the second most accurate over the range of conditions tested in this work.

Based on these findings, recommendations are made as to the most appropriate method for use in a radiation sub-model within an existing zone model software. The accuracy shown by the point source model, coupled with its ease of implementation, means that it should be suitable for such a use.

ACKNOWLEDGEMENTS

The author would like to offer sincere thanks to the following people and organisations who have assisted with this research, including:

- Supervisors Mike Spearpoint and Charley Fleischman for generously giving their time, knowledge and guidance
- The Foundation for Research, Science and Technology for providing funding for the project
- Building Research Association of New Zealand Ltd for providing the project itself, with special thanks to Greg Baker, Colleen Wade and Amanda Robbins of BRANZ Ltd for their support
- The University of Canterbury and the Fire Engineering programme
- Grant Dunlop and Bob Wilsea-Smith whose expertise in the laboratory was invaluable
- Roger Nokes for the use of the *ImageStream* software and assistance in applying it
- Finally, the New Zealand Fire Service Commission for their continued support of the Fire Engineering Programme at the University of Canterbury

TABLE OF CONTENTS

LIST OF FIGURES

LIST OF TABLES

NOMENCLATURE

A	Fire/pool surface area (cross-sectional)	(m²)
A_2	Finite rectangle area (rectangular planar model)	(m²)
dA_1	Differential target element	(-)
c_p	Specific heat of air at constant pressure	(kJ/kgK)
c_v	Coefficient of variation	(%)
D	Fire/pool diameter	(m)
E	(Effective) emissive power of flame	(kW/m²)
E_{max}	Equivalent black body emissive power	(kW/m²)
E_s	Emissive power of smoke	(kW/m²)
F_{12}	Configuration/shape/view factor from fire to target	(-)
$F_{12,max}$	Maximum configuration factor at a point	(-)
F_α	Configuration factor from Plane α to target	(-)
F_β	Configuration factor from Plane β to target	(-)
g	Gravitational acceleration	(9.81 m/s²)
H	Flame height	(m)
H_T	Height of target relative to height of equivalent point source at $H/2$	(m)
ΔH_c	Heat of combustion	(kJ/kg)
L	Distance of target from centre of fire/pool	(m)
ℓ	Path length from flame surface to receiving target	(m)
l_f	Length of flame (rectangular planar model)	(m)
m_f	Final mass of gas bottles	(kg)
m_i	Initial mass of gas bottles	(kg)
$\dot{m}''_\infty$	Mass burning rate per unit area	(kg/m²s)
$\overline{n}$	Unit normal vector to differential target element	(-)
p'_w	Partial pressure of water vapour	(atm)
$p_w\ell$	Partial pressure path length parameter	(atm·m)
$\dot{Q}$	Heat release rate of fire	(kW)
$\dot{Q}^*$	Non-dimensional heat release rate	(-)
$\dot{Q}_r$	Radiative energy output of fire	(kW)

$\dot{q}''$	Radiant heat flux	(kW/m²)
R	Distance from point source to target	(m)
r	Fire/pool radius	(m)
RH	Relative humidity	(%)
s	Extinction coefficient	(m^{-1})
$stdev$	Standard deviation of sample	(any)
t	Time	(s)
T_a	Ambient temperature	(K)
T_f	Flame temperature	(K)
u	Component of $\bar{n}$ in i direction	(-)
v	Component of $\bar{n}$ in j direction	(-)
w	Component of $\bar{n}$ in k direction	(-)
w_f	Width of flame (rectangular planar model)	(m)
$\bar{x}$	Sample mean	(any)
x	Position of target relative to origin in i direction	(m)
y	Position of target relative to origin in j direction	(m)
z	Position of target relative to origin in k direction	(m)

Greek Symbols

α_c	Carbon dioxide absorption coefficient	(-)
α_w	Water vapour absorption coefficient	(-)
β	Mean value of θ in Dayan & Tien method	(radians)
ε	Emissivity	(-)
ε_c	Carbon dioxide emissivity	(-)
ε_w	Water vapour emissivity	(-)
θ	Angle between normal to target and line of sight from target to point source location	(radians)
θ_0	Angle between z axis and line of sight from target to centre-top of cylinder, Dayan & Tien method	(radians)
κ	Effective flame absorption coefficient	(m^{-1})
ρ_a	Ambient air density	(kg/m³)
σ	Stefan-Boltzmann constant	(5.67×10^{-8} W/m^2K^4)
τ	Atmospheric transmissivity	(-)
χ_r	Radiative fraction	(-)

Chapter 1

INTRODUCTION

1.1 Context and Motivation

The dominant mechanism for the spread of fire within buildings is direct thermal radiation from the existing flames (Karlsson & Quintiere, 2000). In order to determine if or when certain objects adjacent to the fire may ignite or be damaged, one must be able to predict the thermal radiation field surrounding the fire. This requires the radiant heat flux to be determined at various points in space.

Being able to calculate the radiant heat flux from a fire provides a number of benefits. These include:

- Prediction of if or when adjacent objects may ignite
- Prediction of extent of damage from fire
- Estimate safe separation distances between objects or buildings
- Estimate safe separation distances between a burning object and an escape route
- Prediction of activation of thermal detectors or sprinkler heads
- Helps to determine the total amount of heat transfer occurring between objects
- Prediction of failure of structural elements

Calculating the thermal radiation field surrounding a fire requires one or more equations to be solved. This can either be performed manually or be programmed into a computer model. This research uses the manual method, with the intent of providing recommendations so that programming into a computer model can be achieved. Including a thermal radiation algorithm into a computer model can provide fire engineers with a useful tool to be used in analysis and design. In determining thermal radiation hazard, fire engineers are interested in the maximum heat flux received by a differential area from a given emitting source at a distance (He, 2001).

The specific motivation for this research is that a thermal radiation model is desired to be input into an existing computer program named BRANZFIRE (Wade, 2008). This

comprises part of a larger project being carried out between the Building Research Association of New Zealand Ltd (BRANZ Ltd) and the University of Canterbury (UC). The overall project is being funded by the Foundation for Research, Science and Technology (FRST). The specific part of the project carried out in this research involves evaluating the performance of a number of thermal radiation models under a range of conditions. Sections 1.2-1.5 contain more information.

1.2 BRANZFIRE Software

A performance-based fire engineering design for a building typically requires some form of quantitative analysis. There are a number of ways in which this can be carried out; one of which is using a 'zone model'. The term 'zone model' usually refers to a two-zone model, based on the conceptual representation of the compartment fire process (Quintiere, 2002). Here, the system is assumed to contain two distinct homogeneous gas layers (or zones); a hot upper layer containing products of combustion and a relatively cool layer beneath it. Conservation equations for mass and energy are solved numerically at each time step for both the upper and lower zones. The flow of smoke and toxic products out through compartment openings is also calculated. The fire itself is represented as a source of energy and mass, which governs the amount of air entrainment that occurs into the plume (Quintiere, 2002). The most important input parameters that must be specified by the user of the software are the building geometry and a design fire. Design fires are covered extensively in literature; a good overview is provided by Karlsson and Quintiere (2000).

One such zone model that is commonly used by practising Fire Engineers in New Zealand is BRANZFIRE (Wade, 2008). BRANZFIRE is a computer fire model which integrates a flame spread and fire growth model for room lining materials with a multi-room zone model (Wade, 2004). This research involves helping to develop the next version of BRANZFIRE.

1.3 Probabilistic Design Tool

BRANZFIRE, like most other zone models at the time of writing, currently carries out its modelling in a deterministic fashion. This means that a single set of outcomes is produced

for a set of input parameters. There is, however, much interest in carrying out probabilistic (or risk-based) analysis during fire engineering design. The Society of Fire Protection Engineers (2005) defines Fire Risk Assessment as "a process for estimation and evaluation of fire risk that addresses appropriate fire scenarios and their probabilities and consequences, using one or more acceptability thresholds" which "develops the basis for fire risk management decisions." Fire Risk Management is then defined as "the process of deciding what should be done about the identified hazards, the exposed population, and the foreseeable adverse outcomes. Fire risk management involves implementing a design evaluated using fire risk assessment and managing an ongoing program (e.g., training, maintenance) required to ensure that the adopted design continues to deliver the calculated acceptable risk." The implementation of risk assessment into computer fire modelling is thought to become increasingly popular in the near future (Beyler, DiNenno, Carpenter, & Watts Jr., 2008).

There is currently a research initiative between BRANZ Ltd and the University of Canterbury which aims to include risk-based modelling in the forthcoming version of BRANZFIRE. BRANZ Ltd (2007) describes the research initiative in detail. The following is an excerpt from the document's executive summary:

> *This research will develop a building fire design and analysis tool to simulate building fire outcomes in a risk-descriptive format that will account for the variability and uncertainty associated with the development of a fire, the nature and arrangement of the building contents and the inherent reliability and effectiveness of different fire safety features used to mitigate the risk of fire. The intermediate outcome to which this research is directed is to help ensure that the management of fire risks in buildings is cost-effective as well as socially and politically acceptable, leading to innovation in construction, flexibility in design and robustness in fire safety solutions.*

Furthermore, BRANZ Ltd (2007) outlines that:

> *Our proposed design tool will use an existing mathematical fire model (BRANZFIRE) for predicting the spread of smoke and development of hazardous conditions in a building. The novel feature of the research will be extending existing knowledge to develop a design tool that allows a wide range of fire scenarios for a building to be simulated within the model, using specialised*

random sampling techniques for rare events. The tool would provide designers with a means of conducting a sensitivity analysis by proposing input fire scenarios and corresponding fire characteristics suitable as design assumptions for New Zealand buildings… Results would be expressed as probability distributions. A design tool with this capability has not been developed before in New Zealand or elsewhere.

By having a better understanding of the uncertainty involved in fire engineering designs, it is hoped that the fire risks within buildings will be better managed and that there is more robustness in fire safety solutions. This should lead to more transparency and confidence in the level of fire safety provided in fire engineered designs.

Research for the BRANZFIRE project comprises staff from both BRANZ Ltd and UC and students undertaking a masters or PhD in fire engineering at UC. Beginning in 2008, the project is expected to take five years to complete and is funded by the Foundation for Research, Science and Technology (FRST). The research described in this thesis makes up a small part of the overall BRANZ Ltd – UC project, as outlined in Figure 1. Note that the dates given in the diagram are given as an indication only and actual completion dates may vary.

As can be seen in Figure 1, one element of the project is to develop an item to item fire spread model that is to be included in BRANZFIRE. This technical basis for this item to item fire spread model will come from work carried out in this thesis, coupled with research performed by a PhD student. See section 1.5 for more details.

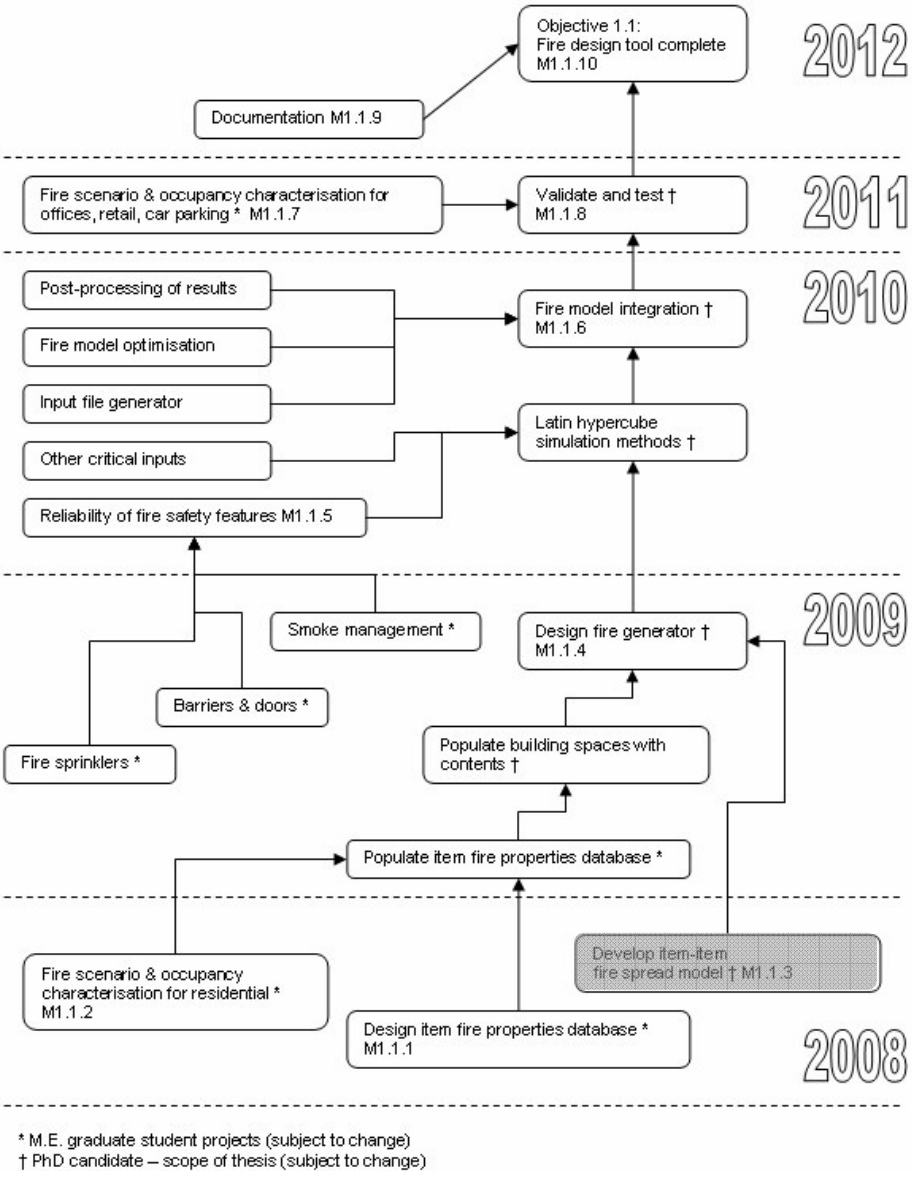

Figure 1: Overview of development scope for risk-informed fire design tool (BRANZ Ltd, 2007). The research outlined in this thesis comprises part of the highlighted section, *Develop item-item fire spread model*

1.4 Thermal Radiation Overview

The three basic modes of heat transfer, namely conduction, convection and radiation, are involved in almost all fire scenarios. It is observed that one mode dominates at different stages of fire growth or in different locations. For example, conduction is of high importance when trying to determine the expected temperature of a structural element during a fire. It is radiation, however, that is the dominant mode of heat transfer for the

spread of flames within compartments (Karlsson & Quintiere, 2000). It is the mechanism by which items at a distance from a fire are heated up, which can lead to ignition without direct flame contact. For these reasons, this thesis investigates thermal radiation only and is not concerned with convective or conductive heat transfer.

Thermal radiation is the transfer of energy by electromagnetic waves. Radiant energy in general can have a wide range of wavelengths; from radio waves with wavelengths of tens of meters to cosmic rays with wavelengths less than 10^{-14} m (Siegel & Howell, 1992). Thermal radiation is detected as heat or light and occupies a narrow window in the electromagnetic spectrum. This includes a small portion of the ultraviolet, all of the visible light region and the infrared, corresponding to a wavelength range of approximately 0.4 to 1000 μm (Siegel & Howell, 1992). Thermal radiation is emitted from tiny soot particles which are present in nearly all diffusion flames (Drysdale, 1999). It is these soot particles which give the flame its characteristic yellow luminosity.

1.4.1 Emissive power and emissivity

The total emissive power of a flame is a function of temperature and wavelength, as described by Planck's Law, given in many radiation references such as Siegel and Howell (1992). Here, the emissive power is for an ideal radiator, known as a 'black body'. However, real surfaces are not ideal radiators and therefore have an emissive power, E, less than that for a black body. The fraction of radiation emitted in relation to the maximum possible emission from a surface is called the emissivity, ε (Karlsson & Quintiere, 2000). Therefore, a black body has an emissivity equal to unity.

In order to simplify thermal radiation calculations, the concept of a 'grey body' (or 'ideal, non-black body') is introduced. For this, the emissivity is assumed to be independent of wavelength (Drysdale, 1999). Furthermore, Kirchoff's law states that the emissivity for a surface is equal to its absorptivity. Karlsson and Quintiere (2000) advise that for enclosure fire radiative exchanges, the grey body assumption is generally satisfactory.

The total radiation emitted, E, per unit area from a grey surface is given by Equation 1:

$$E = \varepsilon \sigma T_f^4 \tag{1}$$

Where ε is the emissivity, σ is the Stefan-Boltzmann constant (5.67×10^{-8} W/m^{2}K^4) and T_f represents the flame temperature (K). E can also be termed the emissive power of the flame.

1.4.2 Configuration factors

The above equation can be used to calculate the radiative heat loss from a surface. However, if one wishes to know the rate of heat transfer to a nearby object, the amount of energy being radiated in that particular direction must be calculated. This can be done using Equation 2, which introduces the concept of a configuration factor.

$$\dot{q}'' = F_{12}\sigma\varepsilon T_f^4 \tag{2}$$

Where $\dot{q}''$ is the radiant heat flux (kW/m²) and F_{12} is the configuration factor.

This factor takes into account the geometrical relationship between the emitter and the receiver. Configuration factors (also known as shape or view factors) have a value between zero and one. For example, when the receiver is very close to the flame and oriented so that it is facing the fire, the configuration factor approaches one, as everything viewed by the receiver is the flame (Iqbal & Salley, 2004). Davis and Bagster (1989) explain that the configuration factor is dependent on three variables:

- The geometry of the emitter and receiver
- Whether the emitter and receiver can be 'viewed' by each other
- The direction of the exchange of thermal radiation

In this work, the configuration factor is determined for radiant energy exchange between a finite surface (the flame) and a differential element at some distance from the flame. The configuration factor is dependent on the dimensions of the finite surface and the distance and angle between the emitter and target. Usually an assumption is made whereby the flame is approximated as a simple shape such as a rectangle or cylinder, which enables calculation of the configuration factor using established equations. Assuming that the flame takes on the shape of a cylinder or rectangle is far from an exact reproduction of the observed geometry. However, due to the rapid fluctuation of the flame shape with time, calculating an accurate configuration factor from the fire to a target would be an extremely complicated and time intensive process. Section 2.3 provides more detail about methods for determining configuration factors.

1.5 Aim

This thesis aims to evaluate the performance of a number of thermal radiation models with respect to item-to-item fire spread within a compartment. Models that are evaluated include the point source and a number of cylindrical models. The effectiveness of these models is tested for a variety of situations and recommendations are made to BRANZ Ltd as to the suitability of different radiation models.

The scope of the analysis is limited to direct radiative impingement on a target and therefore ignores contributions from the compartment surfaces and the hot upper gas layer. Also, internal radiation within the flame is ignored. This radiative feedback to the fuel surface helps to control the rate of burning during a fire. However, in the BRANZFIRE model, a design fire is specified or chosen by the user and therefore the increased burning rate due to radiation feedback within the flame is already accounted for.

Results from this research and analysis feed into work carried out by a PhD student. The combined findings then make up the shaded part of Figure 1 (*Develop item-item fire spread model*) which is a component of the overall BRANZ Ltd – UC project. The intent is that the findings of this research will contribute to the development of the forthcoming version of BRANZFIRE.

In order to evaluate the performance of the thermal radiation models being investigated, the predictions made by these models are compared with experimental data. To obtain this data, a comprehensive experimental programme has been undertaken. In these experiments, measurements of radiant heat flux are taken at various positions surrounding a gas burner. Pure propane gas is used as fuel to the burner, with mass flow controllers regulating the gaseous flow. This allows fires of varying heat release rates to be specified. Three different burner shapes were tested, with length to width aspect ratios of 1:1, 2:1 and 3:1. These aspect ratios are used to represent the likely shapes of furniture found within common New Zealand buildings, such as chairs, sofas, tables and beds.

The measurements of radiant heat flux are taken using heat flux gauges, mounted on steel frames, also called trolleys. Each frame holds four gauges, set at heights ranging from the base of the flame to 1.5 m above the flame base. The trolleys wheels are set on rails,

enabling the gauges to be moved to different distances from the fire. The gauges are also able to be moved laterally across the face of the fire and can be oriented either vertically or horizontally. Furthermore, the gas burner can be rotated to provide the heat flux gauges with a different view of the fire.

By testing many different variables, not only is a vast array of experimental data collected, but the limitations of some of the theoretical models are highlighted. These limitations are usually due to large assumptions being made about the fire, which often do not hold true in the real world. It is useful to know the situations in which the different radiation models perform well and those in which the models become highly inaccurate. This makes for a more comprehensive analysis as the different models can be compared under different scenarios.

Following the comparison between the experimental results and predictions from the radiation models, recommendations must be made to BRANZ Ltd. In terms of implementing a thermal radiation model in the BRANZFIRE software, it is important that the chosen model displays good accuracy coupled with ease of use. Therefore, this research aims to not only evaluate the models, but recommend the most appropriate model to be used by BRANZFIRE. This may involve finding a balance between model accuracy and ease of programming and use.

The context of the investigation is with respect to compartment fires. As such, the fire dimensions and heat release rates tested are restricted to those that are representative of typical single-item compartment fires. In fact, the maximum fire size able to be tested is limited by physical conditions such as the propane fuel supply and the size of the laboratory. The investigation and subsequent findings therefore do not necessarily apply to other fire scenarios; for example, large open liquid pool fires.

1.6 Outline of Thesis

This Master of Engineering in Fire Engineering thesis outlines the processes undertaken and the results found for the evaluation of thermal radiation models for fire spread between objects.

Chapter 2 provides a review of the literature on thermal radiation modelling. Here, six different radiation models are explained in detail, including all equations necessary to use the models.

Chapter 3 outlines the methodology employed for the experimental programme of this research. Details of the fire source, laboratory and instrumentation are given, in addition to an outline of the experimental procedure. Techniques used to extract and analyse the data are then explained. Finally, the method for determining the mean flame height is given.

Chapter 4 provides all of the experimental results, accompanied by a discussion of these results. Results are presented for heat release rate, radiant heat flux and mean flame height.

Chapter 5 compares the experimental data with predictions made by the theoretical radiation models. Here, the different models are closely scrutinised and their performance under different conditions is discussed.

Chapter 6 summarises all of the findings from the research and makes conclusions as to the appropriateness of the radiation models for different circumstances. Recommendations are made to BRANZ Ltd about the most suitable model to be used for the implementation of a radiation sub-model within BRANZFIRE.

Chapter 7 gives a list of references that have been used throughout this research. Finally, the Appendices provide extra material not contained within the main body of the thesis.

Chapter 2

LITERATURE REVIEW

The primary mechanism for injury or damage from large, open hydrocarbon fires is thermal radiation (Beyler, 2002). With respect to fire radiation models, the majority of the work has gone into predicting the thermal radiation from hydrocarbon pool fires (Beyler, 2002) and this will form the basis for this research.

2.1 Types of Model

Rew, Hulbert, and Deaves (1997) outline that two approaches are generally used to determine the thermal radiation surrounding a fire. These are field models and semi-empirical models. Firstly field models, commonly known as Computational Fluid Dynamics (CFD) models, solve the Navier-Stokes equations for fluid flow across a vast grid of cells, known as a mesh. Complex sub-models must be incorporated in order to predict the chemical and physical processes occurring in a fire. The radiant heat transfer is solved by means of an enthalpy conservation term that arises within the Navier-Stokes equations (Cox & Kumar, 2002). The advantage of using field models for radiation modelling is that they are capable of predicting a wide range of scenarios, provided that the input is correctly specified. However, there are disadvantages associated with field models in that they require a lot of time and effort; both human (in terms of the input) and computational (for solving the Navier-Stokes equations).

Semi-empirical models, on the other hand, are comparatively far easier to use and understand. This means that they are more frequently used in risk assessments than field models (Rew, et al., 1997). Semi-empirical models are designed to be simple to use and therefore do not include complicated algorithms for the physical processes involved in fires. As a result, a semi-empirical model designed to predict the radiant heat flux from a fire is not designed to predict other phenomena. The correlations used in semi-empirical models are derived from a wide range of experimental data and can provide more than satisfactory results, provided they are used within their validation limits (Rew, et al., 1997).

This research deals exclusively with semi-empirical models and henceforth all radiation models will be assumed to be semi-empirical.

2.2 General Approach to Thermal Radiation Modelling

Beyler (2002) describes the three major steps involved in estimating the thermal radiation field surrounding a fire:

1. Determine the geometric characteristics of the fire, including the burning rate and the physical dimensions of the fire. These dimensions are based on time-averaged values.
2. Characterise the radiative properties of the fire. This involves the determination of the average emissive power of the flames.
3. Calculate the incident radiant heat flux at the target location. For this to be carried out, steps 1 and 2 must have been completed, as well as knowing the location, geometry and orientation of the receiver.

The radiation models described in the following section use these three steps to varying degrees of accuracy.

2.3 Common Radiation Models

The primary aim of radiation modelling usually is to calculate safe separation distances between fire sources and potential targets that could be damaged or ignited by radiation from the fire. These models range in the level of detail and rigour and some are more suitable for certain applications than others. Some methods are most appropriate for crude initial hazard assessments, while others are capable of more accurate predictions, although more effort is required.

The following sections outline a number of thermal radiation models that are available in the literature. Since the project is investigating compartment fires only, it is assumed that the flames are not wind affected. There are thermal radiation models available in the literature for wind-blown flames, such as the Mudan method (Mudan, 1984).

2.3.1 Shokri and Beyler correlation

Shokri and Beyler (1989) developed a simple correlation based on experimental data from large-scale pool fire experiments. This method calculates the radiant heat flux at ground level as a function of the radial position of a vertical target. Note that the term 'ground level' is loosely used to represent the height of the base of the fire. The heat flux received by the target is given by Equation 3:

$$\dot{q}'' = 15.4\left(\frac{L}{D}\right)^{-1.59} \tag{3}$$

Where L is equal to the distance between the target and the centre of the fire (m) and D is the fire diameter (m).

The correlation was derived for circular pool fires, however, for non-circular pools with a length to width ratio of approximately one, an equivalent area circular source may be used (Shokri & Beyler, 1989). The equivalent diameter is given by:

$$D = \sqrt{\frac{4A}{\pi}} \tag{4}$$

Where A is the cross-sectional surface area of the fire or pool (m).

The following assumptions apply for this method (Beyler, 1999)

- Pool is circular or nearly circular
- Target is vertical and located at ground level

Beyler (1999) lists some limitations with the model. They are as follows:

- The fuels used in the experiments that produced the correlation all produced luminous flames. Therefore, the correlation may not be suitable for non-luminous flames
- In the experiments, pool diameters of 1 to 50 m were used. It is reported (Beyler, 1999) that the correlation systematically over-predicted the results from the 50 m pool fire experiment. Therefore, the model should be used with great care for larger pool diameters. For the smaller pools, the correlation yielded predictions that were within ±100 % of the measured value
- The edge of the circular pool is at *L/D* equal to 0.5. Using Equation 3 above, this yields a radiant heat flux of 46.3 kW/m², which is significantly less than values

that were measured at that location during experimentation. It is recommended that the correlation be limited to *L/D* values ranging between 0.7 and 15

Beyler (1999) then recommends that a safety factor of two should be applied to Equation 3 when being used for design purposes. However, if a realistic result is desired, no safety factor should be applied.

2.3.2 Point source model

The point source model (Modak, 1977) is the simplest configurational model of a radiant source. The essence of the model is that radiation is assumed to emanate isotropically from a single point source located at the centre of the flame, as shown in Figure 2a. The relationship varies with the inverse square of the distance *R* from the source, as given by the following equation:

$$\dot{q}'' = \frac{\dot{Q}_r \cos\theta}{4\pi R^2} \tag{5}$$

Where $\dot{Q}_r$ is the total radiative energy output of the fire (kW), θ is the angle between the normal to the target and the line of sight from the target to the point source location (radians), and *R* equals the distance from the point source to the target (m).

The location of the theoretical point source of energy is at the centre of the fire at the mid-height of the flame (see Figure 2b). The mean flame height, *H*, measured in m, is calculated by the Heskestad correlation:

$$H = 0.23\dot{Q}^{\frac{2}{5}} - 1.02D \tag{6}$$

Where $\dot{Q}$ is the heat release rate of the fire (kW).

The distance, *R*, from the point source location to the target location can be determined using the Pythagorean Theorem, as given below for the given application:

$$R = \sqrt{L^2 + H_T^2} \tag{7}$$

Where H_T is the height of the target relative to the height of the equivalent point source at *H*/2 (m).

Therefore, for a target located on the ground, $H_T = H/2$. For a target at the mid-height of the flame, $H_T = 0$.

As with the Shokri and Beyler correlation, an equivalent diameter can be used for non-circular pools, given that the length to width ratio is near one. The effective diameter is calculated using Equation 4. The total radiative energy output of the fire can be calculated from Equation 8 below.

$$\dot{Q}_r = \chi_r \dot{Q} \tag{8}$$

Where χ_r is the radiative fraction.

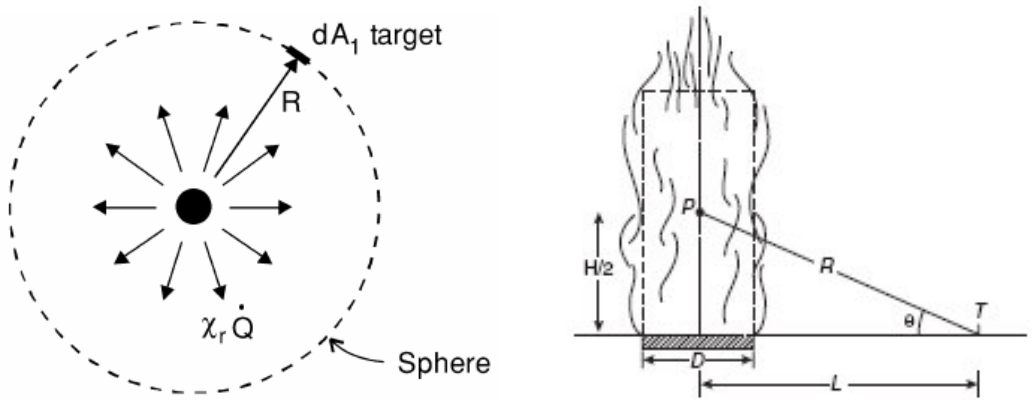

(a) **(b)**

Figure 2: (a) Schematic of point source model (Karlsson & Quintiere, 2000), (b) Schematic and notation for point source model (Beyler, 2002)

Generally, the radiative fraction, χ_r, is dependent on the fuel type, flame size and flame configuration. Its value can vary from approximately 0.15 for low-sooting fuels, such as alcohol, to around 0.6 for high-sooting fuels, such as hydrocarbons (Iqbal & Salley, 2004).

The following assumptions apply for this method (Beyler, 1999):

- Pool is circular or nearly circular
- The point source configuration factor is used, as per Equation 5

Some limitations exist with the point source model. They are as follows:

- The point source model is a very simplistic model of a pool fire (Beyler, 1999)

- The most important parameter in the model is the estimation of the radiative fraction (Mudan, 1984) and therefore great care should be taken when choosing a value for this. The radiative fraction is dependent on the fuel used
- The method is known to under-predict incident heat fluxes at locations close to the fire (Drysdale, 1999). According to Iqbal and Salley (2004) this is primarily because the near-field radiation is greatly influenced by the flame size, shape, and tilt as well as the relative orientation of the target
- The model performs poorly at heat fluxes at the target greater than 5 kW/m², indicating that it is not a good choice when ignition of combustibles is to be considered (Beyler, 2002)
- The point source model is within 5 % of the measured incident heat flux when $L/D > 2.5$ (Modak, 1977)
- The point source model "is a correct assumption at large distances from the fire" (Beyler, 1999)

A safety factor of two is recommended for use with the point source method for design considerations (Beyler, 1999), although it is recommended that this only applies for heat fluxes less than 5 kW/m² as this is the recommended limit of the model. Like the Shokri and Beyler correlation, no factor of safety should be applied if an accurate prediction is desired. Beyler (1999) suggests that the point source model is the most appropriate method for heat fluxes less than 5 kW/m².

Despite its simplicity, the point source model is often used for a range of applications. One such example is for industrial flare design, where the model is seen to provide adequate predictions of the thermal radiation field surrounding the flare (Oenbring & Sifferman, 1980).

2.3.3 Shokri and Beyler detailed method

The methods outlined in sections 2.3.1 and 2.3.2 are known to be simple screening methods (Beyler, 1999) and may not be appropriate if an accurate analysis is desired. There are a number of more detailed methods available, one of which is presented by Shokri and Beyler (1989). The basis of the model is to provide a simple yet realistic model of the flame. To achieve this, the flame is assumed to be a cylindrical, black-body,

homogeneous radiator with an average emissive power. It is assumed that thermal radiation is emitted from the surface of the cylinder and that radiation from non-visible gases is negligible (Iqbal & Salley, 2004). Like many fire radiation models, this method was developed using pool fire radiation data.

Figure 3 provides a schematic and the nomenclature for the Shokri and Beyler detailed method for both vertical and horizontal targets located at ground level. For targets above ground level, the cylinder must be broken down into two individual cylinders, as shown in Figure 4. In such instances, one cylinder represents the flame below the height of the target, while the other represents the flame above the height of the target.

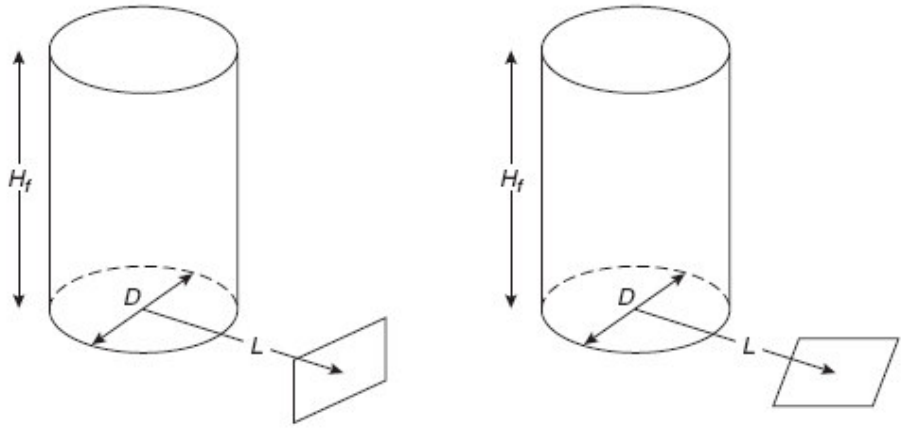

Figure 3: Cylindrical flame shape configuration factor geometry for vertical and horizontal targets at ground level (Beyler, 2002)

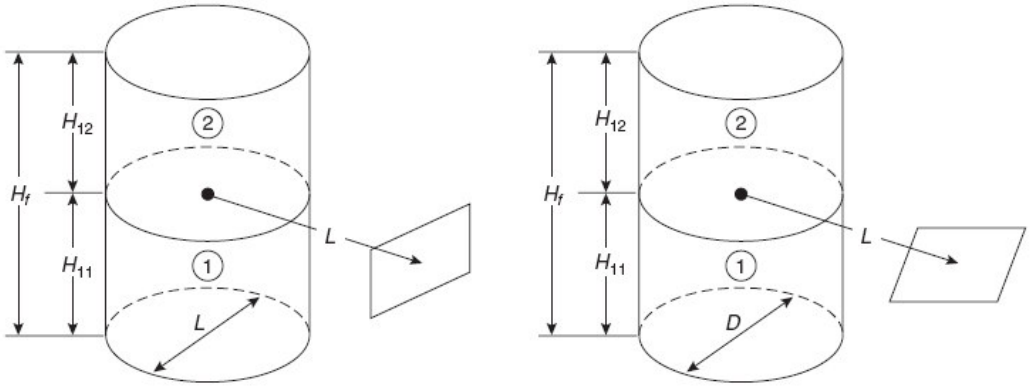

Figure 4: Two-cylinder representations of the configuration factor for target above ground level (Beyler, 2002)

The incident radiative flux to a target outside the flame is given by Equation 9.

$$\dot{q}'' = EF_{12} \tag{9}$$

The configuration factor is a function of the target location and the flame height and diameter. F_{12} always takes a value between zero and one, depending on these factors. For non-circular fires, an effective diameter can be calculated using Equation 4. The flame height can be determined using Equation 6.

Using the flame height and diameter, the configuration factors for horizontal ($F_{12,H}$) and vertical ($F_{12,V}$) targets can be calculated using the Equations 10 and 11.

$$F_{12,H} = \frac{\left(B - \frac{1}{S}\right)}{\pi\sqrt{B^2 - 1}} \tan^{-1}\sqrt{\frac{(B+1)(S-1)}{(B-1)(S+1)}} - \frac{\left(A - \frac{1}{S}\right)}{\pi\sqrt{A^2 - 1}} \tan^{-1}\sqrt{\frac{(A+1)(S-1)}{(A-1)(S+1)}} \tag{10}$$

$$F_{12,V} = \frac{1}{\pi S} \tan^{-1}\left(\frac{h}{\sqrt{S^2 - 1}}\right) - \frac{h}{\pi S} \tan^{-1}\sqrt{\frac{(S-1)}{(S+1)}} + \frac{Ah}{\pi S\sqrt{A^2 - 1}} \tan^{-1}\sqrt{\frac{(A+1)(S-1)}{(A-1)(S+1)}} \tag{11}$$

Where:

$$\begin{aligned} A &= \frac{h^2 + S^2 + 1}{2S}, \qquad & B &= \frac{1 + S^2}{2S} \\ S &= \frac{2L}{D}, & h &= \frac{2H}{D} \end{aligned} \tag{12}$$

The maximum configuration factor at a point, $F_{12,max}$, is given by the vector sum of the horizontal and vertical components:

$$F_{12,\max} = \sqrt{F_{12,H}^2 + F_{12,V}^2} \tag{13}$$

Alternatively, Beyler (1999) provides five figures which display pre-calculated maximum view factors for different ratios of flame height to radius. These may be useful when the target is above ground level.

For vertically oriented targets located above ground level, Equation 11 must be applied for both cylinders 1 and 2 (see Figure 4), yielding two configuration factors, $F_{12,V1}$ and $F_{12,V2}$.

The total configuration factor is given by the sum of the two individual configuration factors.

$$F_{12,V} = F_{12,V1} + F_{12,V2} \tag{14}$$

Horizontal targets, on the other hand, only require one equation as the target will only receive thermal radiation from one of the two cylinders. This is because although the target is infinitely thin, it only receives radiation on one of its faces. The user must decide which surface is required; either the downwards-facing or upwards-facing surface. If the thermal radiation to an upwards-facing surface, such as a desk top, is required then Equation 10 should be employed using cylinder 2 in Figure 4. Conversely, if the user wishes to calculate the radiant heat flux to a downwards-facing surface, such as the underside of a table, cylinder 1 is treated as the sole emitter of radiation.

Shokri and Beyler (1989) explain it is important to note that the 'effective' emissive power of the flame is defined only in terms of a homogeneous flame radiation model. Rather than being the local emissive power measured at a specific point in space, it is more of an averaged emissive power over the whole flame. As the model was developed for pool fire scenarios, an expression for the 'effective' emissive power was formed in terms of the effective pool diameter. It is:

$$E = 58\left(10^{-0.00823D}\right) \tag{15}$$

Shokri and Beyler (1989) observed that the major uncertainty with their model is in the definition of the emissive power and not in the view factor model. In fact, it was found that for pool fires the cylindrical approximation of the flame is highly accurate at predicting view factors over a wide range of conditions.

As with the previous two methods, this model assumes that the fire is circular or nearly circular in shape. Comparison with experimental data suggests that the performance of the method is better at heat fluxes greater than 5 kW/m² at the target (Beyler, 1999). Therefore, the main limitation to the model is that it should only be used when the radiant heat flux to the target exceeds 5 kW/m². Again, a safety factor of two should be used for design purposes (Shokri & Beyler, 1989).

2.3.4 Mudan method

Sometimes known as the 'Mudan and Croce method', this model estimates thermal radiation from pool fires for both wind-free and wind-blown flames. As this research investigates the wind-free condition only, the models for wind-blown flames are omitted. The radiative heat flux to a target is given by:

$$\dot{q}'' = EF_{12}\tau \tag{16}$$

Where τ is the atmospheric transmissivity.

As with various other radiation models, this method centres around the assumption that the flame is cylindrical in shape. Therefore, the flame height and diameter must be determined. For noncircular fires, the effective diameter can be calculated using Equation 4, whilst the flame height correlation for this method is different from the previous methods. Here, the correlation for mean visible height of turbulent diffusion flames, developed by Thomas (1963), is used:

$$\frac{H}{D} = 42\left(\frac{\dot{m}''_{\infty}}{\rho_a\sqrt{gD}}\right)^{0.61} \tag{17}$$

Where $\dot{m}''_{\infty}$ is the mass burning rate per unit area (kg/m²s), ρ_a denotes the ambient air density (kg/m³) and g is the acceleration due to gravity (9.81 m/s²).

The radiation exchange factor between the fire and a target outside the flames is dependent on the flame shape (assumed to be cylindrical), the distance between the fire and the target, and the relative orientation of the target. The maximum view factor at a point is determined using Equations 10 – 13, given in section 2.3.3.

The effective emissive power, E, of the flame can be determined by the following correlation:

$$E = E_{\max}e^{(-sD)} + E_s\left(1 - e^{(-sD)}\right) \tag{18}$$

Where E_{max} is the equivalent black body emissive power (kW/m²), s is the extinction coefficient (m^{-1}) and E_s represents the emissive power of smoke (kW/m²).

As shown in Equation 16, allowance must be given for atmospheric absorption and scattering. This comes in the form of a transmissivity factor, τ. The main atmospheric

constituents that are found to absorb thermal radiation are water vapour (H_2O) and carbon dioxide (CO_2) (Mudan, 1984).

The following procedure, provided by Mudan (1984), is used to calculate the transmissivity. Firstly, calculate the partial pressure of water vapour, p'_w (atm), in the atmosphere:

$$p'_w = \frac{RH}{100}\exp\left(14.4114 - \frac{5328}{T_a}\right) \tag{19}$$

Where RH indicates the relative humidity (%) and T_a is the ambient temperature.

Next, determine the partial pressure path length parameter, $p_w\ell$ (atm·m) :

$$p_w\ell = p'_w\ell\left(\frac{T_f}{T_a}\right) \tag{20}$$

Where ℓ is the path length from the flame surface to the receiving target (m).

For the flame temperature and $p_w\ell$, determine the water vapour emissivity, ε_w, using emissivity plots given in Appendix A, Figure A 1.

Now the water vapour absorption coefficient, α_w, can be calculated from:

$$\alpha_w = \varepsilon_w\left(\frac{T_a}{T_f}\right)^{0.45} \tag{21}$$

The absorption by carbon dioxide is calculated in a similar fashion. Knowing that the partial pressure of CO_2 remains relatively constant at about 3×10^{-4} atm (Mudan, 1984) and using Figure A 2 (Appendix A), the carbon dioxide absorption coefficient, α_w, is:

$$\alpha_c = \varepsilon_c\left(\frac{T_a}{T_f}\right)^{0.65} \tag{22}$$

Where ε_c is the carbon dioxide emissivity.

Finally, the transmissivity can be determined from:

$$\tau = 1 - \alpha_w - \alpha_c \tag{23}$$

Alternatively, the method can be simplified by assuming that $\tau = 1$ (Beyler, 1999). This eliminates the need for the user to consult plots, meaning that the method can be easily programmed into a computer model or spreadsheet.

As with previous methods, the fire is assumed in to be circular or nearly circular in shape. Comparison with experimental data shows that the Mudan method is inherently conservative for predicting radiant heat fluxes. Despite this, a safety factor of two should still be applied when using the method for design purposes (Beyler, 1999).

2.3.5 Dayan and Tien method

A method presented by Dayan and Tien (1974) again approximates the flame as a homogeneous cylinder of uniform temperature and other properties. Their method calculates the incident radiant heat flux from the flame to a target element, *dA*, with a unit normal vector $\bar{n} = u\bar{i} + v\bar{j} + w\bar{k}$. Figure 5 depicts Dayan and Tien's model.

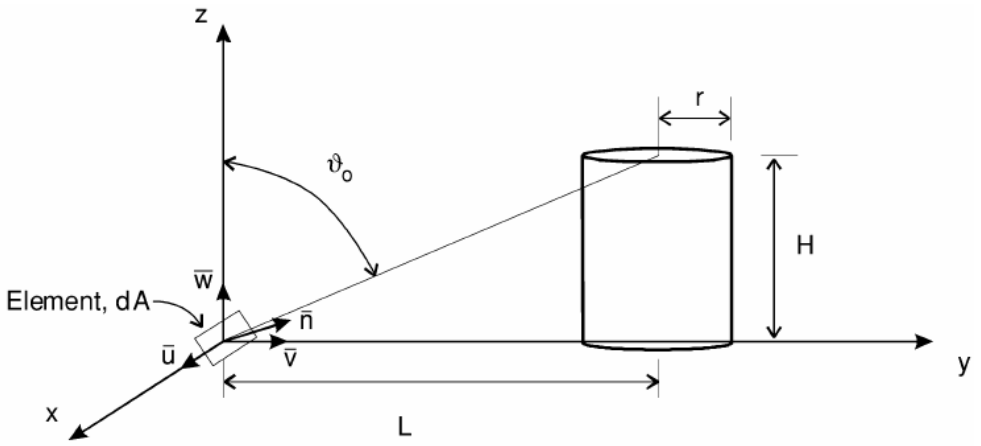

Figure 5: Schematic of radiation exchange between a target element, dA, and a homogeneous cylindrical flame (Karlsson & Quintiere, 2000)

The heat flux to the target is given by:

$$\dot{q}'' = \sigma \varepsilon T_f^4 \left(F_1 + F_2 + F_3 \right) \tag{24}$$

Where:

$$\varepsilon = 1 - e^{-0.7\mu} \tag{25}$$

$$\mu = \frac{2r\kappa}{\sin\beta} \tag{26}$$

$$\beta = \frac{\theta_0 + \frac{\pi}{2}}{2} \tag{27}$$

$$F_1 = \frac{u}{4\pi}\left(\frac{r}{L}\right)^2 \left(\pi - 2\theta_0 + \sin 2\theta_0\right) \tag{28}$$

$$F_2 = \frac{v}{2\pi}\left(\frac{r}{L}\right)\left(\pi - 2\theta_0 + \sin 2\theta_0\right) \tag{29}$$

$$F_3 = \frac{w}{\pi}\left(\frac{r}{L}\right)\cos^2\theta_0 \tag{30}$$

Where κ is the effective flame absorption coefficient (m^{-1}), β is the mean value of θ (radians), θ_0 represents the angle between the z axis and the line of sight from the target to the centre-top of the cylinder (radians), while u, v and w are the components of $\bar{n}$ in the i, j and k directions, respectively (see Figure 5).

This method can be employed for predicting the radiant heat flux to targets located both at ground level and at elevated positions (Dayan & Tien, 1974). For targets above ground level, the cylinder which approximates the fire must be divided into two cylinders, in a similar fashion to the Shokri and Beyler detailed method (see section 2.3.3).

The approximations provided in Equations 28 to 30 are deemed to be applicable for $L/r \geq 3$ (Dayan & Tien, 1974), where r is the fire radius (m). An investigation by He (2001) found that the Dayan and Tien method is not as accurate as the Shokri and Beyler detailed method when predicting the shape factor in the x direction. This is because Equations 28 to 30 are seen to be approximations of the exact configuration factors between a cylinder and a differential element. Equations 10 and 11 represent the exact solutions in the y and z planes. The x component was assumed to be negligible. However, the advantage of Dayan and Tien's method over that of Shokri and Beyler is the relative simplicity in its mathematical expressions.

2.3.6 Rectangular planar model

In addition to the existing models and methods available in the literature, an attempt was made to develop an original model. The objective for this new model was to move away from the common assumption of a cylindrical flame shape. This is because the cylindrical models were mostly developed for liquid pool fires, which are often contained in a tank of circular cross section. However, compartment fires usually relate to burning solids such as furniture, which typically have a rectangular cross section as opposed to circular. A rectangular based model allows calculation of radiant heat flux to targets from fires that are far from circular. In fact, in this research, fires are tested which have a length to width aspect ratio of 3:1.

The basis for the determination of the shape factor for this model is that the flame can be approximated as two perpendicular intersecting planes (see Figure 6a). The line of intersection between these two planes extends vertically from the centre of the fire. The two intersecting planes represent the centreline planes of a rectangular cuboid, as shown in Figure 6b. The intent is that this represents a more universal flame shape assumption than the cylindrical assumption. Plane α has a length, l_f(m), equal to the base length of the fire source while Plane β has a width, w_f(m), equal to the base width of the fire source. Both planes have a height, H, equivalent to the mean flame height.

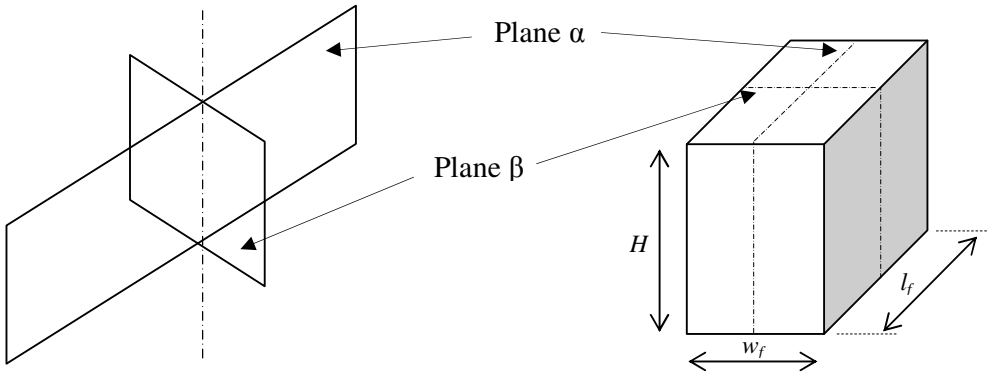

Figure 6: (a) The rectangular planar model is made up of two perpendicular intersecting planes, (b) The planes intersect at the centre of the fire, which can be approximated as a rectangular cuboid

The rectangular flame shape assumption for this method is not an original concept. Drysdale (1999) describes that "the flame can be approximated by a simple geometric

shape, such as a rectangle of height between 1.5 and 2 times the fuel bed diameter…" Assuming a flame height based on the fire diameter is a very simple but crude method. A method presented by Seeger (1974) also uses a rectangular surface assumption; however, just one plane is used. The method is only valid for vertical targets and the plane must be parallel to the target. Seeger's method was derived as a simplification to the cylindrical assumption for circular pool fires. Its applicability to fires of other shapes, such as rectangular cuboids, was not tested. This type of method is also known as an 'equivalent radiator' model (Crocker & Napier, 1986). Robertson (1976) suggests that for circular tank fires the equivalent radiator be a rectangle of width D and height $2D$. For fires that approximate a rectangular cuboid (as the one depicted in Figure 6b), Robertson (1976) recommends a similar method to that outlined above; with a rectangle of length equal to the horizontal flame length and height equal to the flame height. Only one rectangle is specified.

The radiant heat flux received by a differential target from planes α and β is calculated using Equation 2, reproduced below.

$$\dot{q}'' = F_{12}\sigma\varepsilon T_f^4 \tag{2}$$

Calculation of F_{12} uses an existing formula for the configuration factor between a finite rectangle and a differential element located at some distance from the rectangle (see Figure 7). Given by Howell (2008), the formula allows for the differential element to be oriented at any angle to the rectangle. This feature makes it suitable for use in this research, as then it can be programmed into a computer model which is able to calculate the configuration factor for any situation. The configuration factor from a finite rectangle to a differential element can be calculated using Equation 31.

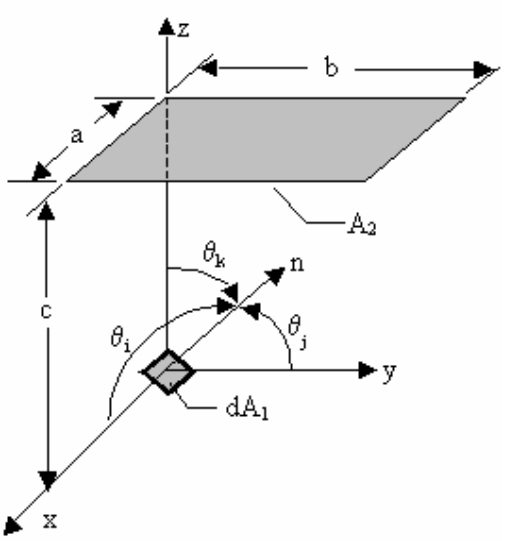

Figure 7: Pictorial representation and notation for the configuration factor from a finite rectangle to a differential element (Howell, 2008)

$$F_{12} = \frac{1}{2\pi}\left[\begin{array}{l}\tan^{-1} B\times\cos\theta_i + \tan^{-1} A\times\cos\theta_j + \dfrac{A\cos\theta_k - \cos\theta_i}{\sqrt{1+A^2}}\tan^{-1}\dfrac{B}{\sqrt{1+A^2}} \\ + \dfrac{B\cos\theta_k - \cos\theta_j}{\sqrt{1+B^2}}\tan^{-1}\dfrac{A}{\sqrt{1+B^2}}\end{array}\right] \tag{31}$$

Where:

$$A = \frac{a}{c}; \qquad B = \frac{b}{c} \tag{32}$$

Figure 7 shows that the target must be directly in line with one corner of the finite rectangle in a direction normal to the plane of the rectangle. This would appear to greatly limit the utility of the formula as targets must always correspond to a corner. Clearly, in fire situations a target will not always meet this criterion, as there would be potential targets for ignition all over the room. In order to solve this problem, one must add or subtract various components that make up the overall configuration factor. This is most easily explained diagrammatically.

Figure 8 depicts just one of the fire planes for simplicity, that being Plane α (labelled A_2). In the situation shown, when a normal is taken from the zy plane towards the target (dA_1), the normal lies within the bounds of A_2. At the point where the normal intersects A_2, horizontal and vertical lines are projected out to the boundaries of the rectangle. This

creates four individual rectangles, each with a configuration factor to dA_1 which can be calculated using Equation 31. Each of the four individual configuration factors F_1 to F_4 contribute to the overall configuration factor, F. For the situation described by Figure 8, the overall configuration factor is:

$$F = F_1 + F_2 + F_3 + F_4$$

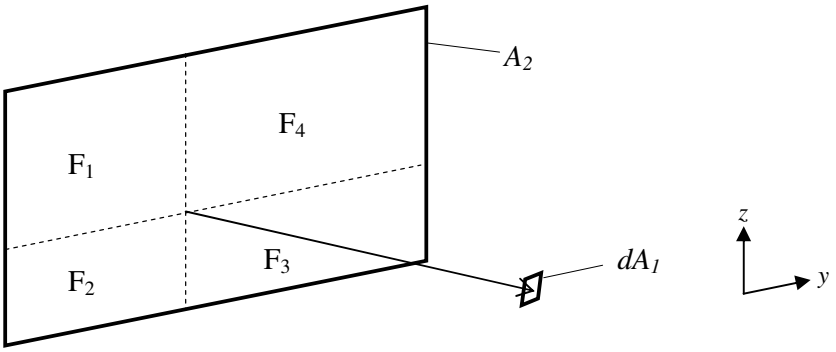

Figure 8: Example situation where the normal of the rectangle to the target lies within the bounds of the fire (area A_2). The fire must be divided into four individual rectangles and the configuration factors for each added to achieve the overall configuration factor

A different situation is outlined in Figure 9. Here, when a normal is taken from the zy plane towards the target, the normal does not actually intersect A_2. To calculate the overall configuration factor, the factors F_1 and F_2 must be added and then F_3 and F_4 must be subtracted as these are not part of A_2.

$$F = F_1 + F_2 - F_3 - F_4$$

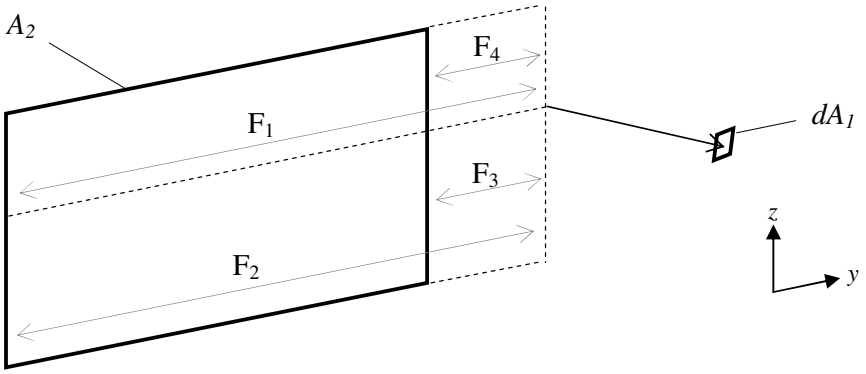

Figure 9: Example situation where the normal of the rectangle to the target lies outside of the bounds of the fire (area A_2). The overall configuration factor is found by adding factors F_1 and F_2 then subtracting factors F_3 and F_4

The same method can then be employed for calculating the configuration factor from Plane β to the target. The only requirement is that the definition of $\theta_{i,j,k}$ is consistent with that for Plane α. The overall shape factor is found by addition of the two components F_α and F_β.

$$F = F_\alpha + F_\beta \tag{33}$$

Where F_α is the configuration factor from Plane α to the target and F_β is the configuration factor from Plane β to the target.

The flame emissivity is calculated using the following equation:

$$\varepsilon = 1 - e^{-\kappa D} \tag{34}$$

As this is a new model, there is currently no validatory data for the rectangular planar model.

2.4 Variables for Models

As described in section 2.3, some of the models require the knowledge of a number of variables. These variables are essential inputs to the models; therefore, care should be taken in selecting appropriate values. The variables required, along with a review of the literature as to appropriate values, are described in the following sections.

2.4.1 Radiative fraction

In order to accurately predict the radiant heat flux to a target, one must determine the fraction of total combustion energy that results in thermal radiation. Known as the radiative fraction, χ_r, it is a function of the efficiency of combustion and the formation of soot, as well as the heat that is convected away from the fire. Markstein (1976) found that the radiative fraction is independent of the heat release rate of the fire. Table 3-11.12 of Beyler (2002) reports that the radiative fraction of propane gas is between 0.30 and 0.32. In the thermal radiation modelling presented in this thesis, the radiative fraction is treated as a variable. It should be noted that Sivathanu and Faeth (1990) determined a radiative fraction value of 0.28 for propane gas; however, this was for a small and possible laminar

flame. The flames that are of interest in this research are most definitely turbulent; therefore, Sivathanu and Faeth's value has little applicability to this situation.

2.4.2 Effective absorption coefficient

An important parameter that is required in both the Dayan and Tien model and the rectangular planar model is the effective flame absorption coefficient. Given the symbol κ, it is a measure of how easy it is for the radiation to penetrate the flame (Karlsson & Quintiere, 2000). Typical values for the extinction coefficient of pool fires are around 2 m^{-1} (Beyler, 2002). For propane fuel a value of 0.85 m^{-1} is recommended (Rasbash, Ramachandran, Kandola, Watts, & Law, 2004). The sensitivity of the theoretical radiant heat flux to this value is investigated (see section 5.6).

2.4.3 Flame temperature

As shown in section 2.3, some of the thermal radiation models require the flame temperature, T_f, to be known. Flame temperatures are commonly reported in two different ways; the adiabatic or the time-averaged flame temperature. The adiabatic flame temperature refers to the maximum theoretical temperature emitted during combustion, assuming there is no transfer of heat to or from the system (Drysdale, 2002). Clearly, this adiabatic assumption does not hold when one considers heat transfer from the fire to surrounding objects.

The flame temperature values used in radiation modelling of fires are the time-averaged values. These temperatures are observed on the fire centreline over approximately the lower 40 percent of the flame height (Beyler, 2002). Over a wide range of pool sizes, the maximum time-averaged flame temperatures are generally observed to be between 900 and 1100 °C (Beyler, 2002). Karlsson and Quintiere (2000) outline that the flame temperature is dependent on the type of fuel, because flames from different fuels have different luminosities and therefore varying degrees of radiative losses. Specifically for propane flames, Rasbash et al. (2004) advises using a flame temperature of 900 °C.

2.4.4 Heat of combustion

The heat of combustion is the amount of energy released when a unit mass of a fuel combusts. Drysdale (2002) reported a value of 46.45 kJ/g for the heat of combustion of propane fuel. This is in good agreement with values reported by Thomas (1986), NRC, ICC, DBH and ABCB (2005) and NIST (2008).

Chapter 3

EXPERIMENTAL METHODOLOGY

A series of experiments were carried out in which heat flux measurements were taken at various locations surrounding a gas burner. This experimental work was performed in the Special Purposes Fire Engineering laboratory at the University of Canterbury. This laboratory contains a furniture calorimeter, whereby combustion products from a fire are collected and analysed.

3.1 Scope of Experimental Work

The main purpose of the experimental work was to provide a comprehensive set of radiative heat flux data to be used for comparison with the thermal radiation models described in section 2.3. Within the overall BRANZ Ltd – UC project, the aim of this sub-section is to develop an item-to-item fire spread model within the BRANZFIRE software, as shown in Figure 1. This requires knowledge of the radiative heat flux received by an object, which is given off by an already burning object, such as an item of furniture. Therefore, ideally the fire source for these experiments should be burning objects, for example desks or armchairs. However, fires from these objects are highly dynamic in their flame size, shape and heat release rate. This makes for difficult comparison between measured data, as the fire conditions are constantly changing. For example, one cannot compare the radiative heat flux to targets at two different distances from the fire, if these measurements are taken at different times, because the fire conditions are likely to be vastly different at these two times. What is more, in order to attain a comprehensive set of heat flux data, tests on many objects must be carried out, which requires large capital expenditure.

In order to overcome these issues, a simple gas burner is used to model a burning object. The advantages of using a gas burner over real burning objects are as follows:

- Easily controllable heat release rate, via a mass flow controller
- Relatively stable and predictable flame size, shape and heat release rate. By knowing that these properties are somewhat constant for a given gas flow rate, heat

flux measurements at different times and locations should be more comparable than for the more dynamic fires from real burning objects

- Safer environment due to being able to extinguish the fire almost instantaneously by shutting off the gas flow to the burner
- More cost-effective than purchasing many items of furniture and other objects to burn

However, the main disadvantage with using a gas burner is that it does not represent a realistic or common source of fire within a compartment.

A limitation of the experimental work was that only one source of fuel was employed. This limits the analysis somewhat, in terms of parameters such as radiative fraction and absorption coefficient. The analysis is based around the assumption that a simple gas burner provides a good approximation to a burning object. The validity or accuracy of this assumption was not investigated in this work, but could be an area of interest for future research.

The experimental programme undertaken is derived from that of Mason (2003) and Mason et al. (2009), who used three dimensional flame reconstruction to estimate thermal radiation fields. The equipment used in the research presented in this thesis was all original; however, the experimental setup and procedure were similar to that of Mason.

3.2 Fire Source

The fire was provided by one of three rectangular gas burners, each with a different length to width aspect ratio. The aspect ratios tested were 1:1, 2:1 and 3:1. These were thought to represent the shapes of a variety of common items one might find within New Zealand buildings. Constructed of 304SS sheets, each burner had a width and depth of 300 mm and consequently lengths of 300, 600 and 900 mm. The gaseous fuel was delivered to the burner via a ¾" SS tube, containing 2 × 2 mm holes drilled at 100 mm centres, as shown in Figure 10. Holes were drilled at approximately a 45° angle from the centreline of the delivery tube.

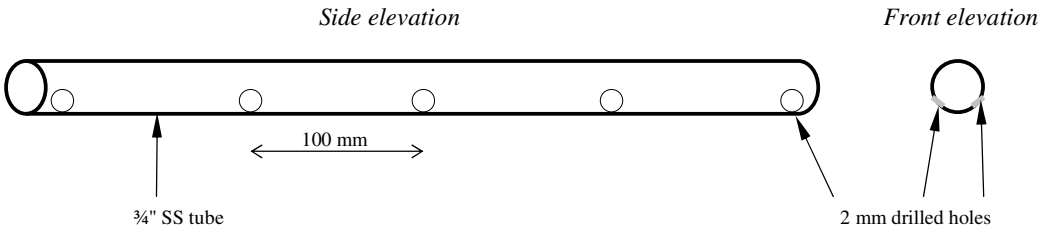

Figure 10: Gas delivery pipe within the gas burners (not to scale)

The burners were filled with ¾" diameter fired clay balls to diffuse the gaseous flow across the top surface area of the burner. This can be seen in Figure 11. The clay balls were filled to the level of the top of the burner, meaning that the base of the flame existed at this height.

Figure 11: The 3:1 aspect ratio burner, filled with fired clay balls to aid in diffusion

The gaseous fuel used was 100 % propane, delivered by four to eight 45 L liquefied propane gas bottles. This simultaneous delivery aimed to prevent any freezing of the propane within the bottles during prolonged periods of operation. The flow rate of propane to the burner, and therefore the heat release rate of the fire, was controlled by two mass flow controllers (see section 3.4.6) arranged in parallel. Using these controllers, heat release rates in excess of 350 kW could be achieved; however, this was limited to 300 kW during experimentation. This is because 300 kW was the maximum heat release rate that could be sustained for the required 15 minutes of burn time without the propane bottles freezing up.

The gas burner was able to be rotated to provide a different field of view to the heat flux gauges. Two different burner angles were tested. Firstly, the burner angle could be set at 0°, meaning that the sides of the burner were parallel with the face of the heat flux gauges. The burner could then be set at 45°. These two positions are shown in Figure 12.

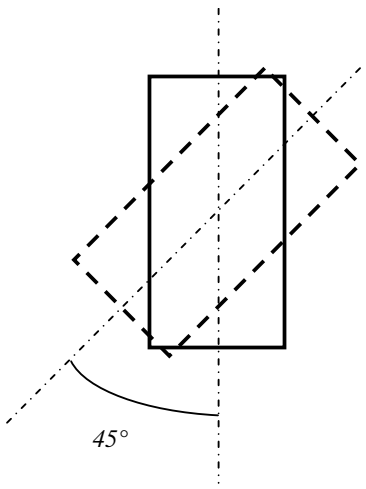

Figure 12: Relative angles of burner positions used in experiments. 2:1 burner aspect ratio depicted

3.3 Laboratory

As mentioned previously, the experimental work was carried out in the Special Purposes Fire Engineering laboratory at the University of Canterbury. The gas burner was placed underneath the large extraction hood, so that the products of combustion could be collected and analysed using oxygen depletion calorimetry. Make-up air was provided to the laboratory via a combination of passive louvred vents and a partially open door. These were adjusted in order to try and eliminate any significant wind effects on the flame. Furthermore, in an attempt to minimise flow disturbance, it was ensured that there was limited movement from personnel within the laboratory whilst data was being recorded. Figure 13 shows a schematic of the layout of the laboratory and Figure 14 shows a photograph taken during a typical experiment.

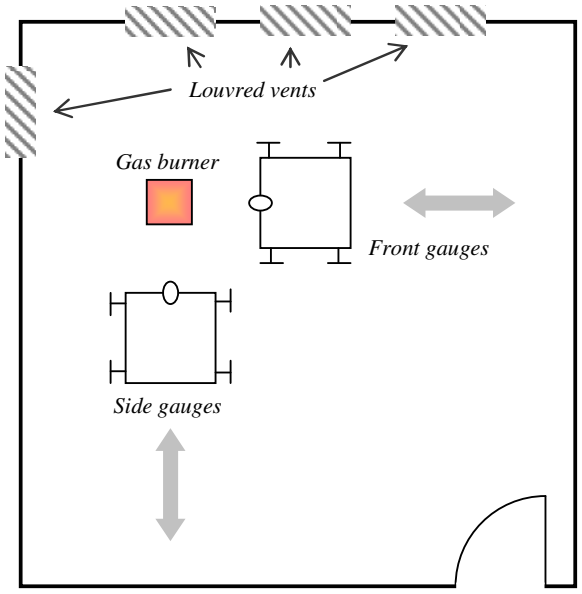

Figure 13: Schematic of laboratory layout (not to scale)

Figure 14: Photograph taken during experimental work, showing heat flux gauge trolleys located at 1.0 m from burner centre. Burner shown has 1:1 aspect ratio

3.4 Instrumentation

All radiative heat flux, temperature and gas analysis data was recorded using a Universal Data Logging (UDL) system, whereby data points were recorded at 1 s intervals for the

duration of the experiments. The following sections outline the instrumentation used during the experiments.

3.4.1 Heat flux gauges

A total of eight heat flux gauges were used to measure the rate of radiative heat transfer from the fire during the experiments. Four gauges were mounted on each trolley, located at heights of 0.0, 0.5, 1.0 and 1.5 m above the base of the flame. Seven of the gauges used were of the Medtherm Schmidt-Boelter variety, with the final transducer being a Gardon gauge. All gauges were able to be oriented either vertically (facing the fire) or horizontally (facing upward). Furthermore, the gauges could be moved horizontally relative to the front face of the fire. As shown in Figure 15, the heat flux gauge trolleys were on steel rails, allowing the heat flux gauges to be moved to different distances from the fire. The two sets of rails were arranged perpendicular to each other allowing a different field of view from the fire. The heat flux gauge positions tested during the experiments were 0.5, 0.75, 1.0, 1.5 and 2.0 m from the fire centre, in each direction.

Figure 16 shows a front view of one of the heat flux gauge trolleys and indicates the position of the offset and central gauge positions. The central position is in line with the centreline of the burner, whilst the offset position is 0.35 m outside the centreline. This arrangement could be installed on both the front and side gauge trolleys.

All gauges were water-cooled and had a claimed range of 0 – 100 kW/m². Water-cooling was achieved by delivering water to each gauge via ¼" OD flexible tubing. Two separate water lines were used, with each line providing water to four gauges in series.

The gauges were calibrated in a cone calorimeter against a previously unused gauge. The output for the heat flux gauges was in mV. For each transducer a conversion factor was obtained so that the measured voltages could be converted to a 'true' radiative heat flux, in kW/m².

Figure 15: Side view of heat flux gauge trolley on its tracks

Figure 16: Front view of heat flux gauge trolley with offset and central gauge positions indicated

3.4.2 Thermocouples

Four ANSI Type K, 24 gauge, bare bead, sheathed thermocouples were employed to measure the flame temperature. These were located at 0.38 m height intervals, up to a height of 1.52 m above the base of the flame. The thermocouples were positioned over the centre of the burner and provided an idea of the flame temperature at various heights. This data could be used as a rough estimation of the mean flame height based on the location of the 500 °C contour.

Also, thermocouples were installed in the water cooling lines to the heat flux gauges. This was so that the water temperature could be closely monitored during the experiments. A fast rise in water temperature may indicate a blockage in the water cooling lines, possibly invalidating the radiant heat flux measurements. Throughout the experimental programme, no such rapid rise in temperature was experienced.

3.4.3 Calorimetry

One form of measurement for the heat release rate of the fire employed the use of oxygen depletion calorimetry. The principle behind calorimetry originates from Thornton (1917), who found that the heat released per unit amount of oxygen consumed during the complete combustion of a large number of organic gases and liquids was fairly constant. This rule implies that one can determine the net heat released from a combustion system if the amount of oxygen consumed is measured.

In order to carry out oxygen depletion calorimetry, it must be ensured that all of the products of combustion are collected and removed through an exhaust duct (Janssens, 2002). Measurements of gas flow rate and composition are carried out downstream, at a distance sufficient to allow adequate mixing. For the work carried out in this experimental programme, the oxygen, carbon dioxide and carbon monoxide components of the combustion products were measured. This allowed calculation of the heat release rate of the fire. The equations used for these calculations and more information on oxygen depletion calorimetry are given by Janssens (2002).

3.4.4 Video equipment

All of the experimental work was filmed using a Canon XM2 digital video camcorder. This was located behind a protective glass window in the control room adjacent to the main laboratory. The camera was mounted on a steel frame and the lens was fitted with a UV filter. The main function of the video was to use it in the determination of the flame height during the experiments. This technique is discussed in detail in section 3.7.

It was ensured that the same camera settings were maintained throughout the entire experimental programme. These are summarised below:

- The camera was set to "TV" mode as this allowed greater flexibility in settings
- Manual focus was enabled to ensure that the flame was in focus
- The movie mode was set to "Frame" which allows the user to play back the video frame by frame, free from field slippage
- The exposure could be set between -11 and +11, with negative values suited to situations where there is a bright image against a dark background. An exposure setting of -5 was found to give good definition of the flame without 'washing out' the picture
- A shutter speed of $1/500^{th}$ of a second was selected for the videoing. This relatively fast shutter speed resulted in a darker image, which aided in the video analysis by the computer software

It was important that reflections from other surfaces surrounding the flame were limited, in order to prevent interference with the video images. To achieve this, a non-reflective canvas was hung against the wall behind the flame and the laboratory lights were switched off during all experiments. Prior to turning off the lights or igniting the burner, however, a period of film was captured in which the thermocouple tree was clearly visible to the camera. Knowing the distance between certain points on the thermocouple tree allowed the scale of the video images to be established.

3.4.5 Load cell

To check that the expected heat release rate was actually being delivered by the gas burner, the propane bottles were weighed before and after burning. This was achieved by

placing the four bottles on a stand and attaching said stand to a load cell. The load cell provided a mass measurement via a digital readout on a Mettler Toledo Hawk terminal. By recording the mass reading immediately preceding and following any period of burning, the heat release rate could be calculated using Equation 35.

$$\dot{Q} = \frac{\Delta H_c \left(m_i - m_f \right)}{t} \tag{35}$$

Where ΔH_c is the heat of combustion (kJ/kg), m_i and m_f are the initial and final mass readings of the gas bottles (kg) and t represents time (s).

In Equation 35, t refers to the exact duration of burning at a constant heat release rate. Before altering the heat release rate, the gas flow would have to be ceased whilst a mass reading was taken. It was assumed that complete combustion of the propane gas occurred.

On particularly cold days and during long periods of burning at heat release rates of 250-300 kW, the mass flow controllers would occasionally begin to show a decrease in the flow being provided by the propane bottles. When this was the case, the number of bottles being drawn from would be increased from four to eight and the test repeated. By supplying propane from eight bottles rather than four, a relatively constant flow of gas could be achieved. However, the mass measurements were no longer valid as only four bottles could be weighed.

3.4.6 Mass flow controllers

The heat release rate of the fire was controlled via two mass flow controllers, arranged in parallel. The type of controller used was an MKS Digital Mass Flow Controller Type 1579A. Each controller was electrically connected to a mass flow controller power supply/readout unit, which allowed a set-point to be specified corresponding to a percentage of the maximum flow through the valve. The mass flow controllers attempted to achieve the set-point value by adjusting the valve position until the measured flow rate equalled the desired flow rate, in terms of the percentage of the maximum. For consistency, both valves were always programmed to the same set-point, regardless of whether a single valve could have provided adequate flow. Each valve had a claimed maximum flow rate of 300 L/min of gaseous nitrogen.

Prior to any experimental results being taken, the mass flow controllers were calibrated so that any desired heat release rate (within the limits of the controllers) could be obtained by adjusting the valve set-point. This was achieved by carrying out periods of burning (at least 20 minutes each) at a range of set-point settings and determining the heat release rate at each setting. The heat release rate calculated by Equation 35 was compared with the oxygen depletion calorimetry result to achieve a trusted value. Using the data collected over the range of set-points, a correlation was established which related set-point settings to heat release rates.

3.5 Experimental Procedure

The total experimental programme consisted of 16 individual tests, where a test is defined as obtaining data at all distances for each heat release rate setting of a single burner geometry. For example, the heat flux data for one test consisted of the measurements taken at each of the four heights and each of the five horizontal distances for each of the five heat release rate settings. Table 1 outlines the settings used for each of the 16 runs performed. Note that test 13 is a repeat of test 9 to check repeatability.

Table 1: Gauge and burner settings for each experimental test

Test #	Gauge Orientation	Gauge location	Aspect ratio	Burner angle
1	Vertical	Offset	2:1	0
2				45
3			3:1	0
4				45
5			1:1	0
6				45
7		Centre	1:1	0
8				45
9			3:1	0
10				45
11			2:1	0
12				45
13*			3:1	0
14	Horizontal		3:1	0
15			1:1	0
16			2:1	0

** Repeat of Test 9*

The procedure for carrying out each experimental test is outlined below.

1. Ensure all equipment is in place and ready to operate. This includes extraction fan running, water to heat flux gauges flowing, louvred vents open, ODC analyser calibrated and heat flux gauge trolleys located at distance of 2.0 m from centre of burner. Record load cell mass reading.
2. Begin data logging and collect 3 minutes of baseline data. Turn video camera on and adjust settings to those outlined in section 3.4.4.
3. Ignite burner, ensuring that mass flow controller set-point corresponding to 300 kW fire is reached. Collect 3 minutes of data.
4. Move heat flux gauge trolleys inwards to distance of 1.5 m from centre of burner. Collect 3 minutes of data.
5. In turn, move heat flux gauge trolleys to distance of 1.0, 0.75 and 0.5 m from centre of burner, collecting 3 minutes of data at each distance.
6. Extinguish burner by closing mass flow controller. Adjust set point to 250 kW setting. Record load cell mass reading.
7. 3 minutes after extinguishment, re-ignite burner at 250 kW heat release rate.
8. In turn, move heat flux gauge trolleys to distance of 0.75, 1.0, 1.5 and 2.0 m from centre of burner, collecting 3 minutes of data at each distance.
9. Continue in same fashion for 200, 150 and 100 kW fires.
10. Collect further 3 minutes of data after final extinguishment. Turn off all logging equipment.

Following each experiment, one of the variables from Table 1 would be changed, and then the above procedure repeated for the new set up. For example, the burner would be rotated to the 45° angle or the gauges moved from the offset to the central position. This was repeated until all of the conditions outlined in Table 1 had been tested.

3.6 Experimental Data Analysis Technique

3.6.1 Heat release rate

The primary form of analysis of the experimental data was to check that the heat release rate delivered by the gas burner was as expected from the mass flow controller set-points. This was achieved by comparing the expected heat release rate (based on the set-point input to the mass flow controllers) with the heat release rates determined by both Equation

35 and Oxygen Depletion Calorimetry. If either of these latter results were greater than ± 5 % of the expected value, that part of the experiment was repeated.

3.6.2 Radiant heat flux

The most important results obtained from the experiments were the heat flux data. The output from each of the eight heat flux gauges was a voltage, measured in mV. The raw data for one complete experimental test, including all heat release rate settings and all distances from the fire, appeared similar to the plot shown in Figure 17 below. The result shown is for the side gauges from Test 13. Figure 18 details the first 18 minutes of the same test. This corresponds to the 300 kW heat release rate at all five distances from the fire centre (2.0, 1.5, 1.0, 0.75 and 0.5 m respectively). Each different distance setting can be seen as a separate step on the plot. It is evident from Figure 17 and Figure 18 that there is considerable noise in the voltage signal from the heat flux gauges. This is expected, due to the highly turbulent nature of the fire itself, meaning that the radiant heat flux to the gauges is also highly dynamic.

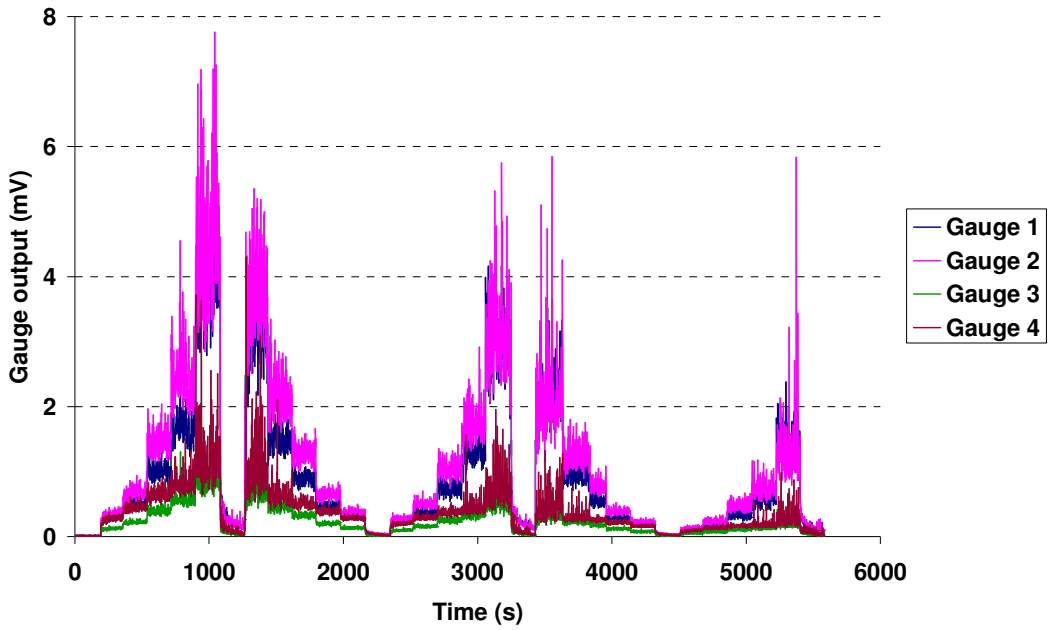

Figure 17: Example of raw heat flux gauge data, from side gauges of Test 13

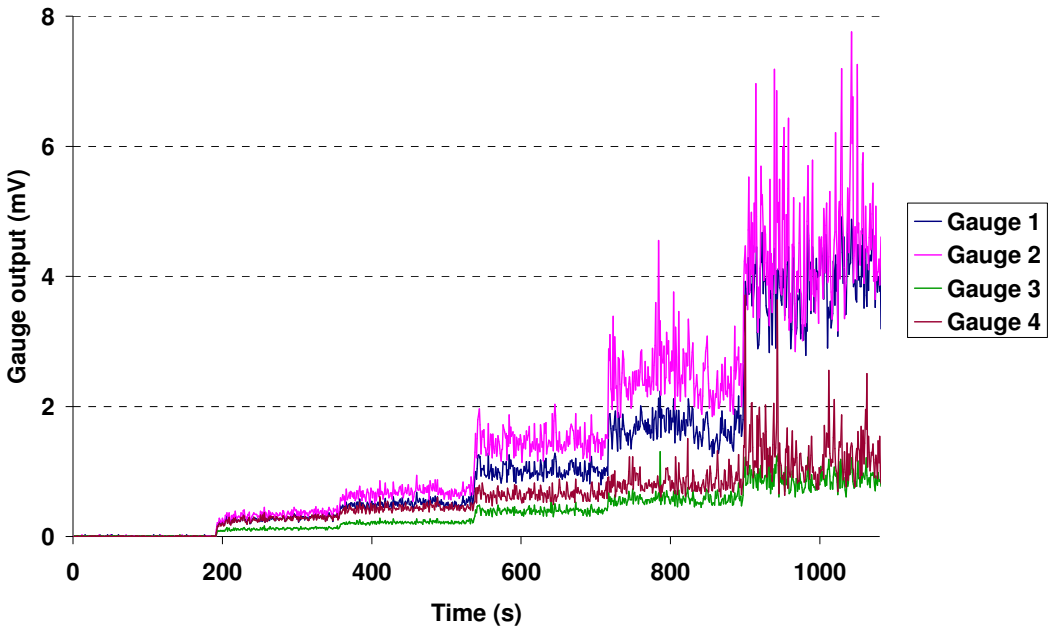

Figure 18: First 18 minutes of Test 13, corresponding to the 300 kW heat release rate

In terms of obtaining meaningful radiant heat flux results, the noise needed to be removed. Therefore, at each distance setting the central 2 minutes of data was averaged to yield a single voltage, which was used for the analysis. The first 30 seconds of data at each setting was discarded because the gauges needed to be given a small amount of time to adjust to the new radiant heat flux being received due to the new distance setting. The final 30 seconds was also discarded, as during this time there was movement in the laboratory in preparation to move the heat flux gauge trolleys.

With the average voltage from each gauge now known at each setting, the conversion factor for each gauge was applied to yield the radiant heat flux at a range of distances and heights. The use of a single time average value for each gauge position is justified because the raw data is normally distributed around its mean value. An example of 2 minutes worth of raw data is shown in Figure 19. Note that in this instance the voltage output has been converted to radiant heat flux. It can be seen that the heat flux data approximates a normal distribution over the 2 minute period of sampling. Therefore, the mean value represents an appropriate statistic of the data set as a whole.

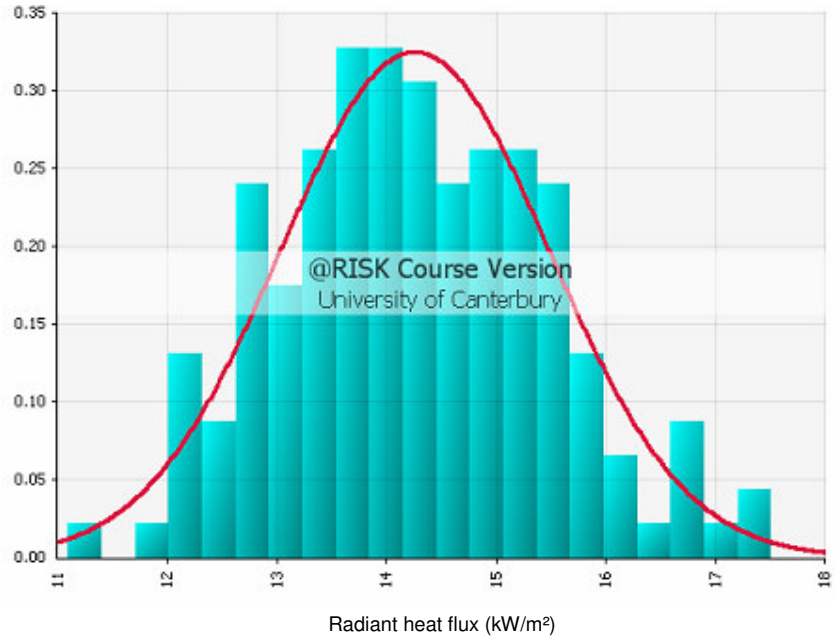

Figure 19: Distribution of raw heat flux data for Test 11, 300 kW, 0.5 m from fire centre, 0.0 m above flame base

3.7 Flame Height Determination

As outlined in section 2.3, some of the thermal radiation models require the flame height, *H*, as an input. Before describing how this might be determined, it is important to define what the term 'flame height' actually refers to. The visible flames above a fire source are where the combustion reactions take place. Heskestad (2002) describes that "the luminosity of the lower part of the flaming region appears fairly steady, while the upper part appears to be intermittent. Sometimes vortex structures, more or less pronounced, can be observed to form near the base of the flame and shed upward." This variation in flame intermittency with height above the fire source forms the basis for the definition of the flame height. As the flame is highly dynamic and turbulent in nature, the highest point that the flame exists is constantly changing. Therefore, it is convenient to define the flame height in terms of its mean value.

The graph shown in Figure 20, first proposed by Zukoski, Cetegen and Kubota (1985), is commonly used to help define the mean flame height. The intermittency, *I*, shown on the vertical axis ranges from 0.0, at which height the flame never exists, to 1.0, where the flame is always visible over the time period of interest. The mean flame height, *H*, is

defined as the height at which the intermittency has reduced to 0.5, meaning that flames appear above this point half the time.

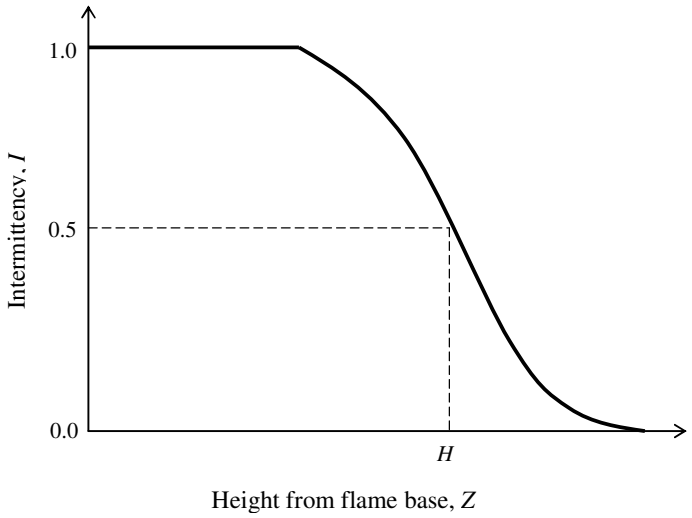

Figure 20: Definition of mean flame height, H, from measurements of flame intermittency, I

Various correlations have been created for the mean flame height, the most well known being that from Heskestad, given in Equation 6. This correlation is employed by some of the thermal radiation models, such as the point source model, Shokri and Beyler detailed method and the Dayan and Tien method. Experimentally, accurate determination of the mean flame height usually involves video equipment (Karlsson & Quintiere, 2000). This was the case for the experimental work carried out as part of this research. An alternative to video analysis for determining the flame height is to rely on visual observation during the experiments; however, this method tends to overestimate the actual flame height (Beyler, 1986).

3.7.1 Video image analysis

In order to determine the mean flame height from the video footage of the experiments, an image processing computer software was employed. Developed at the University of Canterbury, *ImageStream* (Nokes, 2008a) employs a systematic process for manipulating the video images, eliminating the need for the individual's visual perception of the flame height. The software was designed as a "simple image processing package aimed at experimental fluid mechanics applications" (Nokes, 2008b). However, previous work by Goble (2007) demonstrated that it could be readily applied in the analysis of fire.

The required input to *ImageStream* is a series of image files, achieved by breaking down a video into individual frames. This series of images is called an image sequence. The software evaluates the red, blue and green (RGB) colour intensities at each pixel of every image in the sequence and stores them as an integer ranging from 0 to 255. The images can be manipulated by applying transformation algorithms, known as filters. A filter takes the pixel intensities of the digital images as input, transforms these intensities according to its specific rules, and produces new pixel intensities as its output (Nokes, 2008b). In this way, the user is able to clarify the images in order to extract useful pieces of information. An intensity field, based on a rectangular grid applied across each image, allows this pixel information to be extracted and displayed in a useful format, such as a single time-averaged image.

For the analysis of the experiments undertaken in this research, the captured video was broken into individual still images using the *Adobe Premiere Pro* software (Adobe Systems Incorporated, 2007). For each heat release rate setting of each burner aspect ratio, two minutes of video was uploaded and converted using the program. The two minute section was taken from a longer period of relatively stable fire behaviour. This video, recorded at 25 frames per second, yielded 3000 still images for each heat release rate tested. These 3000 images were then created as an image sequence in *ImageStream*. After cropping to remove unnecessary information, a distance scale was applied in both the horizontal and vertical directions, based on the known lengths of the burner and thermocouple tree, respectively.

Next, a series of filters were applied to the image sequence so that the software would be able to accurately determine the outline of the flame. This was best done by extracting a single colour from the images; red was used at it provided the best differential between the luminous flame and the darker background. Following this extraction filter, a threshold filter was applied which removed pixels from the image that were below a given red intensity. The purpose of this was to remove any visible objects from behind the flames. A threshold value of 200 in the red colour gun was applied, as used by Goble (2007). Next, the remaining red colour intensities were amplified so that all had a maximum value of 255 and then normalised to a value of 1. Finally, a convert type filter was employed to convert the red intensities in the RGB image into a ‘real value’. The outcome of the

filtering process was a series of images with Boolean value pixel intensities; that is intensity values of either 1 (where flames existed) or 0 (where there was no flame).

The 3000 images in the image sequence were then time averaged over the two minute period. This created an intensity plot with contours illustrating the probability of a flame existing at any particular location during that period. From this the 0.5 probability, corresponding to 50 % flame intermittency, could be determined by placing the mouse curser at the highest point of that contour. The *ImageStream* display would then give the co-ordinates of that point, corresponding to the flame height. A full set of step-by-step instructions for forming the contour plots of probability is given in Appendix C.

The process of manipulation from the initial still image to the fully filtered image is summarised in Figure 21. To demonstrate the process, one frame is selected at random from the 300 kW burn of the 2:1 burner. It can be seen that the flame shape depicted in the manipulated image of Figure 21e corresponds well with the raw image given in Figure 21a. This visual test was used for all experimental runs as a check that the computer software was carrying out the manipulation process as intended. The final time-averaged contour plot for one particular burner aspect ratio and heat release rate is given in Figure 22.

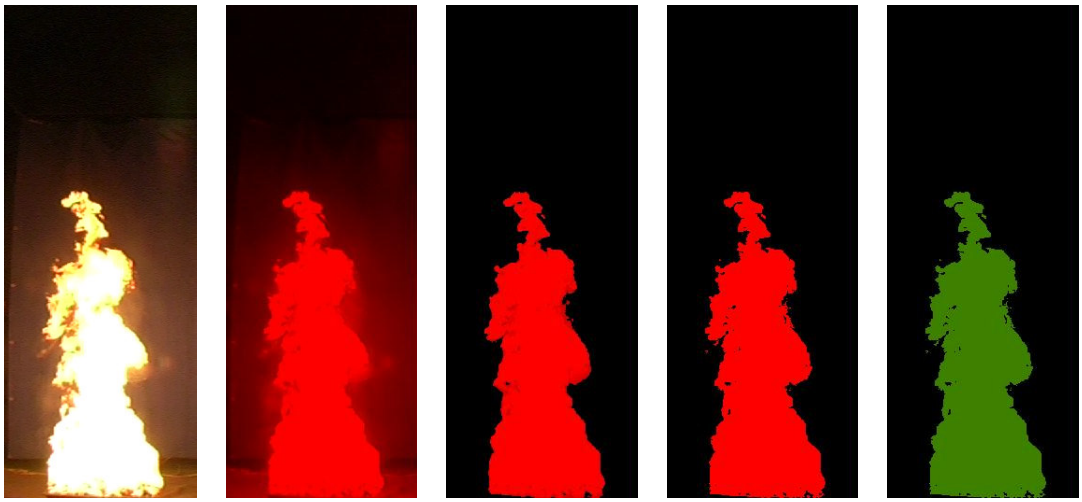

(a) **(b)** **(c)** **(d)** **(e)**

Figure 21: Process of image manipulation using *ImageStream* by applying filters. (a) raw image from single frame of video, (b) extraction of red colour intensity, (c) colour removed below certain red colour threshold, (d) amplification of red colour intensity, (e) intensities converted and normalised to real Boolean values

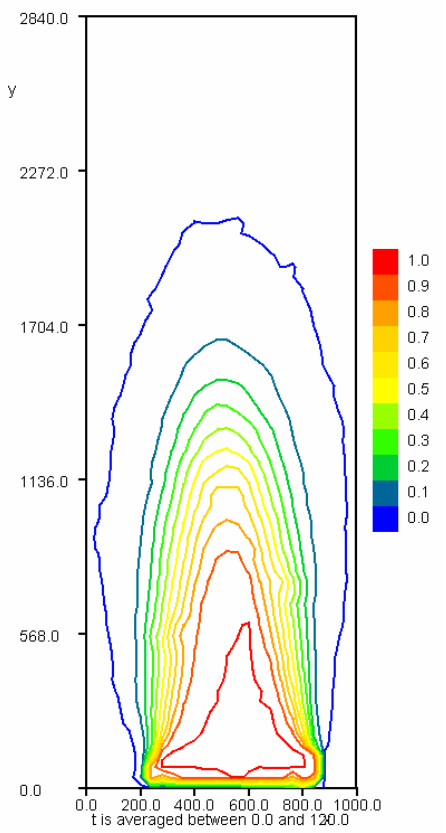

Figure 22: Time averaged contour plot for the 2:1 burner at 300 kW. Vertical axis gives flame height (in mm). Scale on right hand side gives probabilities of flames existing at different locations

There are alternative ways in which the output of the *ImageStream* analysis can be presented; the contour plot given in Figure 22 being one of them. Other forms of display are given in below. Figure 23a is an average colour image from the 2 minute section of film taken for the 2:1 burner at 300 kW. The image shown contains the average colour of the original image sequence of 3000 images at each pixel. Figure 23b is similar to the contour plot; however, the entire image is coloured based on the probability of flame existing within any particular grid cell.

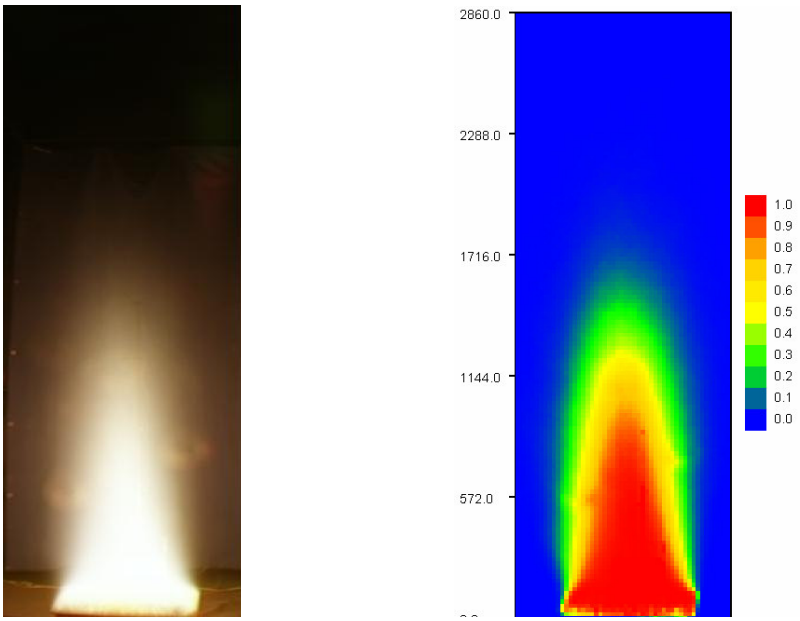

(a) **(b)**

Figure 23: Alternative forms of *ImageStream* output for 2:1 burner at 300 kW

When creating the time-averaged intensity plot, the user must specify a grid size to be applied across the domain of the image. A smaller grid size provides better resolution of the probabilistic flame shape but is more computationally demanding. For this application, the smallest possible grid size did not necessarily provide better results, as the only value of interest was the peak flame height of the 0.5 intensity. The highly detailed contours provided by the finer grids only added unnecessary clutter to the intensity plots, in addition to increased computational time and demand.

In order to determine the most appropriate grid size, a grid independence study was carried out. It was found that a 40 mm grid gave an accurate enough contour shape, whilst still providing adequate resolution for the flame height measurement. Figure 24 compares the probability contour plot resulting from a range of grid sizes. It can be seen that the level of detail in the flame shape decreases with increasing grid size. The 40 mm grid, depicted in Figure 24c, was deemed to be adequate because the difference between the flame heights evaluated at each contour for the 40 mm and 20 mm grids was on average less than 1 %.

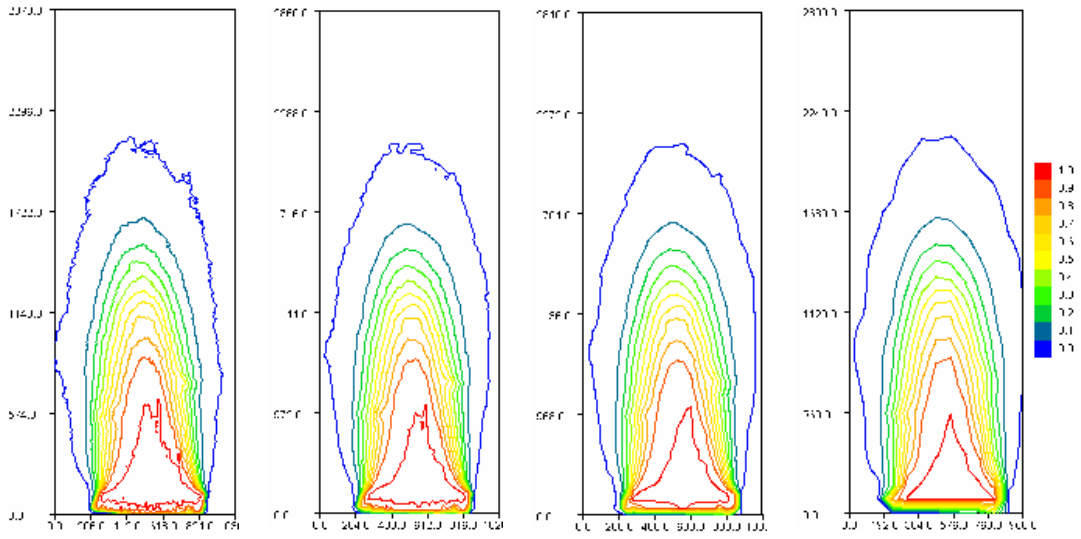

(a) (b) (c) (d)

Figure 24: Time-averaged contour plots of the 2:1 burner at 300 kW resulting from (a) 10 mm grid, (b) 20 mm grid, (c) 40 mm grid and (d) 80 mm grid

In order to validate the mean flame heights determined by the *ImageStream* software, a manual method was also undertaken. Here, the raw images (such as those shown in Figure 21a), were brought up on a computer screen and then a clear overhead projector sheet was placed over the screen. Using markers on the projector sheet, a scale was established, again using the burner and the thermocouple tree as reference points. The images were then cycled through in turn, with the height of the flame being recorded for each image. After 125 images, corresponding to 5 seconds worth of film, the flame heights for all of these images were averaged and compared with the results from the *ImageStream* analysis. This validation was performed for two different experiments; the 1:1 burner at 300 kW and the 2:1 burner at 300 kW. Table 2 compares the flame heights determined computationally and manually for these two settings.

Table 2: Results of flame height validation

	Mean flame height, *H* (m)		
Experiment	***ImageStream* result**	**Manual result**	**% Difference**
1:1 burner, 300 kW	1.49	1.53	2.5%
2:1 burner, 300 kW	1.25	1.31	5.0%

Given the relative crudeness of the manual method, the percentage differences displayed in Table 2 were deemed to be small enough to give confidence to the flame heights determined by the *ImageStream* software.

Chapter 4

EXPERIMENTAL RESULTS AND DISCUSSION

The experimental work described in Chapter 3 yielded a large amount of data. This data is best viewed and compared graphically. In accordance with the aim of this research, the main quantity of interest is the radiant heat flux to the heat flux gauges. As such, the analysis deals almost exclusively with the radiant heat flux, while results taken of other quantities, such as temperature, will not be presented here. This is because the other variables were measured purely so that they could be monitored during the experiments.

It is useful to view the experimental data on its own prior to comparison with the theoretical models to become familiar with the general behaviour of the radiant heat flux under different conditions. The radiant heat flux results presented in this chapter come accompanied by error bars, representing the standard deviation of the sampled data.

Given the amount of experimental data that has been recorded, it would be of little use to present all of the data on a single graph. Therefore, to demonstrate some of the general trends evident in the experimental results, single experiments are selected and presented in detail. The results from these tests are representative of the trends shown by the majority of the experimental tests.

4.1 Heat Release Rate

As described in section 3.6.1, the heat release rate expected from the burners was validated against two independent forms of measurement; the calculated heat release rate (using Equation 35) based on mass loss of the propane fuel and the heat release rate calculated using Oxygen Depletion Calorimetry. It should be noted that the calculation method based on mass loss of propane could not be carried out during all experimental runs due to freezing of the propane. A comparison of the different methods based on results from a typical test is presented in Figure 25. In this figure, each distinctive step represents one heat release rate setting during the experiment, starting at 300 kW and stepping down to 100 kW at 50 kW intervals.

The dashed line represents the desired heat release rate, which is expected to be delivered by the mass flow controllers based on the appropriate set-point being manually inputted. The solid green line is the heat release rate that is calculated using Equation 35. This is calculated using the mass of propane at the start and end of each heat release rate step, resulting in an average value being presented. The final, more dynamic, line is the heat release rate as calculated by Oxygen Depletion Calorimetry. It should be noted that this data has been smoothed somewhat, in the form of a 30 second moving average, to make the data more readable. This time averaging results in an apparent delay in the heat release rate data, as can be seen in the figure.

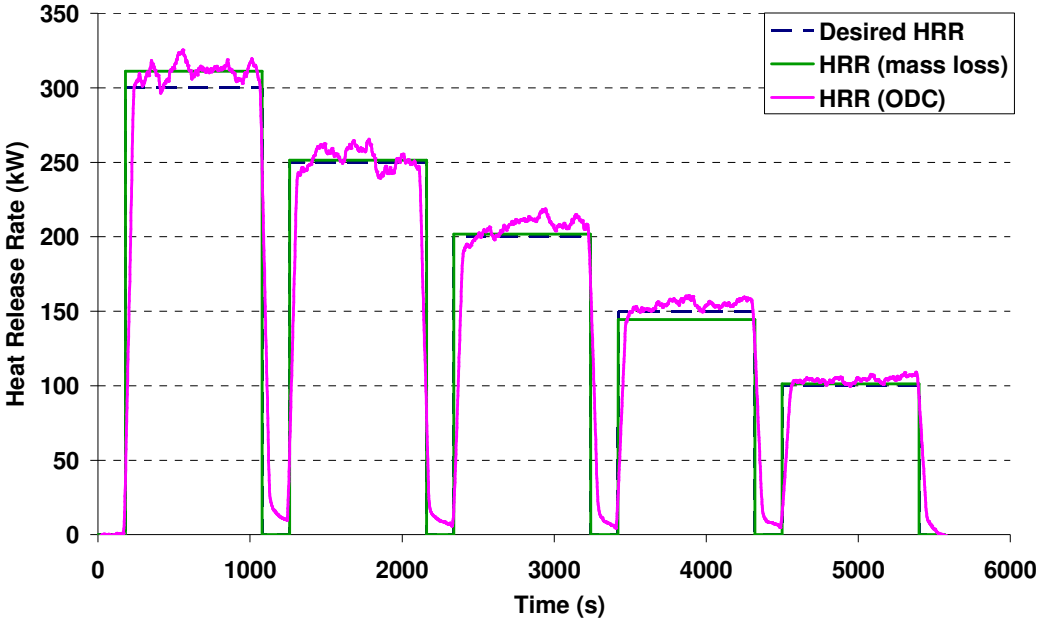

Figure 25: Comparison of heat release rates (from Test 2). Shown are desired values from mass flow controllers, calculated values based on propane mass loss and calculated values based on ODC (30 second moving average plotted)

On the whole, the two different calculation methods showed good agreement with the expected heat release rates. It proved to be difficult to get an exact match all of the time, as the calculated heat release rate appeared to vary unpredictably based on various factors, including the ambient temperature and propane pressure. A fairly comprehensive calibration procedure attempted to limit these variations as much as was practicably possible; however, small differences still appeared at times.

4.2 Radiant Heat Flux

The following sections outline how the radiant heat flux varied with different experimental variables.

4.2.1 Variation of heat flux with distance from fire

As shown in Figure 26 below, the radiant heat flux to the gauges decreases as the gauge moves further away from the fire. This is intuitive, as from experience one knows that close to a heat source the heat energy that can be felt is greater than when one is at a larger distance from the source. This phenomenon is mainly due to the configuration factor that exists between the source (in this case the fire) and the target (the heat flux gauge). One of the contributing factors to the configuration factor is the distance between the objects, as explained in section 1.4.2.

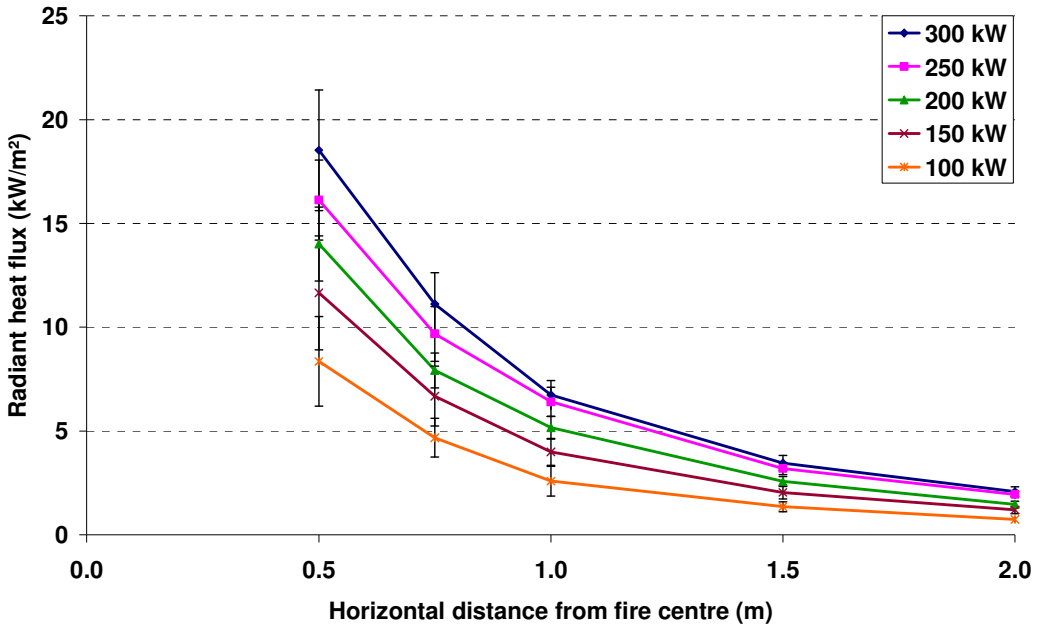

Figure 26: Radiant heat flux vs horizontal distance from fire centre. From Test 11, 2:1 burner, front gauges, gauge height above flame base = 0.5 m

The magnitude of the error bars show that the standard deviation of the data taken close to the fire is much greater than when further away from the fire. This was also indicated in Figure 18, where a lot more noise could be seen in the raw heat flux gauge data at distances closer to the fire. To investigate this phenomenon closer, it is useful to get a

measure of the standard deviation relative to the mean. This is called the coefficient of variation, denoted c_v (%), and is defined by Lohninger (2009) as:

$$c_v = 100\frac{stdev}{\bar{x}} \tag{36}$$

Where *stdev* is the sample standard deviation (any units) and $\bar{x}$ is the sample mean (in same units as *stdev*).

Table 3 below summarises the coefficients of variation for the data presented in Figure 26. It can be seen that the general trend is for the coefficient of variation to decrease as the target moves away from the fire and also as the heat release rate increases. Therefore, relative to the mean values, the radiant heat flux did indeed exhibit more noise when closest to the fire. Also, smaller heat release rates resulted in greater noise in relation to the mean values measured. These facts should be kept in mind when viewing the error bars for the experimental data.

Table 3: Coefficient of variation data for Test 11, front gauges, gauge height above flame base = 0.5 m

	Coefficient of variation, c_v				
Distance from fire centre	**100 kW**	**150 kW**	**200 kW**	**250 kW**	**300 kW**
0.50	26%	24%	13%	12%	16%
0.75	20%	22%	11%	14%	14%
1.00	27%	16%	11%	11%	10%
1.50	18%	16%	9%	9%	11%
2.00	17%	14%	10%	10%	11%

4.2.2 Variation of heat flux with heat release rate

Also shown in Figure 26 above is the fact that the radiant heat flux increases with increasing heat release rate from the fire. The maximum heat flux values at each horizontal distance setting resulted from the 300 kW fire – the maximum heat release rate tested. This result was as expected, as a larger source of energy would give a larger rate of energy transfer per unit area of target. Figure 27 shows that there is roughly a linear relationship between the radiant heat flux to a target and the heat release rate of the fire. This supports the findings of Markstein (1976), who also conducted radiation measurements around propane turbulent diffusion flames. This researcher observed that the total radiative power of the flame was directly proportional to the total heat release rate.

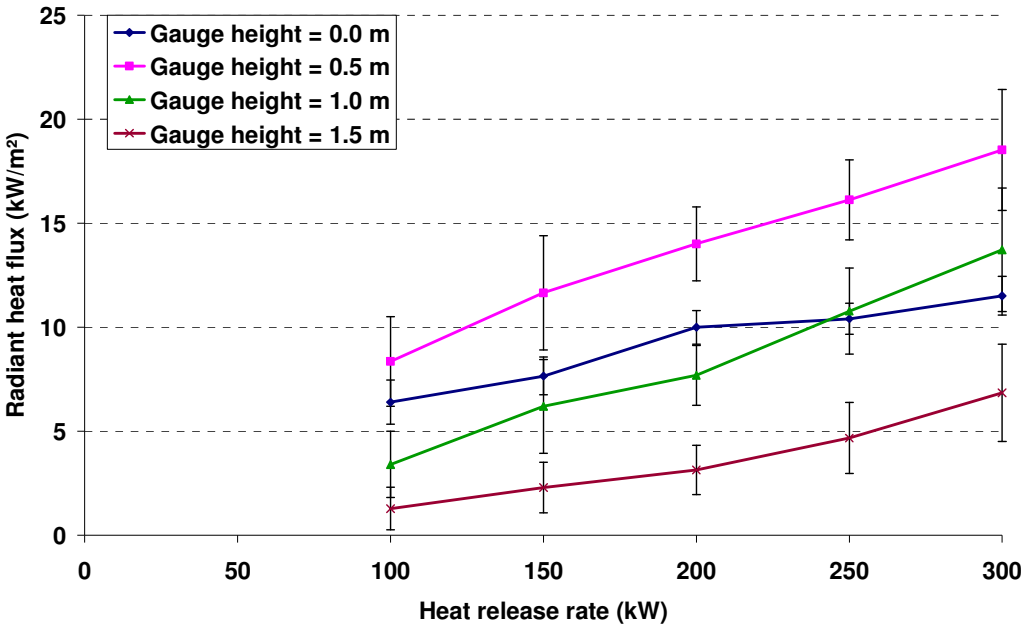

Figure 27: Radiant heat flux vs heat release rate of fire. From Test 11. Front gauges, distance from fire centre = 0.5 m

4.2.3 Comparison between front and side gauges

For the burner with the 1:1 aspect ratio, one would expect the radiant heat fluxes received by the front and side gauges to be roughly equivalent. On the whole, this was the case for the experimental work carried out as part of this research. For non-square burners, however, there are likely differences in the heat fluxes to the front and side gauges due to the different effective surface areas of flame viewed by these targets.

The convention in the theoretical models in section 2.3 for measuring the distance, *L*, between a radiating body and a target is that this distance is between the target location and the centre of the fire. In keeping with this, in the experimental work the distance is also measured to the centre of the gas burner, not to the edge of the flame. Therefore, for the 2:1 and 3:1 aspect ratio burners, due to the orientation of the burner, the side gauges are actually closer to the edge of the burner than the front gauges. For example, when the gauges are located at 0.5 m from the centre of the 2:1 burner, they are 0.35 m from the front edge of the burner but only 0.20 m from the side edge. This may result in a higher heat flux being received by the side gauges (when at the same distance from the centre of the burner) because these gauges are closer to the flame. However, these side gauges, although closer to the flame edge, actually view a smaller surface area of the flame, as

shown in Figure 28. The actual heat flux to the gauges will depend on a combination of factors, such as the distance away, heat release rate of the fire, height of flames and gauge height. Of course, the edge of the flame does not necessarily correspond with the edge of the burner, as shown in Figure 28b. The actual distance from the target to the flame edge is difficult to measure, due to the flame shape changing with time, and the position of the flame edge changing with height. Section 5.6 discusses how the predictions from the radiation models change when a different convention for the distance between the fire and target is used.

(a) **(b)**

Figure 28: Typical view of a 300 kW fire from the 3:1 aspect ratio burner when viewed from (a) the side and (b) the front

Figure 29 below indicates that at high heat release rates, the side gauges appear to receive a greater radiant heat flux than their counterparts located to the front of the fire. As the heat release rate decreases, however, the difference between the heat flux to the side and front gauges lessens, until at 100 kW, the front gauges are measuring a greater heat flux than the side devices when close to the fire. This may mean that at higher heat release rates (at least 300 kW) the heat release rate dominates the radiant heat flux, while as the heat release rate tends to 100 kW and below, the proximity to the fire dominates.

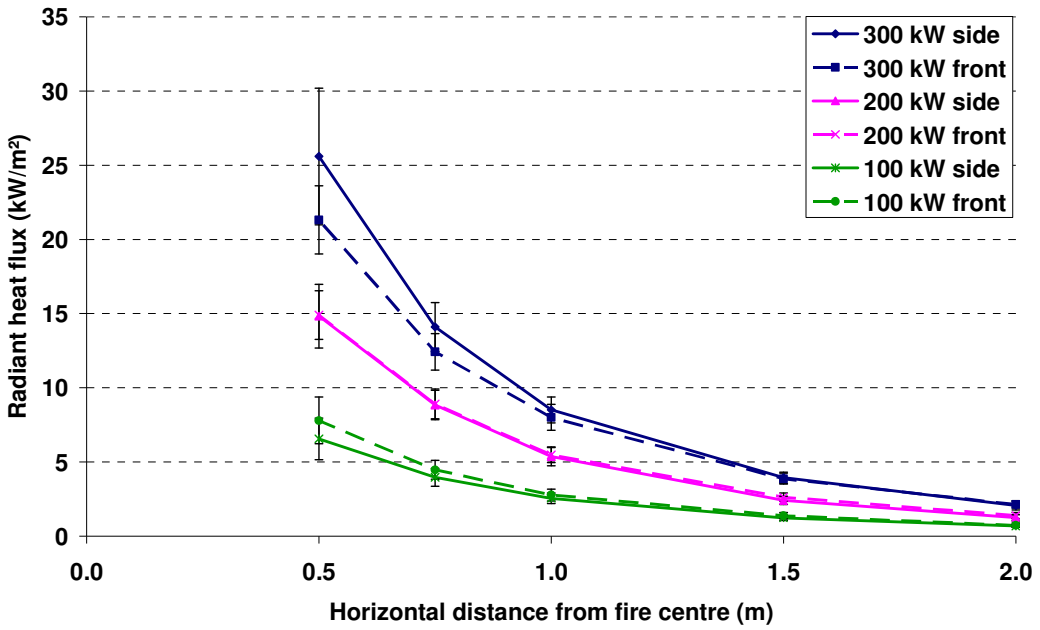

Figure 29: Radiant heat flux vs horizontal distance from fire centre. From Test 9, 3:1 burner, gauge height above flame base = 0.5 m

4.2.4 Variation of heat flux with height above fire

As mentioned previously, heat flux gauges were located at heights of 0.0, 0.5, 1.0 and 1.5 m above the base of the fire. Figure 30 clearly shows that the radiant heat flux to a target located at some horizontal distance from the fire centre (0.5 m in this case) achieves a maximum value at a height somewhere between 0.0 and 1.0 m above the base of the fire. The exact height at which this maximum occurs will depend on the fire geometry and heat release rate; however, for all fires the behaviour exhibited in Figure 30 should be seen. That is, the radiant heat flux at some point above the base of the flame will be greater than what is measured at the base height. The reason for this is also due to configuration factors.

To simplify matters, assume that the fire can be approximated as a cylinder, as in the methods of Shokri and Beyler (1989), Mudan (1984) and Dayan and Tien (1974). When a target is located at ground level, as in Figure 31a, the target receives a much larger measure of radiation from the bottom half of the cylinder than from the top half. This is due to configuration factor theory and is discussed in section 1.4.2. In contrast, for a target located at the mid-height of the cylindrical flame, as in Figure 31b, the target receives equally large measures of radiation from both the top and bottom segments of the

flame. In other words, the target located at the flame mid-height can "see" more of the flame.

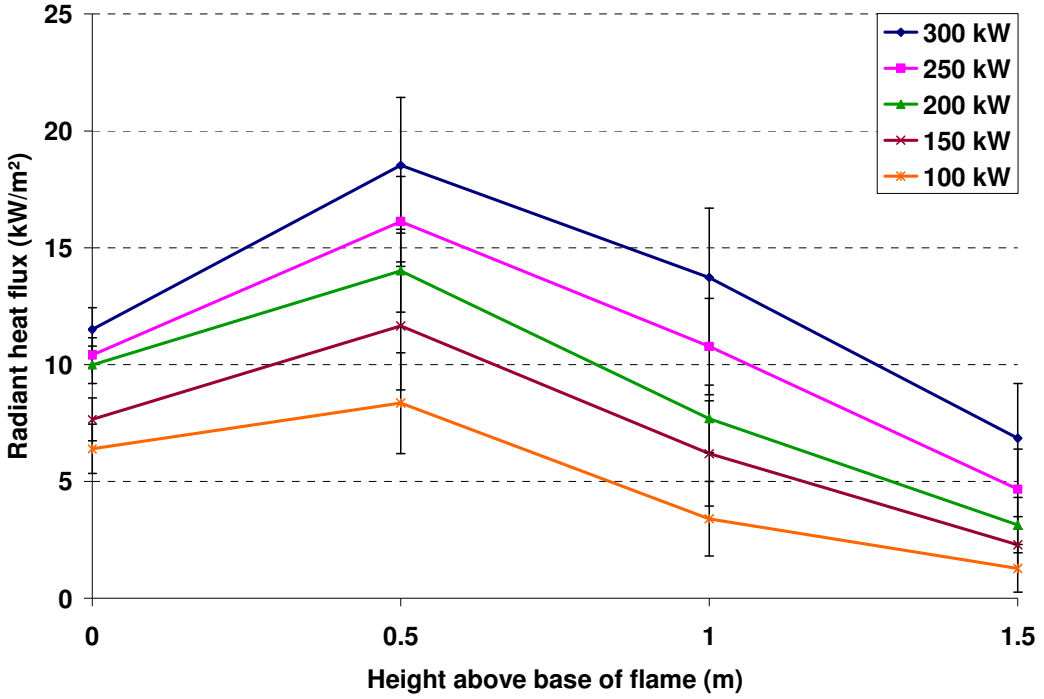

Figure 30: Radiant heat flux vs height above base of flame. From Test 11, 2:1 burner, front gauges, horizontal distance from fire centre = 0.5 m

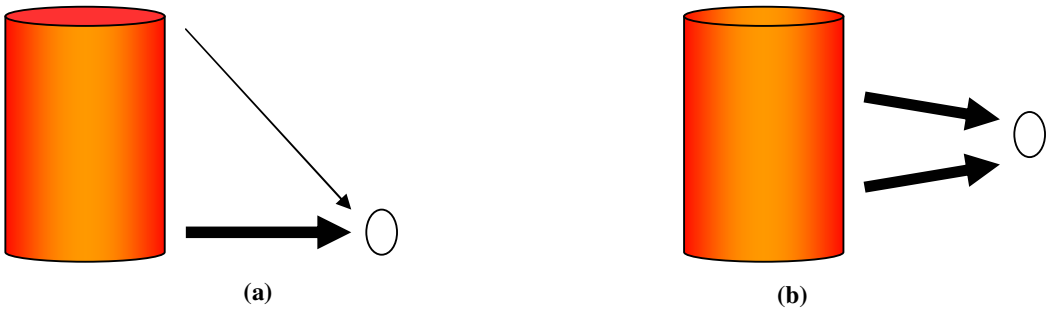

Figure 31: Schematic of radiation from a cylindrical fire to a target located at (a) the base height of the flame and (b) the mid-height of the flame. The thickness of the arrows represent the amount of radiation being received from different areas of the fire (not to scale)

4.2.5 Comparison between burner aspect ratios

For the front heat flux gauges, the three different burner aspect ratios tested provide significantly different flame shapes from which thermal radiation is emitted. More specifically, as the aspect ratio increases the flame base becomes wider whilst the flame

height decreases. This affects the configuration factor between the flame and the heat flux gauges.

Figure 32 shows that for the front gauges, the higher aspect ratios result in greater radiant heat fluxes. This implies that for the burners tested, the width of flame visible to the target has a greater bearing on the radiant heat flux than the flame height. Figure 33 compares the heat flux against heat release rate for all three burners from both the front and side gauges. For the side gauges, there is little difference in heat flux between the different burner aspect ratios. This is because the target is essentially viewing the same flame for each aspect ratio, just with slightly different flame heights. Although the flame height is greatest for the 1:1 aspect ratio, the distance from the gauge to the flame edge is greater, as explained in section 4.2.3. It is therefore somewhat of a trade-off between the flame height and the distance from the burner edge. The front gauges, however, as seen in Figure 33b, show a much greater difference between the three aspect ratios, with the 3:1 burner resulting in the greatest heat flux. This effect is much more evident at higher heat release rates. For the front gauges, the distance to the burner edge is independent of the aspect ratio; therefore the configuration factor is mainly a function of the flame base width. Note that the error bars have been removed from Figure 33 for clarity.

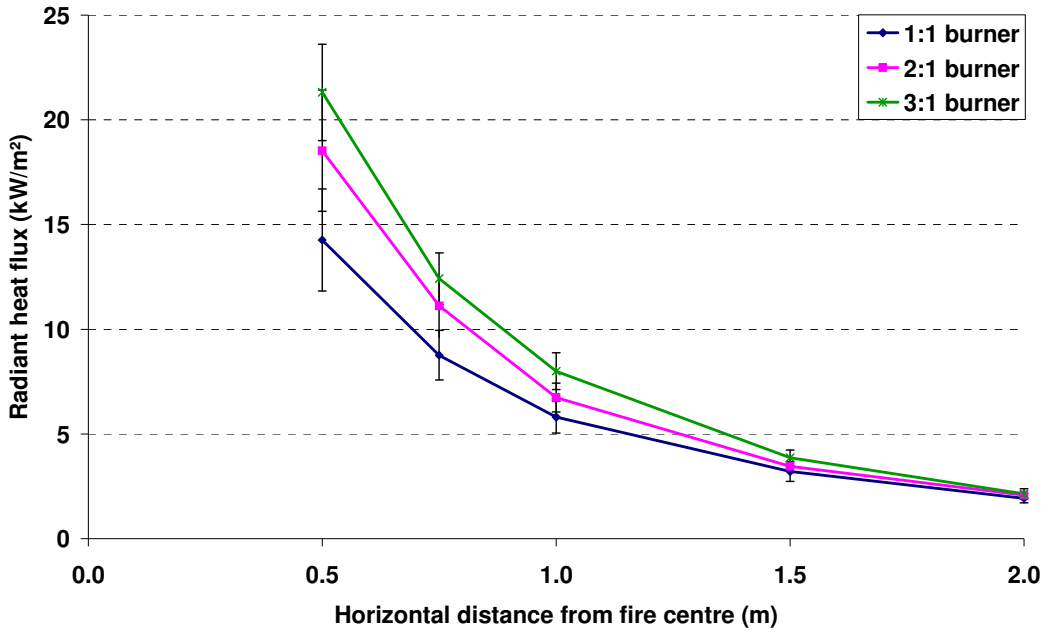

Figure 32: Radiant heat flux vs horizontal distance from fire centre. From Tests 7, 9 and 11. Heat release rate = 300 kW, front gauges, gauge height above flame base = 0.5 m

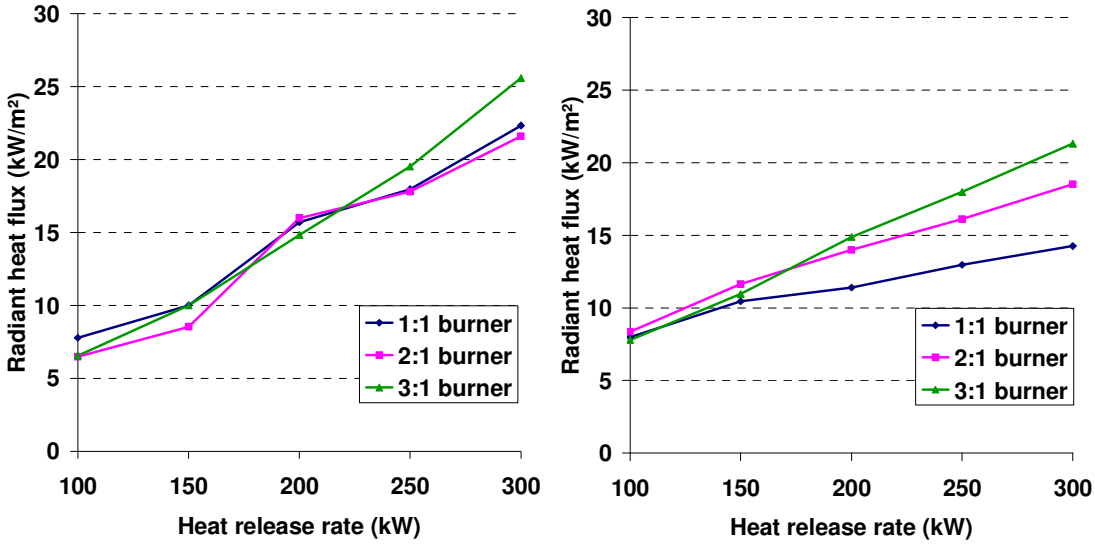

Figure 33: Radiant heat flux vs heat release rate for (a) side gauges and (b) front gauges. From Tests 7, 9 and 11. Horizontal distance from fire centre = 0.5 m, gauge height above flame base = 0.5 m

4.2.6 Variation of heat flux with burner angle

Two different burner angles were tested: firstly, with the burner sides parallel to the heat flux gauges and then at an angle of 45°. As shown by Figure 34, there was very little difference between the heat fluxes measured for the 0° and 45° burners. To better represent all data collected, a log-log scale has been used.

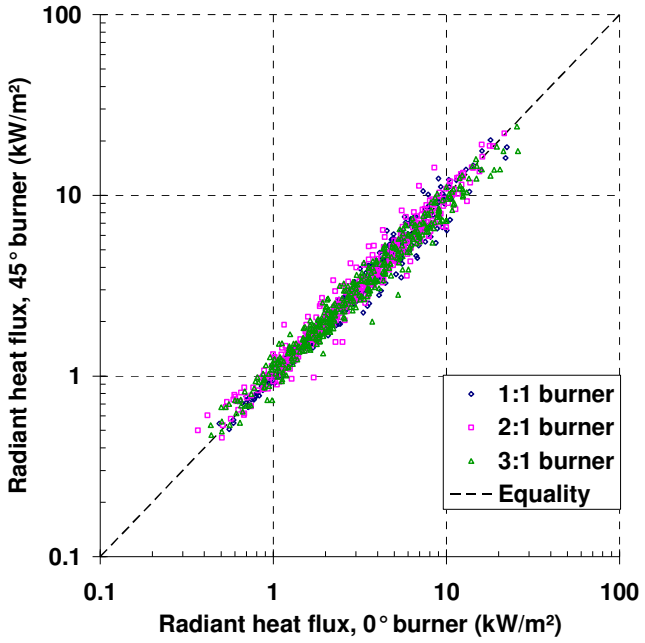

Figure 34: Comparison of radiative heat flux measurements from burners oriented at 0° and 45°. Data is presented from all burner aspect ratios, gauge positions, heat release rates, distances from fire and heights above flame base. From tests 1-12

In Figure 34 it can be seen that most of the data lies very near the equality line. This means that in general the data measured for the 0° burner was very similar to that of the 45° burner. These two data sets have a correlation coefficient of 0.971, indicating a strong relationship between the two arrays. 90 % of the data was found to be between -23 % and +16 % of the equality line.

From the data analysis presented, it can be concluded that there is insignificant difference between the radiant heat flux measured from the different burner angles.

4.2.7 Comparison between central and offset gauges

As described in section 3.4.1, the heat flux gauges could be arranged so that they were in line with the centreline of the gas burner (the central position) or 0.35 m out to one side of the centreline (offset position). Both of these positions were tested under a variety of burner scenarios, as shown in Table 1.

As expected, the gauges positioned centrally to the burner resulted in a higher heat flux than gauges positioned radially outwards from the burner centreline (see Figure 35). This

is exactly the same principle as in section 4.2.4 with regards to configuration factors. The centrally located gauges have a better 'view' of the fire than the offset gauges. Markstein (1976) investigated this in some depth using propane turbulent diffusion flames and concluded that the thermal radiation is at a maximum at approximately the centre of the flame, then tapers off on either side of the centre, forming a Gaussian distribution. As only two lateral gauge positions were tested in this work, the data is unable to be matched to a Gaussian distribution.

Figure 35 compares radiative heat flux measurements between central and offset gauges for both the 1:1 and 3:1 burners. In both cases, it can be seen that the centrally positioned gauges received considerably greater radiant heat flux, especially when located very close to the fire centre. Figure 36 is a summary of all of the data taken from Tests 1-12. In this scatter plot, the data from the centrally positioned gauges (x axis) is plotted against the corresponding data taken for the offset gauges (y axis). For example, one particular data point represents the radiant heat flux measured for both the central and offset gauges for the 2:1 burner, at 150 kW, 1.0 m above the flame base, 1.5 m from the fire centre, for a burner angle of 0°. Figure 36 clearly shows that the majority of data lies below the line of equality. This means that for the majority of data taken, the radiant heat flux to the central gauges were greater than the radiation to the offset gauges under the same conditions. In fact, 82 % of the data lies below the equality line and 90 % of the data lies within +4 % of the line.

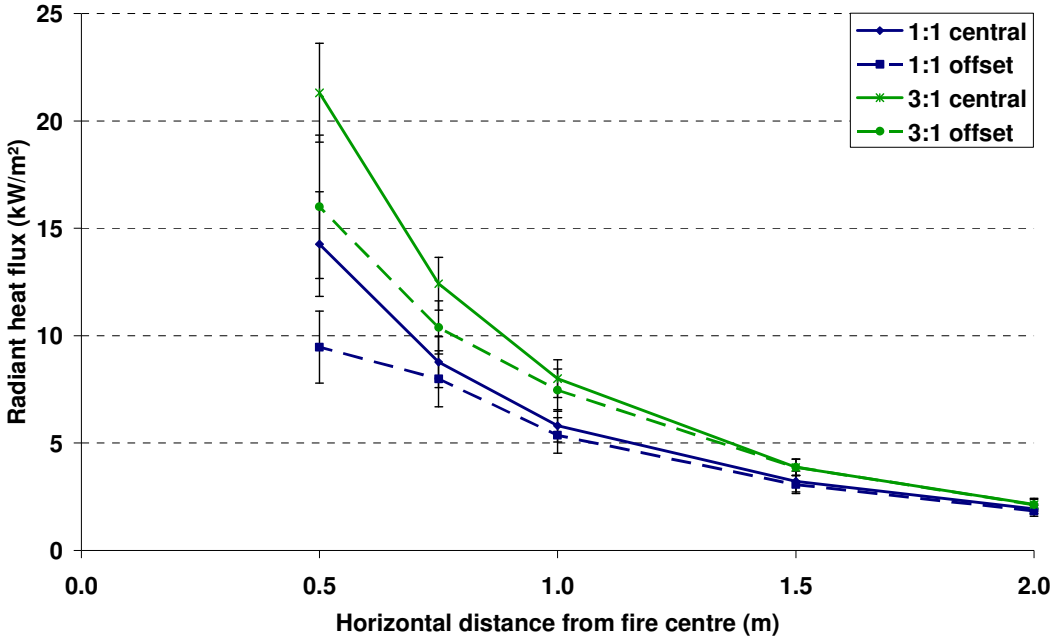

Figure 35: Radiant heat flux vs horizontal distance from fire centre, comparing central and offset gauge positions. From Tests 3, 5, 7 and 9. Heat release rate = 300 kW, front gauges, gauge height above flame base = 0.5 m

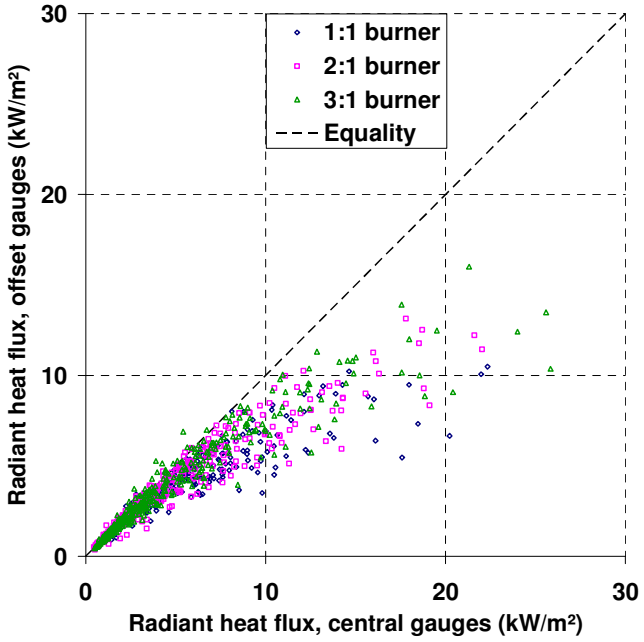

Figure 36: Comparison of radiative heat flux measurements from central and offset gauges. Data is presented from all burner aspect ratios, burner angles, heat release rates, distances from fire and heights above flame base. From tests 1-12

4.2.8 Comparison between vertical and horizontal gauges

Three tests were performed with gauges located in the horizontal position. All three burners were tested; all in the 0° position. Figure 37 shows that horizontally oriented gauges receive considerably less radiant heat flux than vertically oriented gauges in the same position. This occurs at any distance from the fire and at any height.

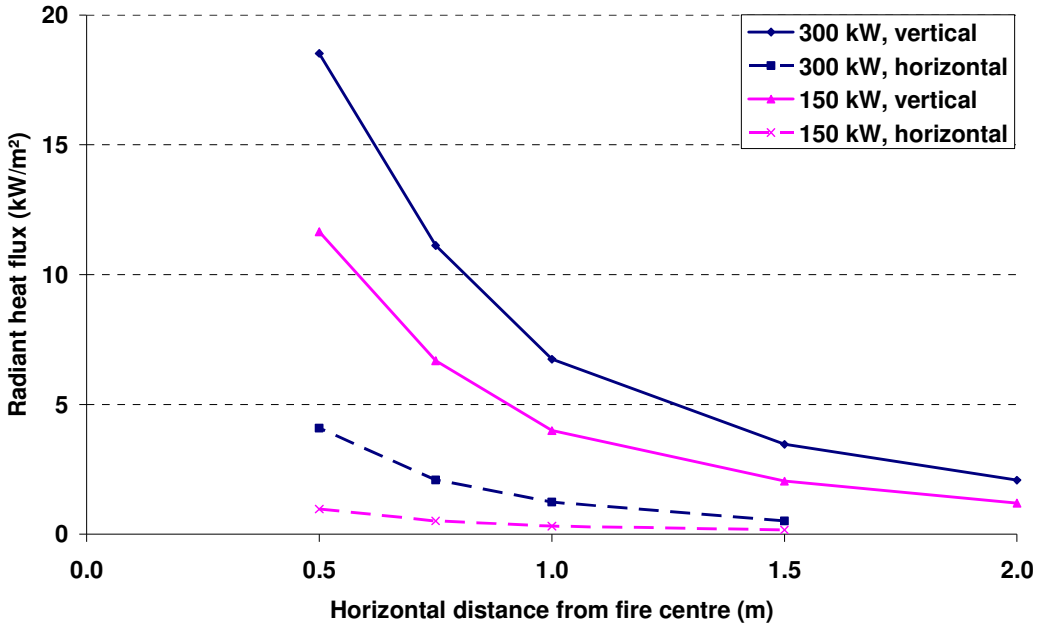

Figure 37: Radiant heat flux vs horizontal distance from fire centre. From Tests 11 and 16, 2:1 burner, front gauges, gauge height above flame base = 0.5 m

Figure 38 shows how the radiant heat flux varies with height above the flame base at different heat release rates for horizontal gauges. Compare the shape of this graph with Figure 30, which is the equivalent plot for vertically oriented gauges. When the gauges are vertical, the radiant heat flux passes through a maximum somewhere between 0.0 and 1.0 m; whereas for the horizontal gauges, the maximum heat flux is experienced at ground level. This is because the horizontal gauges only receive thermal energy from that part of the flame located above the height of the gauge. At a particular distance away from the fire, the more surface area of flame that can be viewed by the gauge, the higher the heat flux to that gauge. Therefore, the gauge located at the base height of the flame receives the highest heat flux for horizontal gauges.

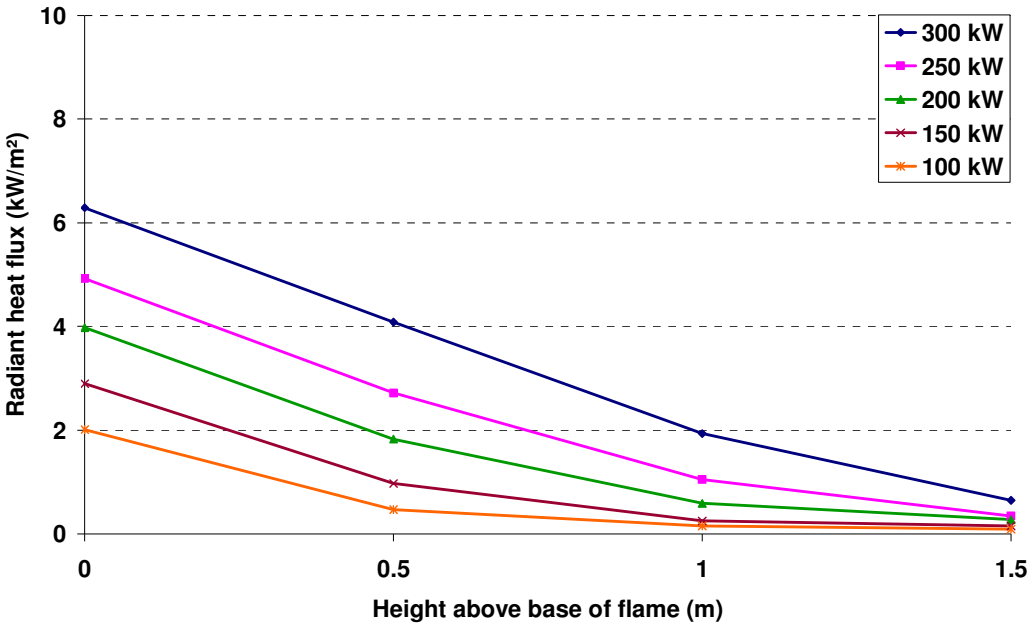

Figure 38: Radiant heat flux vs height above base of flame. From Test 16, 2:1 burner, front gauges, horizontal distance from fire centre = 0.5 m

When the variation in heat flux with burner aspect ratio was reviewed in section 4.2.5, it was found that for vertically oriented gauges at the front of the fire, the heat flux was higher for the higher aspect ratios. For horizontal gauges, however, the opposite is true; that is, lower aspect ratios actually result in higher heat fluxes. This can be seen in Figure 39. Where the base width of the fire was found to dominate the configuration factor for the vertical targets, the flame height appears to dominate for horizontal targets. As the horizontal targets are perpendicular to the plane of the fire, the flame width has less effect than the height of the flame. The 1:1 burner had the greatest flame heights therefore this burner resulted in higher heat fluxes than the non-square burners.

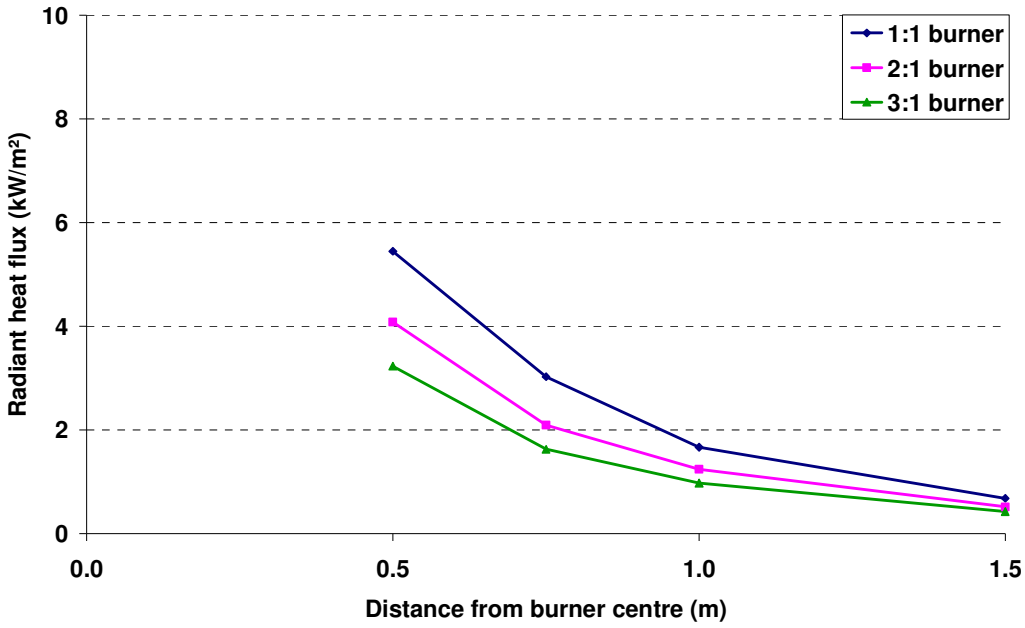

Figure 39: Radiant heat flux vs horizontal distance from fire centre. From Tests 14-16. Heat release rate = 300 kW, front gauges, gauge height above flame base = 0.5 m

4.2.9 Repeatability of results

To test the repeatability of the experimental results, one of the tests was replicated. The test replicated was test 9 and the repeat test (test 13) was performed on a different day from the original. As expected, the two tests provided very similar results, as shown in Figure 40. The correlation coefficient between the two data sets is 0.990 and the percentage of data points that lie below and above the equality line is 50.5 % and 49.5 %, respectively.

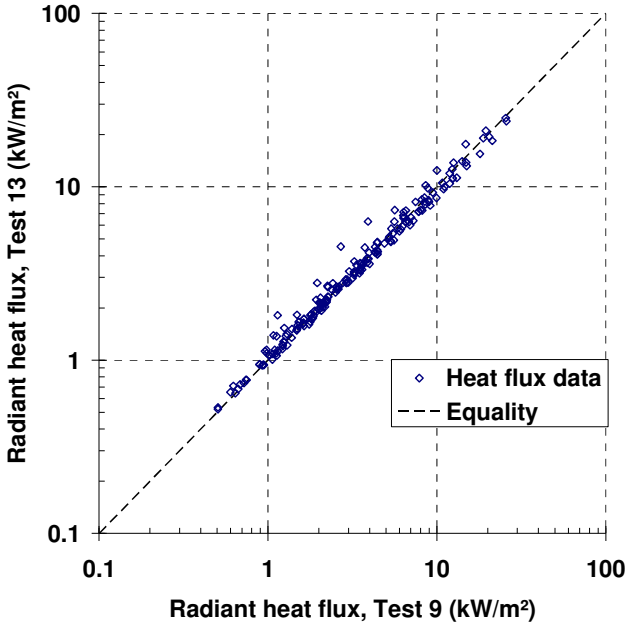

Figure 40: Comparison of radiative heat flux measurements from Tests 9 and 13 (replicate tests)

The fact that the results from the repeat test compare very well with the original give confidence in the experimental data. Ideally, one would like to repeat all of the tests; however, this was not a realistic alternative. One cannot say for certain that all of the data recorded would be matched by repeat tests, but it must be assumed that the data is representative of what would be measured if the experiments were repeated many times. Minor variations will always occur due to a range of factors such as the dynamic behaviour of the fire and differing ambient conditions. Averaging the data over time attempts to smooth out some of these variations.

4.3 Flame Height

Using the method outlined in section 3.7.1, the mean flame heights were determined for each heat release rate setting of the three different burners. The results are displayed in Figure 41, where the values shown correspond to the 0.5 intensity level. These are the values that are fed into the theoretical radiation models. The contour plots from which the flame heights were determined are provided in Appendix B.

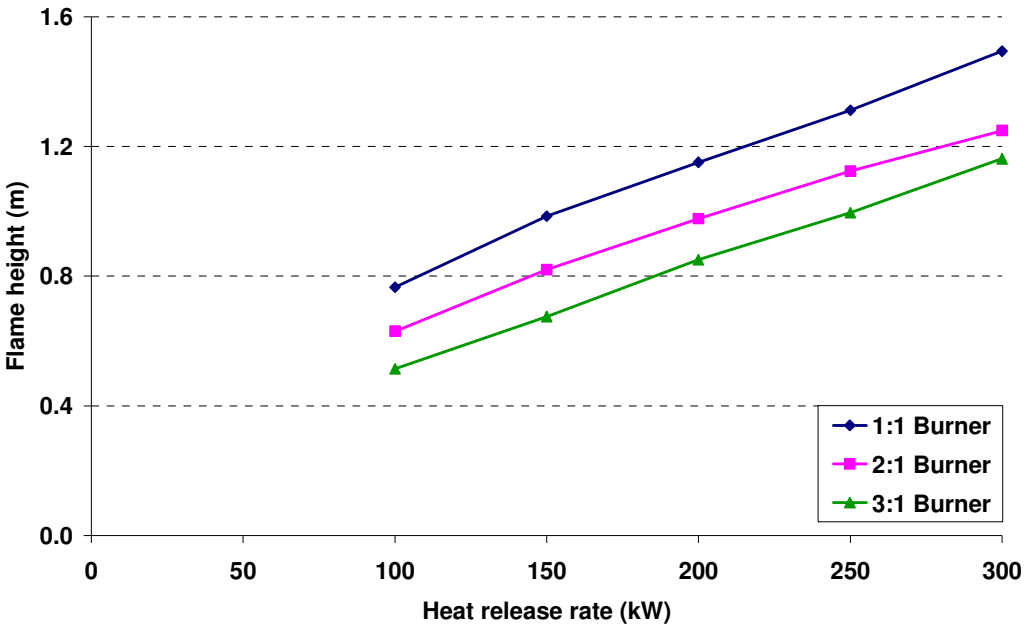

Figure 41: Mean flame heights vs heat release rate for all three burner aspect ratios, generated by *ImageStream*

As well as the mean flame heights shown in Figure 41 above, the contour plots were used to find out the height at which flames existed at a range of probabilities. Figure 42 summarises all of the flame height data collected, from each heat release rate setting of each burner. The flame heights are presented as normalised values; meaning that flame heights for all probabilities are divided by the mean flame height (0.5 intensity value) for that particular burner and heat release rate. This is so that the results from different burner aspect ratios and heat release rates can be easily compared. By normalising the flame height, the 0.5 flame intermittency corresponds to a normalised flame height value of 1.0. It can be seen that this plot takes the same shape as the general curve defining the mean flame height presented in Figure 20.

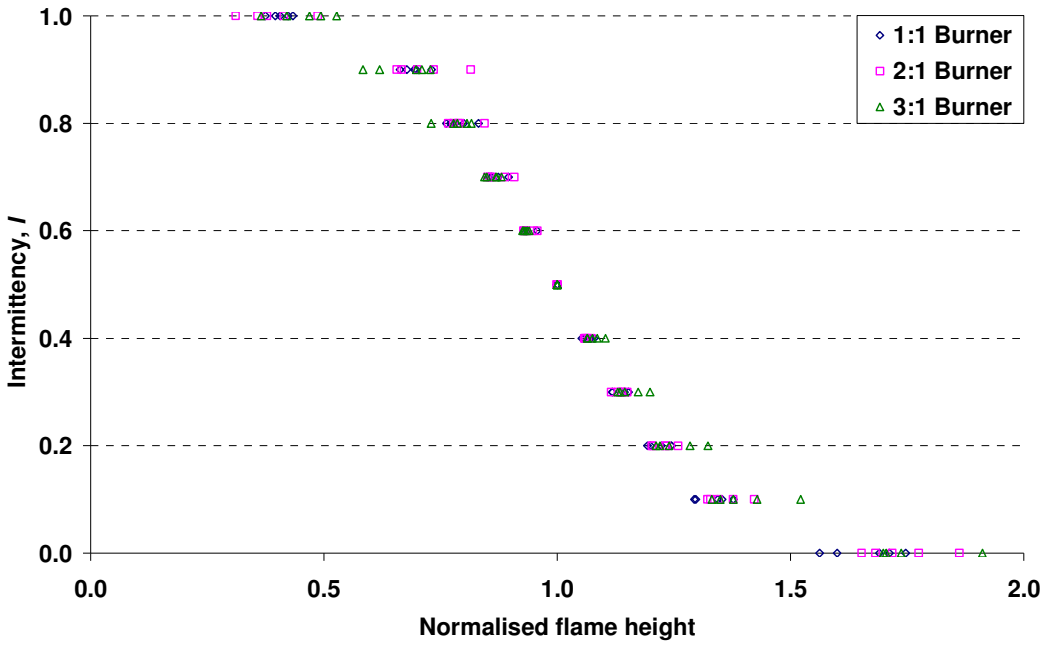

Figure 42: Flame intermittency vs normalised flame height for all burner aspect ratios and heat release rates tested, generated by *ImageStream*

4.3.1 Comparison with correlations

The flame height values determined from the video image analysis were found to be considerably lower than predictions given by the Heskestad correlation (Equation 6) for the same scenario. In fact, Heskestad's correlation predicted mean flame heights up to 66 % greater than those obtained from the computational analysis. The results predicted by Thomas' flame height correlation (Equation 17) also over-predict the flame heights determined by *ImageStream*. For the 2:1 aspect ratio burner, Figure 43 compares the mean flame heights at different heat release rate settings using the three different determination methods. The Thomas correlation, used in the Mudan method only, is seen to provide approximations of flame height that are closer to the results obtained from *ImageStream* than the predictions from the Heskestad correlation. The trends shown for the 1:1 and 3:1 burner aspect ratios are very similar to those presented in Figure 43. On average, Thomas' correlation yielded predictions that were 17 % greater than the *ImageStream* results, whereas Heskestad's correlation was 46 % greater on average. This is of little concern because the manual technique for validating the flame heights explained in section 3.7.1 returned close matches to the computational values.

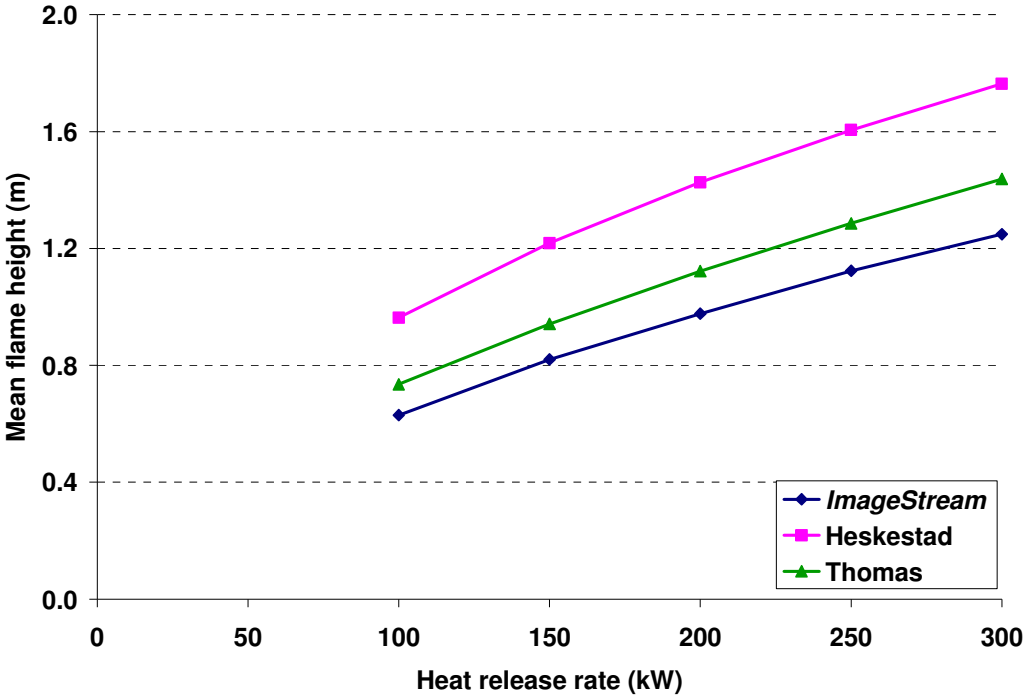

Figure 43: Mean flame height vs heat release rate for the 2:1 burner as determined using *ImageStream*, the Heskestad correlation and the Thomas correlation

Differences between experimental measurements of flame height and published correlations do not appear to be unique to this research. For example, Cox and Chitty (1985) conducted experiments using square burners and found that their measured flame heights were less than previous measurements by Zukoski, Kubota and Cetegen (1981) and the Heskestad correlation given in Equation 6. Cox and Chitty (1985) write that "The reason for the differences are not clear except that the current work has been conducted with square burners while Zukoski's experiments were on circular burners. Square burners do appear to produce shorter flames than circular ones perhaps because of the extra mixing induced at corners." This perhaps highlights a limitation to the Heskestad correlation; the conformation of which will not be investigated in this work.

4.3.2 Buoyancy driven flame validation

Much research has gone into relating the flame height to the heat release rate and fire source diameter (Karlsson & Quintiere, 2000). Experimenters commonly express the data in terms of the non-dimensional heat release rate, $\dot{Q}^*$, also referred to as the Froude

number within the field of fire engineering. Equation 37 provides the definition of the non-dimensional heat release rate:

$$\dot{Q}^* = \frac{\dot{Q}}{\rho_a c_p T_a \sqrt{gD} D^2} \tag{37}$$

Where c_p is the specific heat capacity of air at constant pressure.

Figure 44 compares the mean flame height normalised by the source diameter with the non-dimensional heat release rate. Note that the vertical axis on this figure denotes the mean flame height as *L*, whereas in this work the mean flame height has the symbol *H*. Both have the same definition, however. The horizontal axis is presented as $\dot{Q}^{*2/5}$ in order to compress the scale and match the non-dimensional nature of the vertical axis. The plot includes data taken from a wide range of researchers, with each letter and corresponding line on the plot originating from a different researcher. Plotted as solid symbols are the experimental data collected as part of this research. The plot represents a wide range of fire scenarios. On the far left are data from pool fires, where the mean flame height is of the same order of magnitude as the source diameter, *D*. Here, and in the intermediate section, the flame is said to be buoyancy-dominated (Karlsson & Quintiere, 2000). The far right of the plot represents the high-momentum jet flame regime, where the flame is momentum-driven. As all of the experimental data collected as part of this research falls within the bottom end of the intermediate section, one can have confidence that all of the fires tested were indeed buoyancy-dominated. This is of importance as momentum-driven flames have different radiative properties and therefore need to be treated differently within the models.

Figure 45 shows an expansion of Figure 44 in the region of the experimental data collected in this research. More detail is given about how the different burner aspect ratios performed. It can be seen that the lower aspect ratios tend towards the upper right section of the graph, indicating taller and thinner flames. For each burner geometry, the higher plot points result from higher heat release rates.

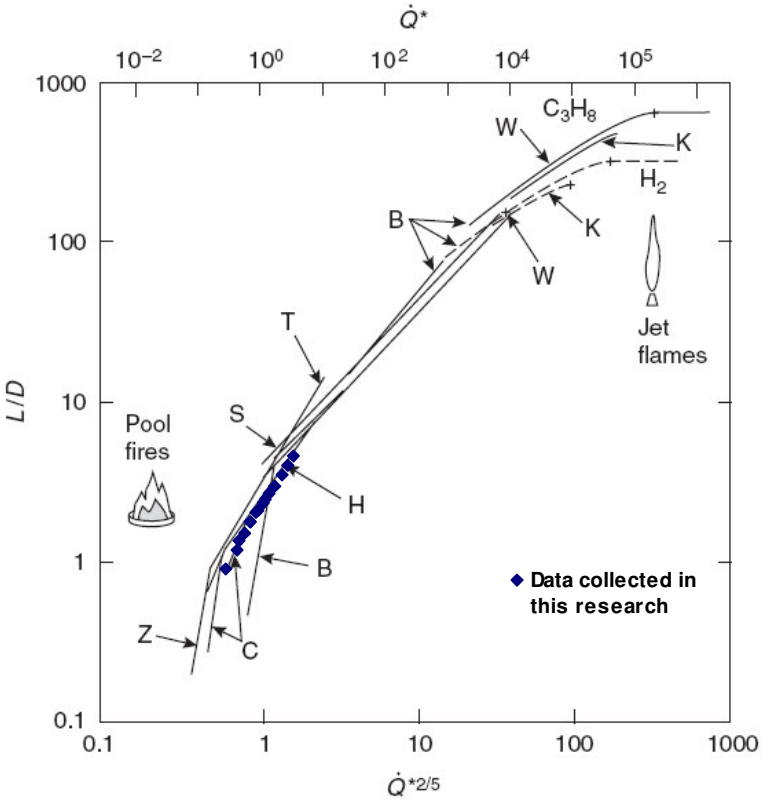

Figure 44: Mean flame height normalised by source diameter vs non-dimensional heat release rate for large number of independent experiments (adapted from Heskestad (2002)). Solid symbols represent experimental data collected as part of this research

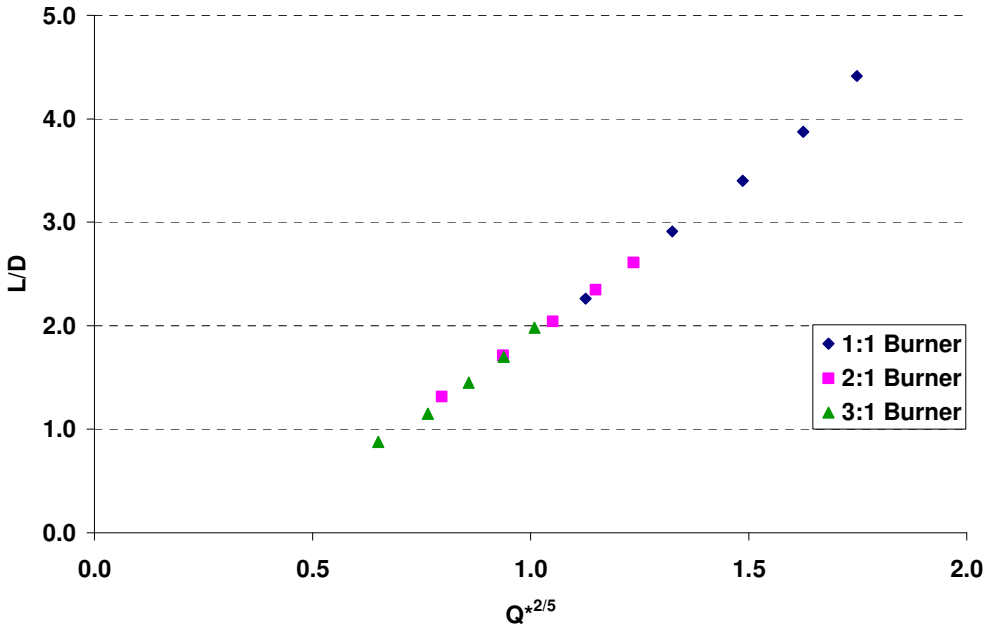

Figure 45: Mean flame height normalised by source diameter vs non-dimensional heat release rate for different burner aspect ratios

Chapter 5

THEORETICAL MODEL ANALYSIS

To evaluate the performance of the different radiation models (section 2.3), the experimental results were compared with predictions made by the models using the experimental parameters as inputs. To make these comparisons, a spreadsheet tool was created. This spreadsheet calculated the radiant heat flux to targets located at positions surrounding the fire, using all of the theoretical methods. Inputs required to be entered by the user included the burner aspect ratio, burner angle, flame height (from experiments), target orientation (vertical or horizontal) and target location. Averaged heat flux measurements from the experiments (section 4.2) were imported into the spreadsheet tool so that comparisons with the theoretical results could be made.

5.1 Variables and Constants used in Radiation Models

Section 2.4 presented a review of the literature on appropriate values to use for propane fuel for the effective absorption coefficient, flame temperature, radiative fraction and heat of combustion. The actual values that were used in the theoretical radiation models to produce the results shown in sections 5.2 – 5.5 are as follows:

- Radiative fraction, χ_r = 0.32
- Effective absorption coefficient, κ = 0.85 m^{-1}
- Flame temperature, T_f = 900 °C (1173 K)
- Heat of combustion, ΔH_c = 46.45 kJ/g

To calculate the effective emissive power of the flame using the Mudan method, three constants are required. Their values, as given by Beyler (1999), are as follows:

- Equivalent black body emissive power, E_{max} = 140 kW/m^2
- Extinction coefficient, s = 0.12 m^{-1}
- Emissive power of smoke, E_s = 20 kW/m^2

5.2 Overview of Model Results

Before reviewing each individual model, it is useful to compare all models in order to get a feel for the relative difference between them. Figure 46 gives such a comparison. Depicted is the change in radiant heat flux with distance away from the burner centre for the 2:1 burner at 300 kW. The target height is 0.5 m above the fire base, centrally located and vertically oriented.

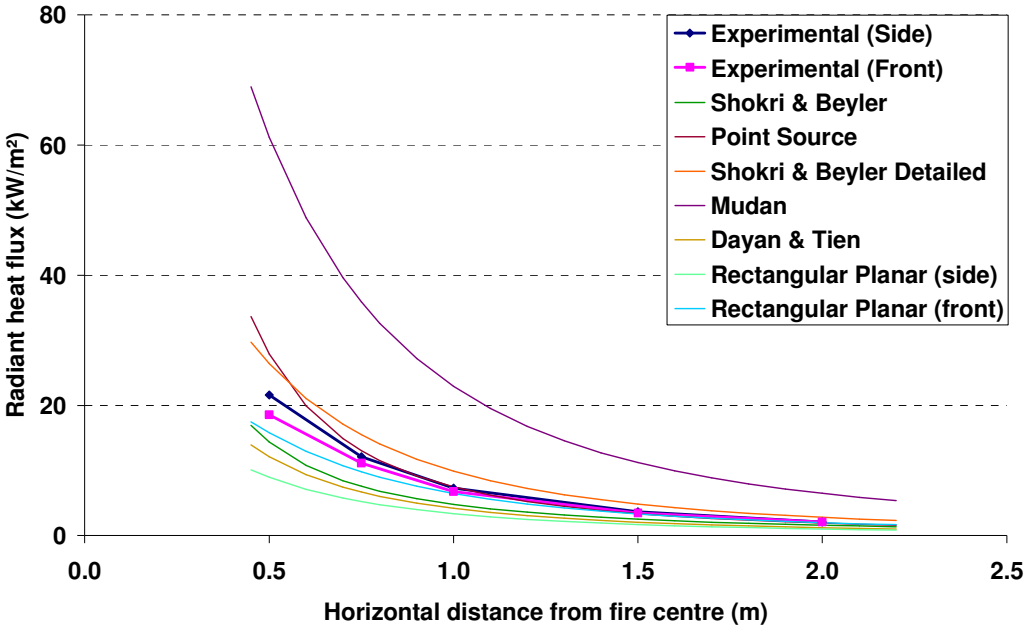

Figure 46: Radiant heat flux vs horizontal distance from fire centre. Comparison of experimental results with all models. From Test 11, 2:1 burner, 300 kW, gauge height above flame base = 0.5 m

The first noticeable feature in Figure 46 is that there is a fairly significant range of results as predicted by the thermal radiation models. The exact detail of which methods best match the experimental results will be discussed in more detail in the following sections. However, this plot does highlight one important aspect: that the models all vary in their predictions, based on the different assumptions made, and methods used, in their calculations.

Figure 47 and Figure 48 show how the different methods vary with height above the flame base and with heat release rate, respectively. From the three graphs shown in this section, certain trends are evident. For example, the Mudan method seems to predict considerably higher heat fluxes than any other method, whilst there are several models which

consistently under-predict the heat flux. These plots act as a good reference point for the relative closeness of fit between the theoretical models and the experimental data.

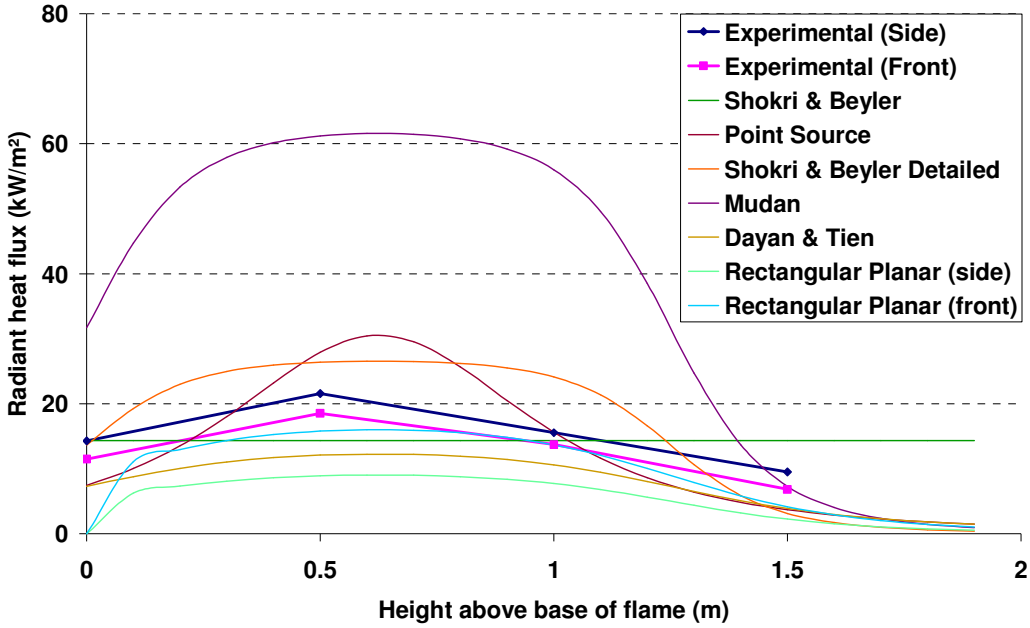

Figure 47: Radiant heat flux vs height above flame base. Comparison of experimental results with all models. From Test 11, 2:1 burner, 300 kW, gauge distance from fire centre = 0.5 m

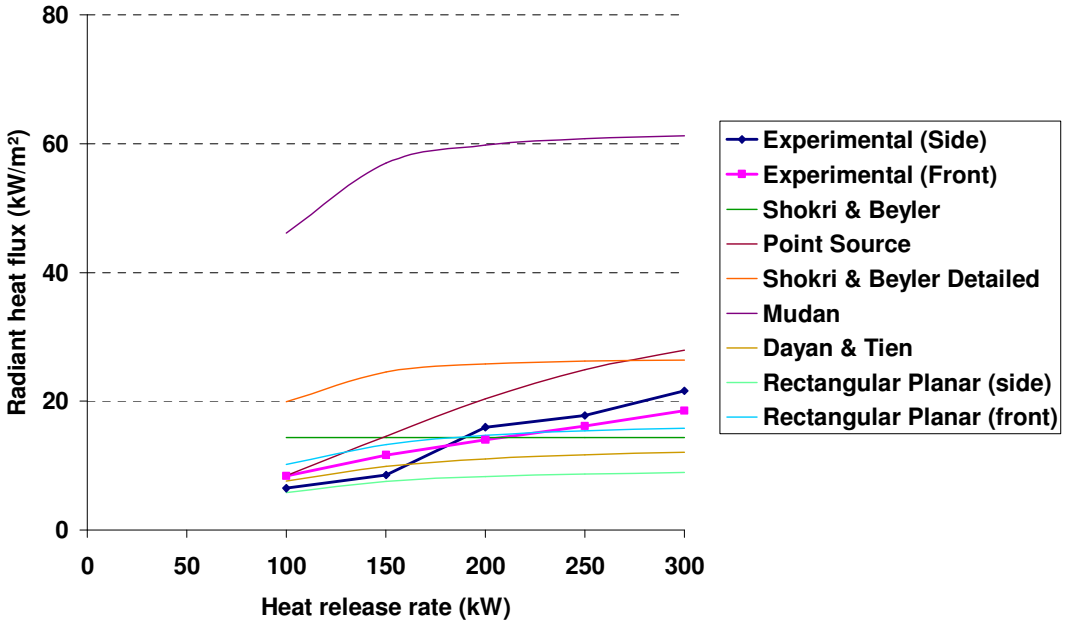

Figure 48: Radiant heat flux vs heat release rate of fire. Comparison of experimental results with all models. From Test 11, 2:1 burner, gauge distance from fire centre = 0.5 m, gauge height above flame base = 0.5 m

Rather than reviewing each individual model separately, the theoretical models will be grouped into three distinct categories: basic, cylindrical and planar models. The results from these categories are presented in sections 5.3 – 5.5.

5.3 Basic Models

The comparisons between the experimental and theoretical data begin with the two simplest models: the Shokri and Beyler correlation and the point source model. As both of these models are designed to be a quick and easy way of predicting the radiant heat flux from a fire to a target, one may expect a fairly rough approximation. After all, one of these models is purely a correlation of experimental data and the other is a very crude approximation of an energy source. Despite these matters, both of these models provided a reasonably good match to the experimental data, as shown in Figure 49 for one particular scenario. The predictions made by the point source model in particular were especially good, which was somewhat of a surprise, given the relative simplicity of the model compared with the cylindrical models. Figure 49 shows that the point source model provides better predictions when further away from the fire centre. At a distance of 0.5 m from the fire centre, the model over-predicts the radiant heat flux by 30-50 % for the side and front gauges, for the scenario depicted in Figure 49. Although experimental results are given for both the side and front gauges, the two theoretical models have only one prediction each. This is because neither model assumes any shape for the fire. The Shokri and Beyler correlation only requires the fire diameter and the distance between the target and the fire centre, whilst the point source model assumes isotropic energy release from the point source.

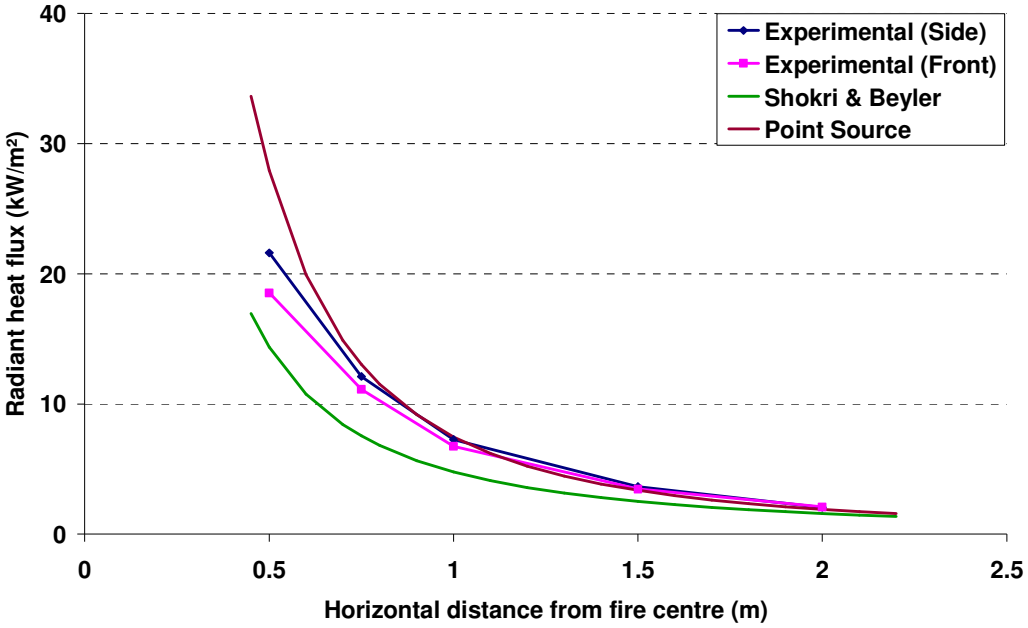

Figure 49: Radiant heat flux vs horizontal distance from fire centre. Comparison of experimental results with basic models. From Test 11, 2:1 burner, 300 kW, gauge height above flame base = 0.5 m

Figure 50 shows how well the two basic models predict the radiant heat flux with varying height above the flame base, again from Test 11. Two different heat release rate settings are given, 300 kW and 100 kW, in Figure 50a and Figure 50b, respectively. Clearly, the point source model does a much better job at predicting the behaviour of how the radiant heat flux varies with height; that is, the heat flux passes through a maximum somewhere near 0.5 m above the base of the flame. In contrast, the Shokri and Beyler correlation is not able to predict how the heat flux varies with height, nor does it change for different heat release rates. This highlights the rudimentary nature of this model.

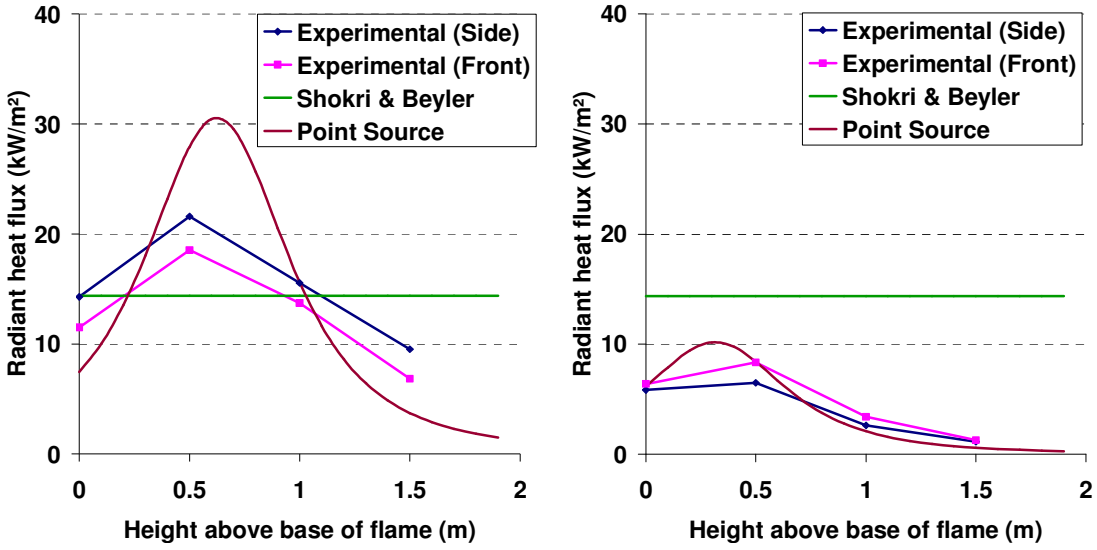

Figure 50: Radiant heat flux vs height above flame base. Comparison of experimental results with basic models. From Test 11, 2:1 burner, distance from fire centre = 0.5 m, at heat release rate of (a) 300 kW and (b) 100 kW

Although it is useful to review specific examples to visualise the trends, it also pays to cluster a large amount of data together. This can provide a much better view of how well the theoretical models perform over a variety of circumstances. In Figure 51, all of the experimental data collected in Tests 7, 9 and 11 is compared with the predicted heat fluxes using (a) the Shokri and Beyler correlation and (b) the point source model. Tests 7, 9 and 11 were chosen as these were seen as the 'base case' for each burner aspect ratio. The conditions for these tests were vertical gauges in the central position, with a burner angle of 0°. To better represent all data collected on a single graph, a log-log scale has been used.

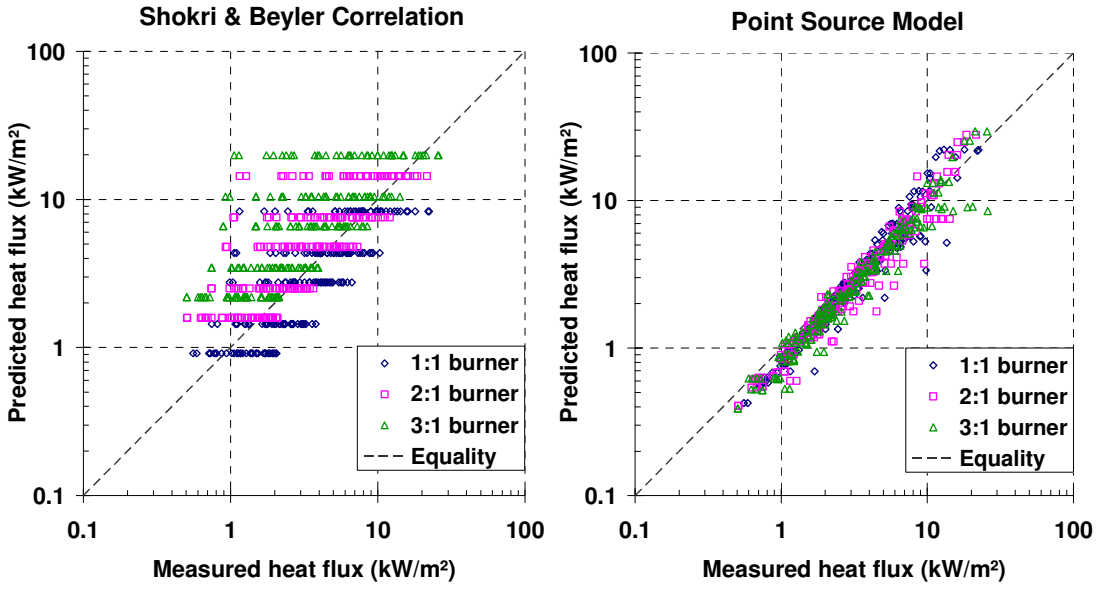

Figure 51: Comparison of measured and predicted radiative heat flux using (a) Shokri & Beyler correlation and (b) point source model. Data taken from Tests 7, 9 and 11

Figure 51a highlights the limitations of the Shokri and Beyler correlation in predicting the radiant heat flux. Clearly, there is significant spread of data from the equality line. It can be seen that there are five distinct lines of data for each burner aspect ratio. These correspond to the five target distances from the fire centre. At each distance, the predicted radiant heat flux is the same, regardless of height. The experimental results do vary with height, as shown in section 4.2.4, thus creating a line of data at each distance setting. The correlation does correctly predict an increase in the radiant heat flux with increasing burner aspect ratio, as a result of one of the model inputs being the effective fire diameter. From the distribution of data on the plot, it appears that with increasing experimental heat flux, the model over-predicts the heat flux more.

The predictions made by the point source model, summarised in Figure 51b, are not only considerably better than the Shokri and Beyler correlation, but they are on average closer to the experimental data than any other model tested in this research. The fact that most data points are clustered around the equality line, at both the high and low ends of the measured heat flux spectrum, is rather surprising, especially given the relative crudeness of the model compared with the more complex cylindrical methods. 90 % of the data presented in Figure 51b is within -40 % and +24 % of the equality line.

As discussed in section 2.3.2, the point source model has been recommended only for heat fluxes at the target less than 5 kW/m² (Beyler, 2002). From Figure 51b, the model seems to give good approximations of the radiant heat flux over the entire range of heat fluxes recorded. However, upon closer inspection of the data, there is in fact an increase in the percentage error with increasing heat flux, as shown by Table 4. This table provides the average absolute percentage errors for the point source model in different heat flux brackets. Note that in this and the following sections, the term 'percentage error' indicates how close the theoretical predictions are from the experimental data. An absolute value is used so that positive and negative values do not have any 'cancelling out' effect. The data used to calculate the average percentage errors presented in Table 4 is all of the data presented in Figure 51b. This takes into account the percentage errors from both the front and side gauges.

Table 4: Summary of percentage errors for point source model. Data from Tests 7, 9 and 11

	$\dot{q}'' < 5$ kW/m²	$5 \leq \dot{q}'' < 10$ kW/m²	$\dot{q}'' \geq 10$ kW/m²
Average absolute % error	17%	17%	31%

From the above table, it can be seen that the predictions made by the point source model are equally good for heat fluxes between 5 and 10 kW/m² as they are for values less than 5 kW/m². Above 10 kW/m² though, the model does not predict the radiant heat flux as accurately. This suggests that for this particular application, the 5 kW/m² limit on the point source model advised by Beyler (2002) could possibly be extended to 10 kW/m². However, this should be validated with a broader range of fire scenarios, such as with liquid hydrocarbon pool fires of varying pool diameter.

Looking again at Figure 51a, the Shokri and Beyler correlation performs better for fires with an aspect ratio nearer to unity. As the aspect ratio increases, the model tends to over-predict the radiant heat flux. The point source model, on the other hand, is much less affected by changes in the aspect ratio (see Figure 51b). This is better illustrated by Table 5, which gives the average absolute percentage errors for the three different burner aspect ratios tested. All data from Tests 1-13 is used in the calculation of the percentages, representing all of the experiments performed with vertically oriented gauges. Clearly, the percentage error increases dramatically with increasing fire aspect ratio for the Shokri and Beyler correlation, however remains essentially constant for the point source model.

Table 5: Summary of percentage errors for basic models. Breakdown of fire aspect ratios. Data from Tests 1-13

	Shokri & Beyler correlation	Point source model
1:1 burner	46%	19%
2:1 burner	90%	18%
3:1 burner	159%	19%

The performance of the theoretical models with horizontal targets was also investigated. As discussed in section 2.3.1, the Shokri and Beyler correlation is not able to predict the radiant heat flux to horizontal targets. The point source model, on the other hand, can deal with horizontal targets by means of the angle θ in Equation 5. A comparison between the experimental results and predictions made by the point source model for the 2:1 burner at 300 kW is given in Figure 52. For this situation, the point source model matches the experimental results from the side gauges very well. In a more general sense, Figure 53 shows that over the range of heat flux data collected, this model has overall good agreement with the experimental data. See Appendix C to compare the scatter plots of all radiation models for horizontal targets.

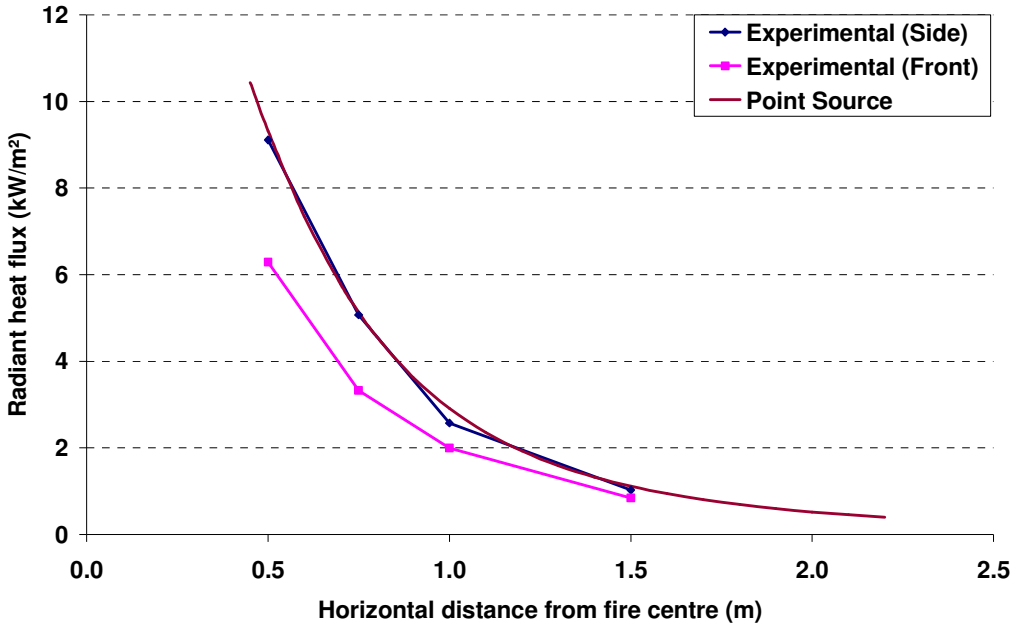

Figure 52: Radiant heat flux vs horizontal distance from fire centre for horizontal targets. From Test 16, 2:1 burner, 300 kW, gauge height above flame base = 0.0 m

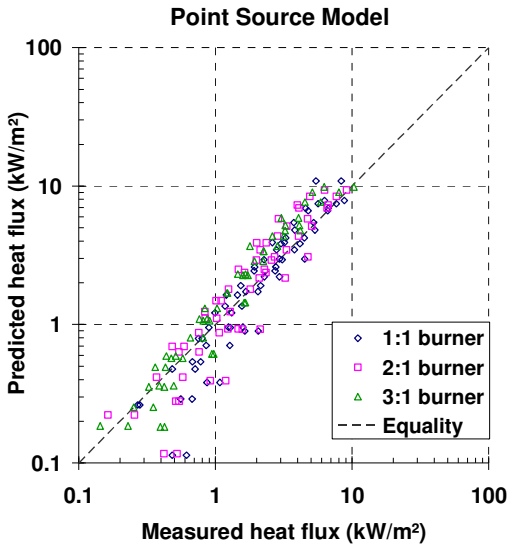

Figure 53: Comparison of measured and predicted radiative heat flux to horizontal targets using point source model. Data taken from Tests 14-16

When all data from Tests 14-16 is reviewed, the point source model yields an average absolute percentage error of 76 % for horizontal targets. This seems relatively high, especially compared with the result shown in Figure 52. This is explained by going back and reviewing some of the initial assumptions made for the point source model. Firstly, as the name suggests, all radiation is emitted from a single point source. This point source is located at the centre of the fire, at a height of half the mean flame height. Furthermore, in this research it is assumed that horizontal targets are facing upwards only. This means that if a horizontal target is located above the point source, it will not receive any radiant energy. This is depicted in Figure 54. When this occurs, the percentage error from the experimental results is 100 %, hence increasing the average considerably.

The problem with this comes from the fact that the mean flame height determines the point source location. When experimentally measuring the radiant heat flux, 50 % of the time the flame is actually taller than the mean flame height. This means that heat flux gauges located higher up do still receive some thermal radiation, due to the fluctuating flame. These fluctuations are lost when the mean flame height is used, hence horizontal targets located above the point source height cannot receive any radiation. The model can easily be modified to predict the radiation heat flux to a downwards-facing target, such as a ceiling; however, allowing targets to receive radiation from below and above is fairly unrealistic in a practical sense. One could argue that a table might be able to receive

radiation on both its top and bottom surfaces, but in this case, the legs and side edges of the table would provide vertical surfaces, to which the radiant heat flux would be greater anyway.

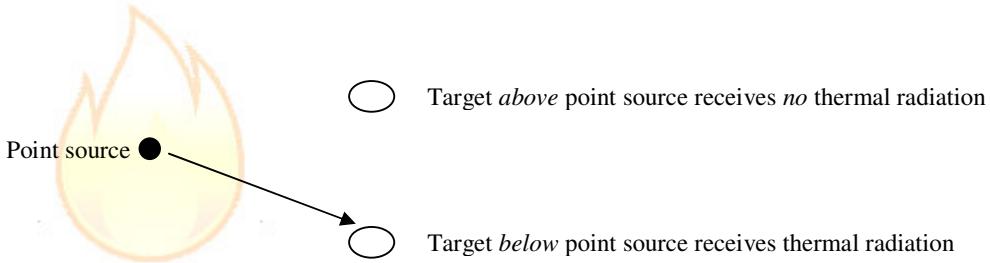

Figure 54: Schematic of thermal radiation from point source to horizontal targets

In summary, these two basic models provided a very straightforward radiant heat flux calculation that yielded results that were closer to the experimental data than expected; especially in the case of the point source model. When each individual experimental data point is compared with the theoretical prediction under the same conditions, the Shokri and Beyler correlation had an average absolute percentage error of 103 % from the experimental results. Remember here that this model was not able to predict the radiant heat flux to horizontal targets; therefore, this figure includes results from Tests 1-13 only. The point source model proved to be a far more accurate model, averaging 29 % error from the experimental results. If the results to the horizontal targets are excluded the average error is just 18 %.

The relatively poor performance of the Shokri and Beyler correlation in comparison to the point source model is likely due to a number of factors. Firstly, the former model is simply a correlation based on large-scale pool fire experiments, where the pool diameter ranged from 1 to 50 m. However, the largest effective fire diameter used in the experiments in this research was only 0.59 m. One could question the validity of the correlation for fires with an effective diameter less than 1 m. Secondly, all of the data on which the correlation was based came from circular pool fires. The burners constructed for this thesis were either square or rectangular in shape. Theoretically, the square 1:1 burner should approximate the circular pool fire the best and this showed in the results (see Table 5). Furthermore, the correlation is designed only to be used for targets at the same level as the flame base. This resulted in fairly substantial over-predictions for

targets located 1.5 m above the base of the fire, where the radiant heat flux tended to be low. In fact, the average percentage error from the experimental results at the height of the base of the flame was only 55 %, compared with 221 % at 1.5 m above the base. Finally, the correlation only requires two inputs: the fire effective diameter and the horizontal distance between the target and the fire centre. With no information about the fire's heat release rate or emissive power, the model is likely to struggle to accurately predict the radiant heat flux in some situations.

5.4 Cylindrical Models

The next group of models all have a common assumption: that the fire can be approximated as a cylinder of uniform properties. The radiation is assumed to emit from the surface of this cylinder, which has a height equal to the mean flame height. In this research, three cylindrical models are investigated; the Shokri and Beyler detailed method, the Mudan method and the Dayan and Tien method.

Despite this common assumption, the three methods all have different ways of calculating the radiant heat flux to a target, resulting in significantly different predictions. Figure 55 compares the predictions made by the models with experimental results for the 2:1 aspect ratio burner at 300 kW. The heat flux gauge height is 0.5 m above the base of the flame. Figure 56 then shows how the different models perform with varying target heights.

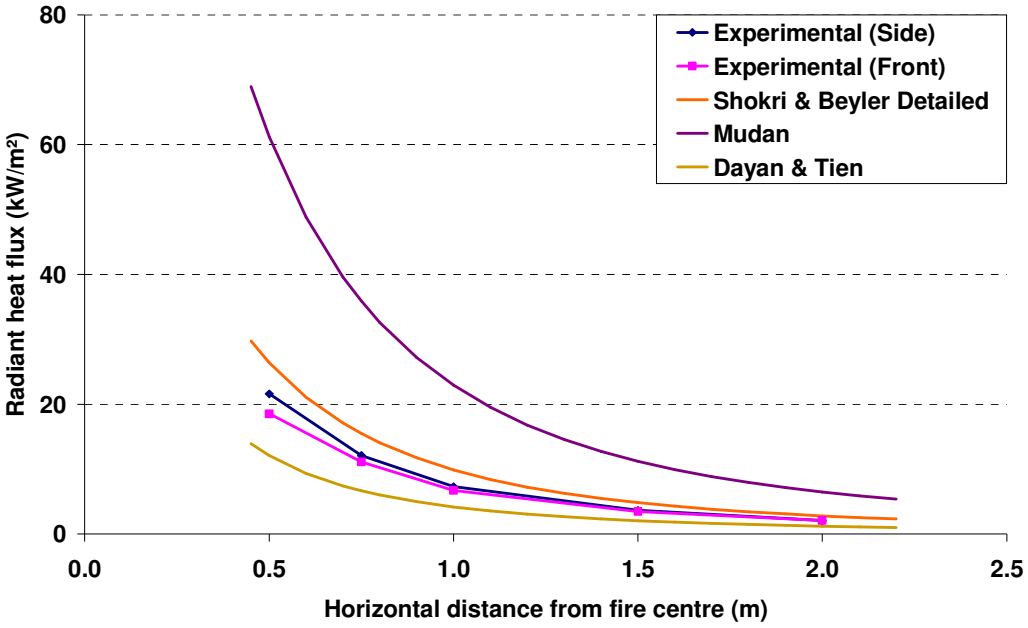

Figure 55: Radiant heat flux vs horizontal distance from fire centre. Comparison of experimental results with cylindrical models. From Test 11, 2:1 burner, 300 kW, gauge height above flame base = 0.5 m

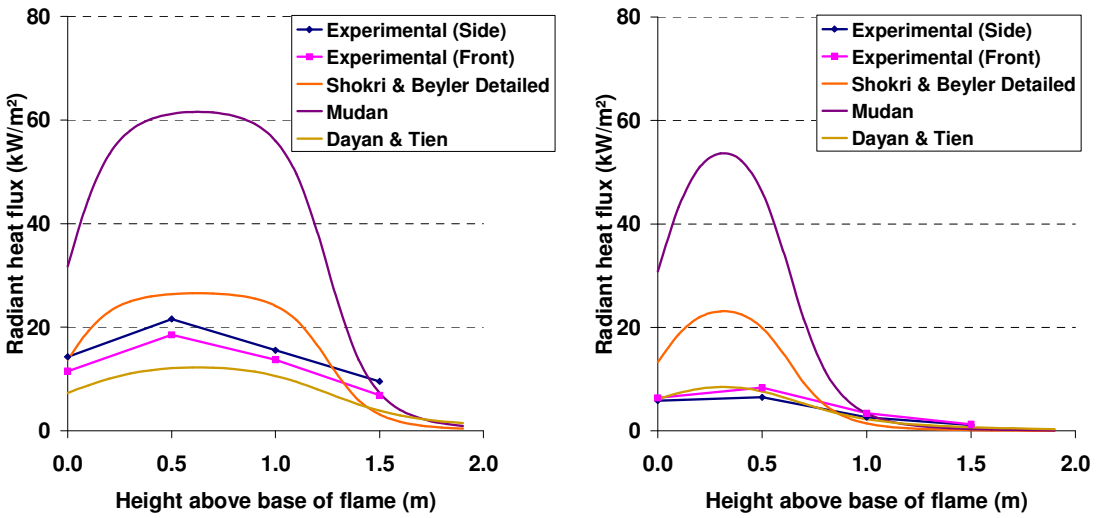

(a) **(b)**

Figure 56: Radiant heat flux vs height above flame base. Comparison of experimental results with cylindrical models. From Test 11, 2:1 burner, gauge height above flame base = 0.5 m, at heat release rate of (a) 300 kW and (b) 100 kW

Perhaps the most noticeable feature of Figure 55 and Figure 56 is that the Mudan method significantly over-predicts the radiant heat flux to the targets. This is in agreement with the findings of Beyler (1999), who states that the heat flux predictions made by the Mudan

method tend to be conservative. This over-prediction is mainly due to the calculation of the effective emissive power. The use of Equation 18 for determining the emissive power is questionable for the fires used in this research (see section 5.6 for more in-depth analysis). The Shokri and Beyler detailed method also appears to over-predict the radiant heat flux to a target; however, to a much lesser degree than the Mudan method.

Figure 57 compares a much wider range of experimental data with the model predictions for the three cylindrical models. Again, the tendency for the Mudan method to over-predict the radiant heat flux is evident (Figure 57b). The scatter of data for the Shokri and Beyler method and Mudan method appears to be very similar, albeit shifted. This is due to the fact that these methods use the same configuration factor calculations, as given by Equations 10 – 13. The Dayan and Tien method, on the other hand, employs a different way of calculating the configuration factor, resulting in a more uniform spread of data (see Figure 57c).

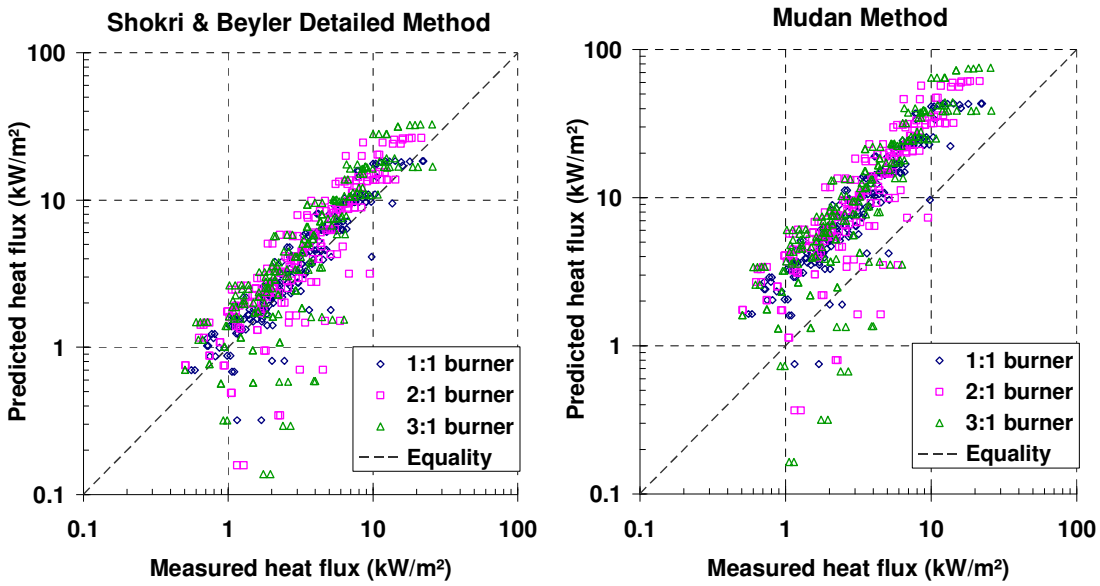

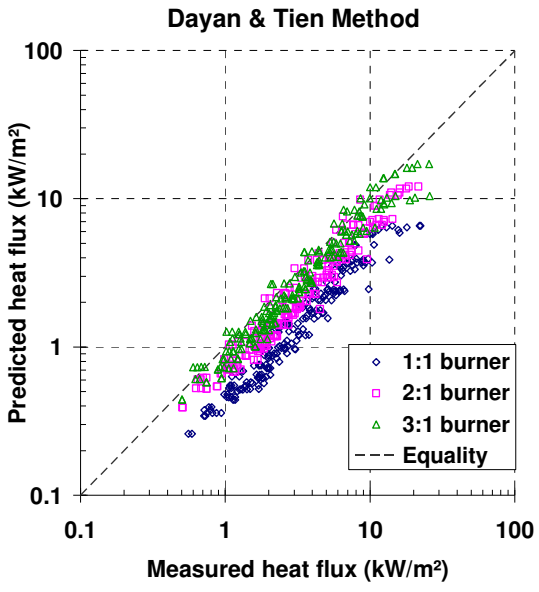

(c)

Figure 57: Comparison of measured and predicted radiative heat flux using (a) Shokri & Beyler detailed method, (b) Mudan method and (c) Dayan & Tien method. Data taken from Tests 7, 9 and 11

For the data presented in Figure 57 above, the Shokri and Beyler detailed method over-predicted the experimental heat flux in 81 % of all cases. 90 % of the data was within -61 % and +120 % of the equality line. The Mudan method over-predicted the heat flux 94 % of the time, with 90 % of the data coming within -11 % and +410 % of the equality line. The Dayan and Tien method tended to under-predict the heat flux, doing so for 94 % of the data in Figure 57c. However, this data was generally closer to the equality line than the other two cylindrical methods, with 90 % of data falling within -64 % and +3 % of the equality line.

Table 6 displays the average absolute percentage errors for the cylindrical methods at each burner aspect ratio. The results are taken from Tests 1-13, representing all data for vertical gauges. The overall average values confirm that the Dayan and Tien method was the best performing cylindrical model, with an average percentage error of 35 % from the experimental data. The remarkably poor performance of the Mudan method for this application is again evident, whilst the Shokri and Beyler detailed method provides relatively good approximations. For the different fire aspect ratios, the percentage errors for both the Shokri and Beyler detailed method and the Mudan method increased with increasing fire aspect ratio. This is expected, because as the fire becomes more rectangular, the cylindrical assumption on which the models are based on begins to break

down. For the Dayan and Tien method, however, Table 6 shows that the percentage error from the experimental results actually decreased as the aspect ratio increased. This does not mean that the model is necessarily better for aspect ratios greater than one. Rather, it is likely that the model tends to under-predict the radiant heat flux in general but as the aspect ratio increases, it begins to over-predict relative to the 1:1 burner results. But due to the inherent under-prediction, this has the effect of bringing the predicted data closer to the experimental results. This point is explained diagrammatically by Figure 58, which is an adaptation of Figure 57c; this time with linear trend lines through each aspect ratio series. Although the trend lines are linear, they do appear to deviate from linearity because of the log-log scale.

Table 6: Summary of percentage errors for cylindrical models. Breakdown of fire aspect ratios. Vertical targets only (Tests 1-13)

	Average absolute % error		
	Shokri & Beyler detailed	Mudan	Dayan & Tien
1:1 burner	34%	199%	54%
2:1 burner	53%	232%	31%
3:1 burner	62%	240%	20%
AVERAGE	50%	224%	35%

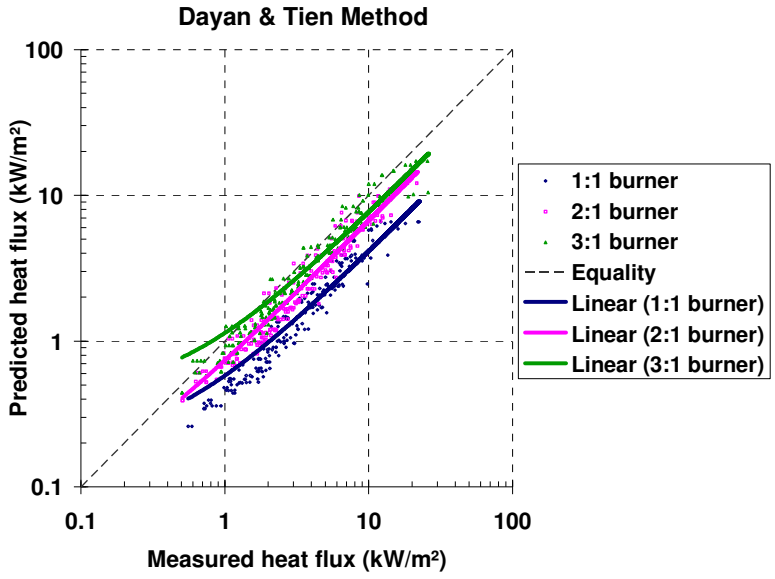

Figure 58: Comparison of measured and predicted radiative heat flux using Dayan & Tien method, including linear trend lines through data series. Data taken from Tests 7, 9 and 11

As it appears that the Dayan and Tien method is the best performing cylindrical model, it is a good idea to break up the results into different heat flux brackets. Table 4 showed that the point source model performed best for heat fluxes less than 10 kW/m². Above 10 kW/m², the point source model had an average percentage error of 31 % from the experimental results, compared with 17 % below 10 kW/m². The Dayan and Tien method, on the other hand, has essentially the same accuracy within any heat flux bracket, as shown in Table 7 below. This means that the model performs equally well for any heat flux within the range that was tested. However, the predictions made by the point source model were closer to the experimental results even within its least accurate heat flux bracket ($\dot{q}'' \geq 10$ kW/m²).

Table 7: Summary of percentage errors for Dayan & Tien method. Data from Tests 7, 9 and 11

	$\dot{q}'' < 5$ kW/m²	$5 \leq \dot{q}'' < 10$ kW/m²	$\dot{q}'' \geq 10$ kW/m²
Average absolute % error	36%	35%	36%

The Shokri and Beyler detailed method, which has been recommended as the method to use for heat fluxes greater than 5 kW/m² (Beyler, 1999), actually performed worse when the measured heat flux was greater than 5 kW/m². For heat fluxes less than 5 kW/m², the Shokri and Beyler detailed method had an average percentage error of 46 % (from Tests 7, 9 and 11). Between 5 and 10 kW/m², the error actually increased to 54 %. Above 10 kW/m², the average error from the experimental results was found to be 49 %. Therefore, for the fire scenario tested in this research, the Shokri and Beyler detailed method performed the best for measured heat fluxes less than 5 kW/m². This is in disagreement with the recommendations of Beyler (1999).

Figure 59 compares the performance of the three cylindrical methods with some experimental data for horizontal targets. The trend shown is very similar to that for vertical targets (see Figure 55), just with lower heat flux values. The Shokri and Beyler detailed and Mudan methods again are seen to over-predict the radiant heat flux, whilst the Dayan and Tien method gives results that are lower than the experimental data. When all data for horizontal gauges is taken into account, the Shokri and Beyler detailed method has an average percentage error from the experimental results of 89 %, whilst the Mudan method has an average error of 205 %. As with the vertical targets, the Dayan and Tien

method performs the best out of the cylindrical models, having an average percentage error of 71 %.

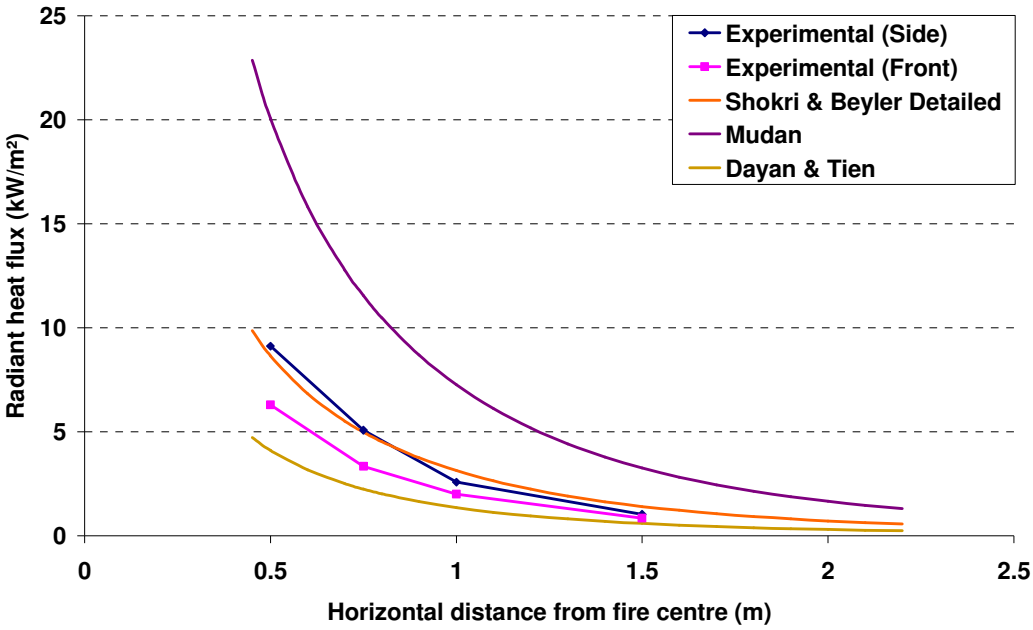

Figure 59: Radiant heat flux vs horizontal distance from fire centre for horizontal targets. From Test 16, 2:1 burner, 300 kW, gauge height above flame base = 0.0 m

Overall, the performance of the cylindrical models for predicting the radiant heat flux to a range of target locations from a propane gas fire was poorer than expected. Using all test data, including results from vertical and horizontal targets, the Dayan and Tien method was the most accurate cylindrical model, with an average error of 41 % from the experimental results. The Shokri and Beyler detailed method was less accurate, having an average error of 58 %, whilst the Mudan method performed very poorly, averaging 221 % error.

5.5 Planar Model

The rectangular planar model is the only model out of those investigated in this research to be able to predict different heat fluxes to the side and front gauge positions. This is due to the fact that the fire is not modelled as a point source of energy or a solid cylinder, but rather two intersecting rectangular planes. Figure 60 displays how the radiant heat flux varies with distance from the fire centre for the experimental data and rectangular planar

model predictions for one particular situation. It can be seen that the predictions for both the side and front gauges are lower than what was measured during the experiments.

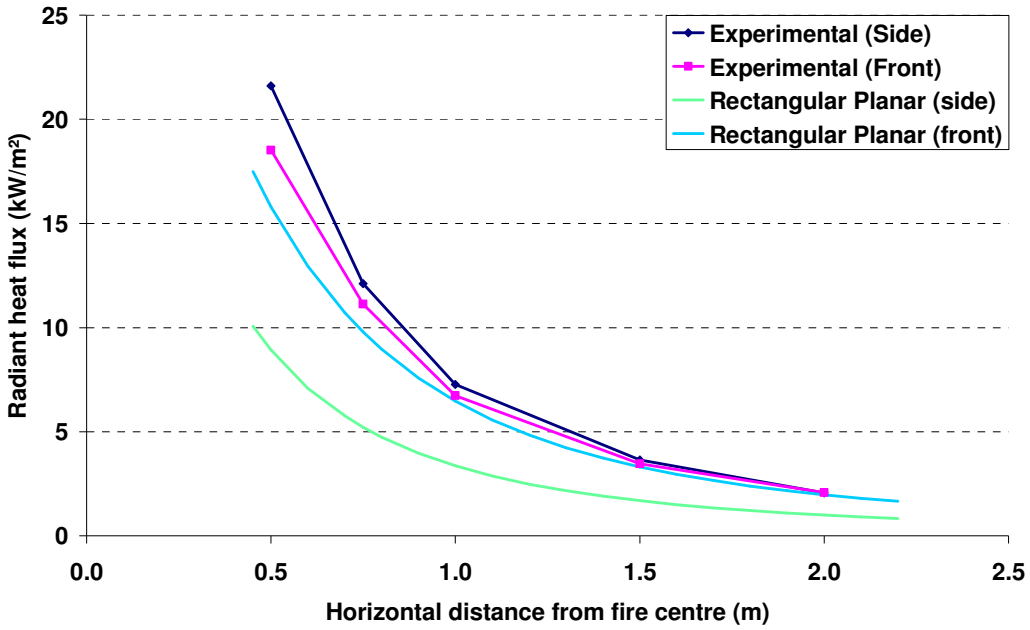

Figure 60: Radiant heat flux vs horizontal distance from fire centre. Comparison of experimental results with rectangular planar model. From Test 11, 2:1 burner, 300 kW, gauge height above flame base = 0.5 m

The experimental results of section 4.2 showed that for fires with a length to width aspect ratio of greater than unity, the side gauges generally recorded a higher radiant heat flux than their front counterparts. This was due to the gauge distance being relative to the centre of the fire, making the side gauges closer to the actual burner edge. As is shown by Figure 60 though, the rectangular planar model predicts the reverse case to occur: that the front gauges will in fact receive a greater radiant heat flux. This is because this model assumes that the radiation is emitted from two intersecting planes, with the line of intersection being above the centre of the fire. In other words, the bulk of the radiation being received by the side gauges is emanating from a plane that is facing those gauges but at the centre of the fire. The front gauges are at the same distance from their facing plane; however, in the case of a 2:1 or 3:1 aspect ratio, this plane is twice or three times as long as the plane facing the side gauges. Due to configuration factor theory, this results in a greater heat flux to the front gauges. Section 5.6 describes the effect of changing the position of the planes on the results.

Figure 61 shows how the rectangular planar model performs with varying height above the base of the flame, again for the 2:1 burner. At 300 kW (Figure 61a), both the front and side gauges are seen to under-predict the radiant heat flux to the targets; however, at 100 kW (Figure 61b) the predictions are closer to the experimental results, even over-predicting nearer the base of the flame.

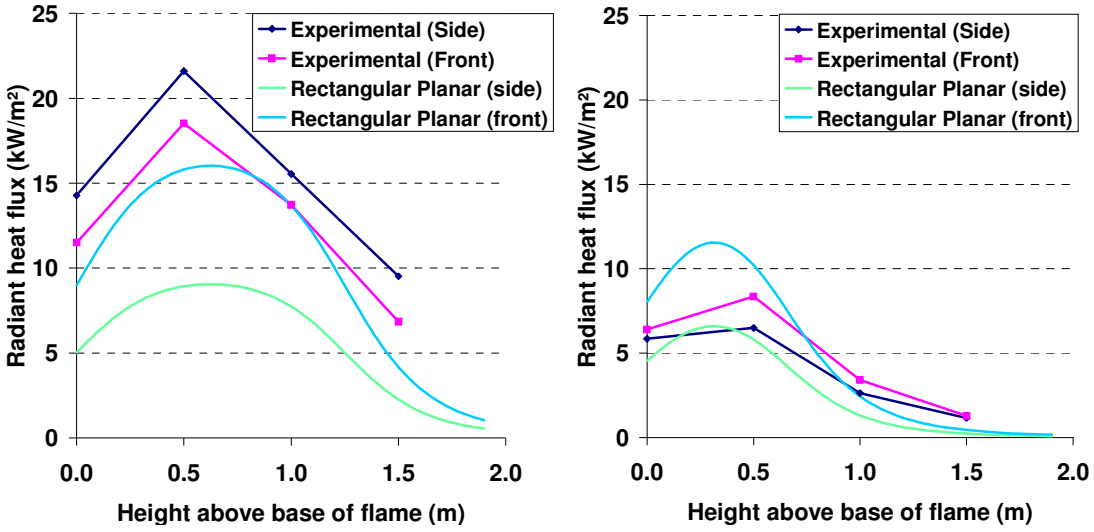

Figure 61: Radiant heat flux vs height above flame base. Comparison of experimental results with planar model. From Test 11, 2:1 burner, gauge height above flame base = 0.5 m, at heat release rate of (a) 300 kW and (b) 100 kW

From the above plots and Figure 62 below, it can be seen that the rectangular planar model generally under-predicts the radiant heat flux. The model provides much better predictions for the front gauges than it does for the side ones. The average absolute percentage error for the front gauges is 35 %, compared with 51 % for the side gauges. This is because for the 2:1 and 3:1 burners, the distance from the edge of the burner to the position of the theoretical rectangular plane is less for the front gauges than for the side gauges. Therefore, the location of the theoretical plane for the front gauges is a better approximation of the real fire than for the side gauges.

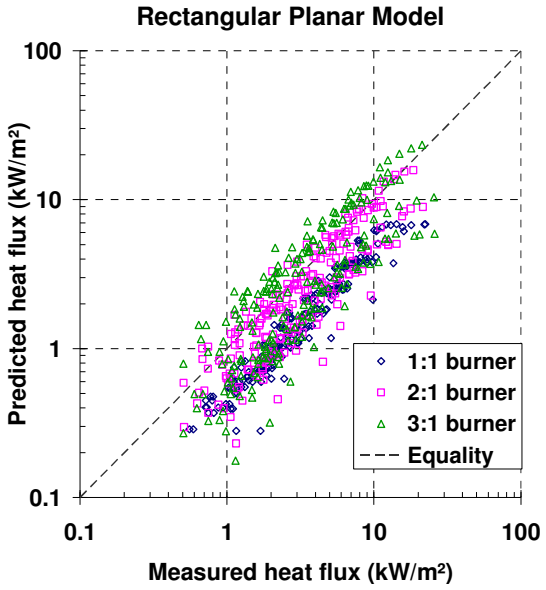

Figure 62: Comparison of measured and predicted radiative heat flux using rectangular planar model. Data taken from Tests 7, 9 and 11

Table 8 shows that there is an unusual trend in the model's behaviour as the aspect ratio increases. There is currently no explanation that can be found to explain this.

Table 8: Summary of average absolute percentage errors for rectangular planar model. Breakdown of fire aspect ratios. Data from Tests 1-13

	Rectangular planar model
1:1 burner	45%
2:1 burner	29%
3:1 burner	45%

In terms of the model's performance for different radiant heat fluxes, the results collected indicate that there is no particular heat flux range that suits the model best. Under 5 kW/m², the model had an average error of 44 % from the experimental results. Between 5 and 10 kW/m², the average error was 40 %, whilst for heat fluxes 10 kW/m² and above it was 42 %. This suggests that there are no limitations on the model in terms of radiant heat flux.

For predicting the radiant heat flux to horizontal targets, Figure 63 shows that the rectangular planar model is again below the experimental results. As with the vertical targets, the predictions made by this model for horizontal targets at the front of the fire are greater than at the side. The rectangular planar model had an average percentage error of

76 % from the experimental results for horizontal targets only. This is the same as was shown by the point source model for horizontal targets.

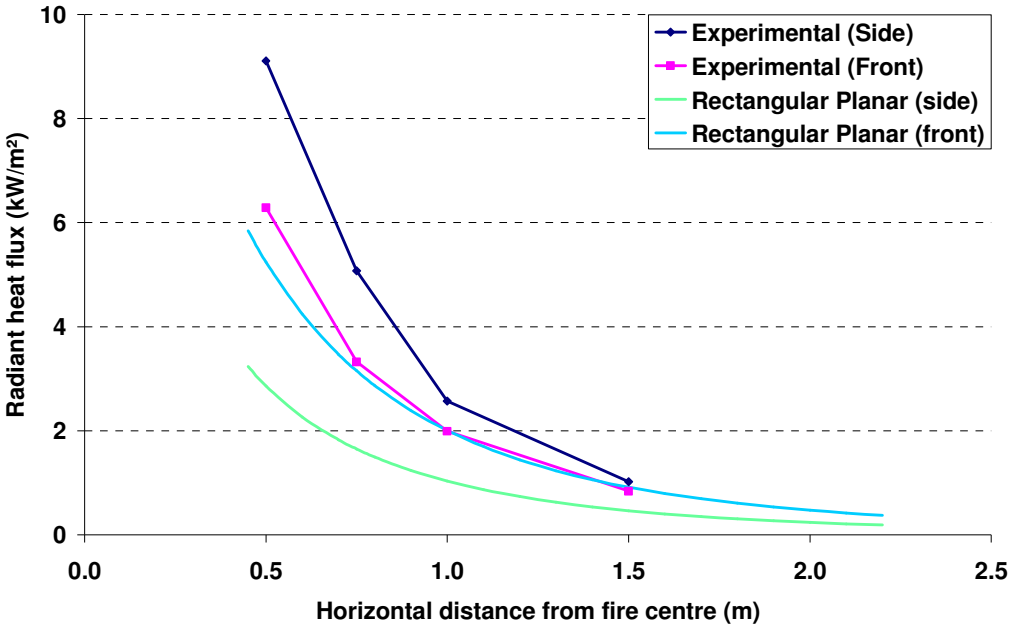

Figure 63: Radiant heat flux vs horizontal distance from fire centre for horizontal targets. From Test 16, 2:1 burner, 300 kW, gauge height above flame base = 0.0 m

When all of the experimental data is taken into account, the predictions made by the rectangular planar model are on average 47 % from the experimental data. This figure is reduced to 40 % when only the vertical target orientation is considered.

The main advantage of the rectangular planar model over the other models reviewed is that the user has more flexibility with fire source geometries. Rather than altering the shape and dimensions of the source to approximate a cylinder, this model uses the actual geometry of the source, then simplifies it to two rectangular planes. However, this way of calculating the configuration factor does not necessarily make the model more accurate; rather it is an alternative approach to some of the more common models. The added flexibility that comes with the model in terms of specifying the geometry has a drawback: the shape factor calculations are fairly complex to program on a computer, in relation to the other radiation models.

5.6 Sensitivity to Inputs

When using the radiation models presented in this work, there are some variables and constants that are required to be input by the user. This requires judgement by the user in selecting an appropriate value for each variable and constant. Section 5.1 explained which values were used in this research, such as 900 °C for the flame temperature. However, such variables seldom have a single, 'correct' value. In order to present the results from the theoretical models (sections 5.2 – 5.5), single values needed to be selected for each variable, but not before the sensitivity of the results to these values was investigated. This section outlines the effect that changing the values has on the radiation model results.

To illustrate how the theoretical model results are altered when different variables are used, a single test is selected rather than presenting all of the experimental data. As with before, Test 11 is used to illustrate the trends that are representative of all of the results.

5.6.1 Radiative fraction

The first variable that was investigated was radiative fraction, χ_r. Used to calculate the radiative energy output of the fire, the radiative fraction is only used in the point source model. Figure 64 compares a sample of predicted results using the standard value of χ_r = 0.32 with results generated using other values. It appears that the radiative fraction used in the calculation of the heat flux by the point source model has relatively little effect on the predictions. This indicates that any value within the 0.30 – 0.32 range of radiative fraction values given by Beyler (2002) should provide acceptable results when used in the point source model.

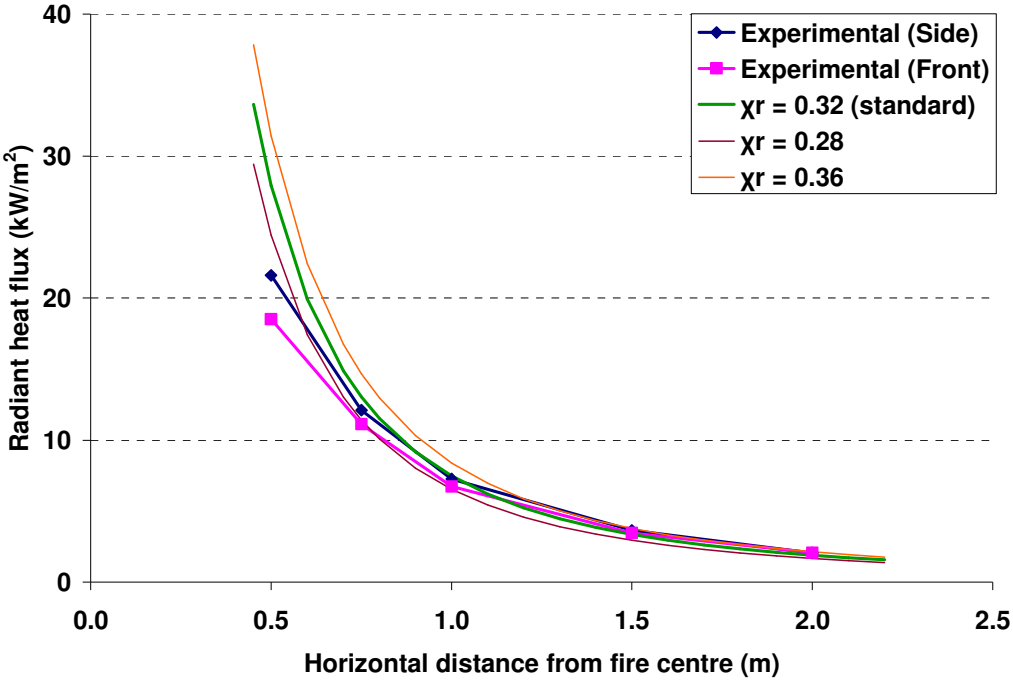

Figure 64: Radiant heat flux vs horizontal distance from fire centre. Comparison of results using different radiative fractions for point source model. From Test 11, 2:1 burner, 300 kW, gauge height above flame base = 0.5 m

The outcome of a sensitivity investigation for the radiative fraction using all of the data from Test 11 is given in Figure 65. The plot shows the average absolute percentage error of the point source model from the experimental results for a wide range of radiative fraction values. The standard value used in the calculations, χ_r = 0.32, is labelled. The minimum of the curve lies to the right of this value, meaning that for this experiment the optimum radiative fraction to minimise the percentage error is χ_r = 0.35. This does not at all suggest that the radiative fraction of propane gas should be 0.35. Rather, this value simply provides the closest match to the experimental results for Test 11. As the point source model was seen to slightly under-predict the experimental results in general, increasing the radiative fraction by a small amount brings the predictions a little closer to the measured data.

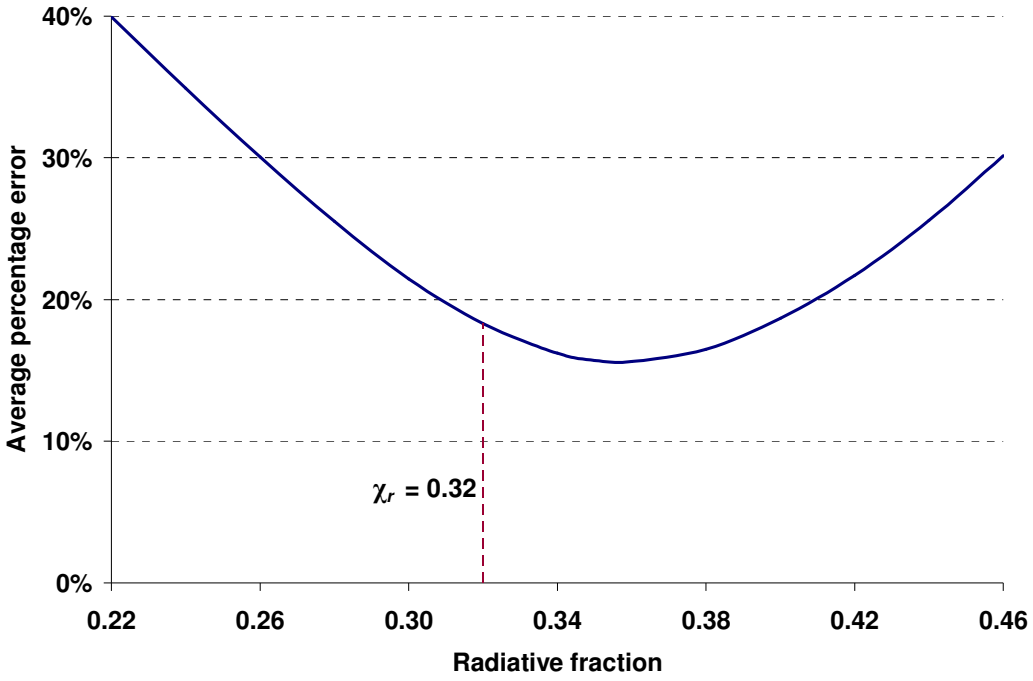

Figure 65: Average percentage error from experimental results vs radiative fraction used in calculation of predictions by point source model. From Test 11 (all data)

5.6.2 Effective absorption coefficient

The second variable that was investigated was the effective absorption coefficient, κ. This has an effect on two of the radiation models: the Dayan and Tien model and the rectangular planar model. In the results presented, a value of 0.85 m^{-1} was used, as recommended by Rasbash, et al.(2004) for propane gas. Figure 66 shows how the predictions change for these models with varying effective absorption coefficient. It can be seen that as κ increases, the predicted radiant heat flux to the target also increases.

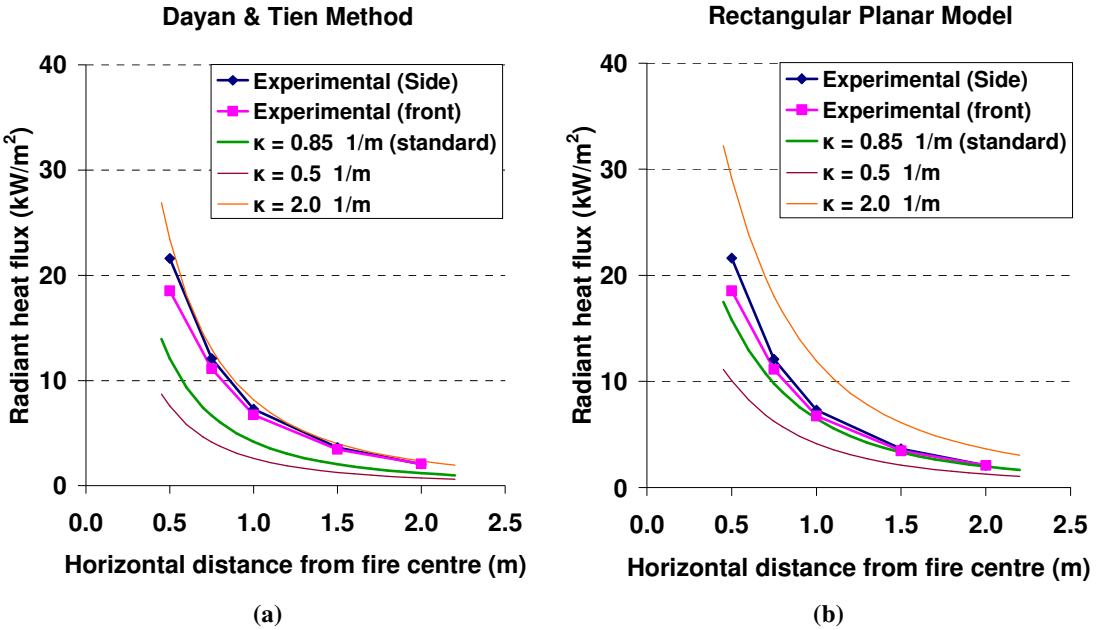

Figure 66: Radiant heat flux vs horizontal distance from fire centre. Comparison of results using different effective absorption coefficients for (a) Dayan & Tien method and (b) rectangular planar model (front gauges). From Test 11, 2:1 burner, 300 kW, gauge height above flame base = 0.5 m

Figure 67 displays the average absolute percentage error from the experimental results for the Dayan and Tien method and rectangular planar model, as a function of the effective absorption coefficient. The average of these two lines is also plotted. All of the data from Test 11 is used to produce this graph. The plot shows that the two methods each have an optimum value of κ in order to minimise the percentage error from the experimental results. The value of 0.85 m^{-1} used to generate the results displayed in sections 5.2 – 5.5 is closer to the theoretical optimum value for the rectangular model than it is for the Dayan and Tien method. However, even at the rectangular planar model's optimal value, the Dayan and Tien method still yields predictions that are closer to the experimental data. This is shown by the fact that the Dayan and Tien method has a lower average percentage error for any effective absorption coefficient above 0.85 m^{-1}. An effective absorption coefficient of 1.20 m^{-1} yields the lowest percentage error when the two methods are averaged. Despite this, the use of κ = 0.85 m^{-1} is justified because it has been determined experimentally for propane gas. The optimum value of 1.20 m^{-1} found here has no experimental measurement involved, but rather is the outcome of an optimisation study that is subject to all of the assumptions of the theoretical models.

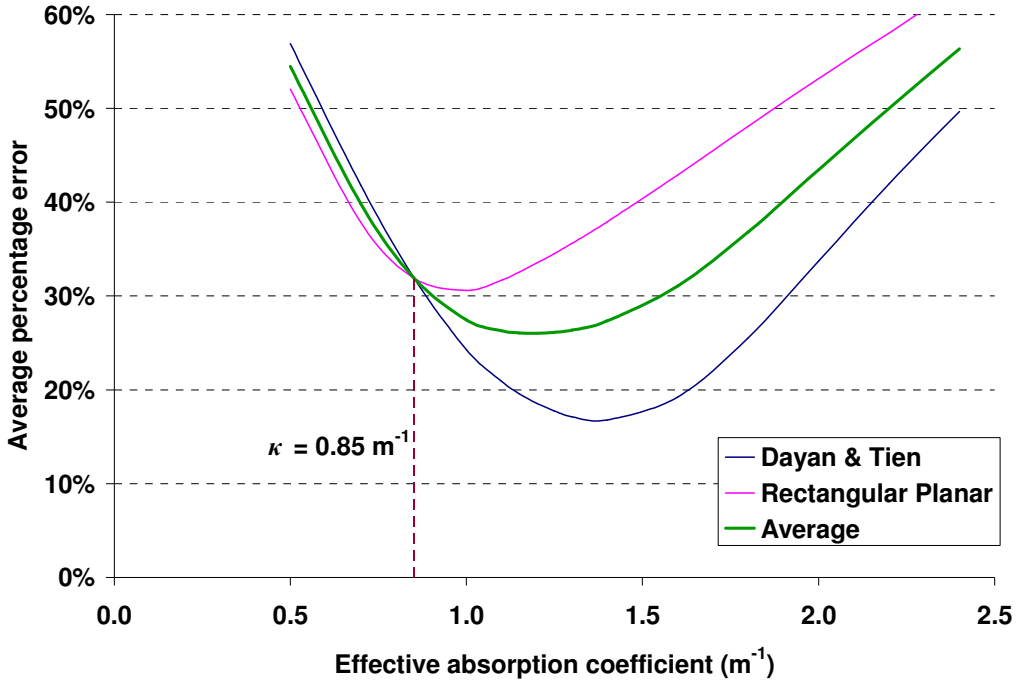

Figure 67: Average percentage error from experimental results vs effective absorption coefficient used in calculation of predictions for Dayan & Tien method and rectangular planar model. From Test 11 (all data)

5.6.3 Flame temperature

The sensitivity of the theoretical results to the flame temperature, T_f, was also investigated. As with the effective absorption coefficient, the flame temperature value affects only the Dayan and Tien method and the rectangular planar model. Figure 68 gives insight into the dependency of these two models on the flame temperature. The standard value of 900 °C again is closer to the optimum temperature input for the rectangular planar model; however, the Dayan and Tien method has lower percentage errors when flame temperatures above 900 °C are input to the models. Averaging the absolute percentage errors from these two models yields an optimum flame temperature of approximately 1000 °C. Again, there is absolutely no experimental measurement involved in the determination of the 1000 °C optimum. Furthermore, this value is only applicable when the effective absorption coefficient is equal to 0.85.

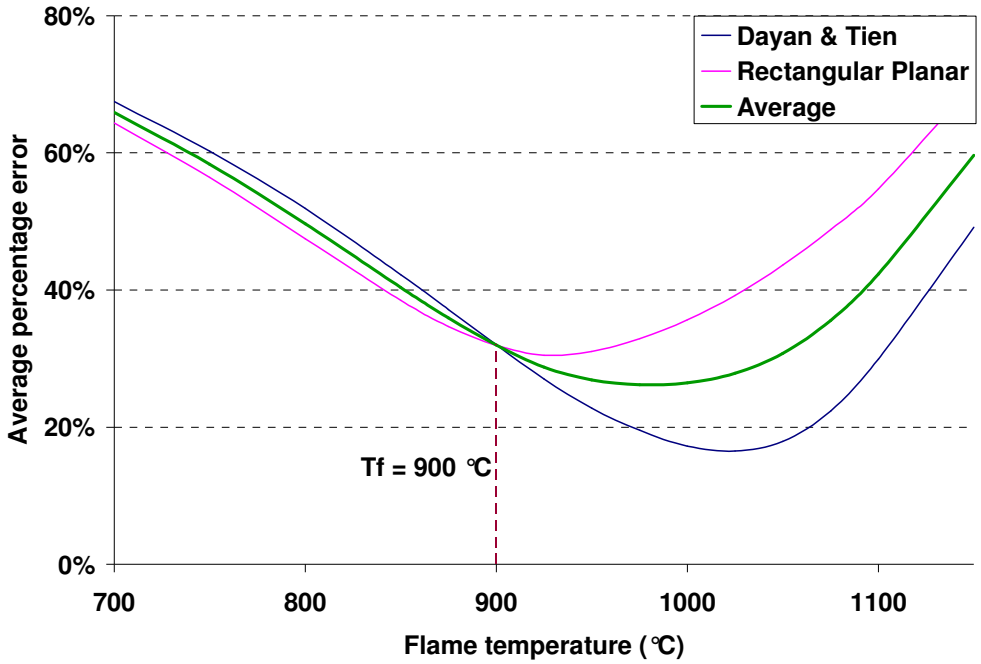

Figure 68: Average percentage error from experimental results vs flame temperature used in calculation of predictions for Dayan & Tien method and rectangular planar model. From Test 11 (all data)

5.6.4 Flame height

As described in section 3.7, the flame height used as an input to the radiation models was that determined from video analysis. However, in many situations an experimentally-determined mean flame height may not be available. When this is the case, flame height correlations must be used. The Heskestad correlation (Equation 6) is utilised in the point source model, Shokri and Beyler detailed method, Dayan and Tien method, and rectangular planar model, as recommended by the models' authors. The Mudan method makes use of Thomas' flame height correlation, given in Equation 17, whilst the Shokri and Beyler correlation does not require the flame height as an input.

Section 4.3.1 described that the correlations over-estimated the mean flame height that was determined using *ImageStream*. For each of the radiation models except the Shokri and Beyler correlation, Figure 69 compares the average percentage errors from the experimental results using the two different methods of determining the flame height. This comparison takes into account all of the experimental data; that is from Tests 1-16. It can be seen that when the flame height is calculated using the recommended correlations,

the performance of the models are on average poorer than when the *ImageStream* flame height is used. In the case of the point source model and Dayan and Tien method, the difference between results is relatively minor, with just a 5 % and 6 % respective difference between the two average values. The rectangular planar model showed a 22 % difference, whilst both the Shokri and Beyler detailed method and Mudan method had differences between results of at least 75 %. This highlights the dependence of the radiation models on the flame height input. The performance of the point source model and the Dayan and Tien method are far less sensitive to changes in the flame height. This, coupled with the fact that these two were the best performing of all of the models tested (section 5.3 and 5.4), makes them strong candidates for the radiation sub-model within BRANZFIRE. On the other hand, the Shokri and Beyler method and the Mudan method not only have greater percentage errors from the experimental results, they also are more sensitive to changes in the flame height.

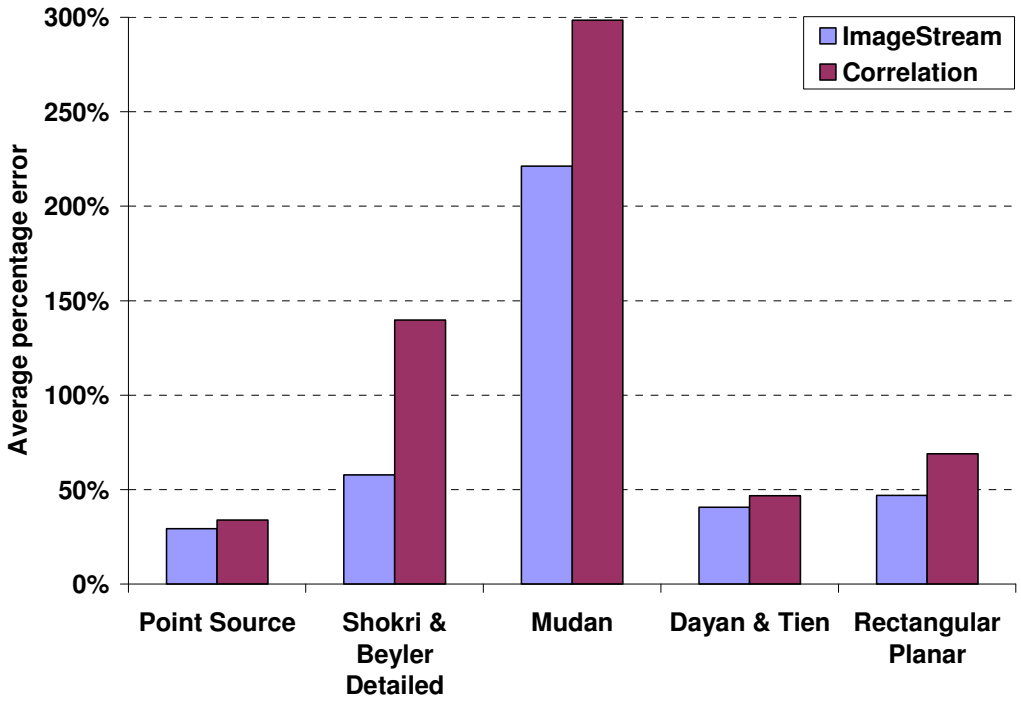

Figure 69: Comparison of average percentage errors from experimental data using two different methods of flame height determination: *ImageStream* and recommended correlations. Data from Tests 1-16

5.6.5 Effective emissive power

The Mudan model was seen to consistently over-predict the radiant heat flux by a significant margin. This model is very strongly affected by the effective emissive power of the flame, *E*. The configuration factor calculation used is the same as in the Shokri and Beyler detailed method, yet the Mudan method gives considerably larger results. Assuming that the atmospheric transmissivity is equal to one, as is usually the case for scenarios on this relatively small scale, the radiant heat flux calculated by the Mudan method is purely just the effective emissive power of the flame multiplied by the configuration factor. Therefore, the value used for the effective emissive power of the flame is very important. Looking again at Equation 18:

$$E = E_{\max} e^{(-sD)} + E_s \left(1 - e^{(-sD)}\right) \tag{18}$$

Section 5.1 provided the values to be used for E_{max}, s and E_s in this equation. These values were held constant during the analysis as they were recommended specifically for use in Equation 18. The only user input required is the effective fire diameter, *D*. For fires used in this research, the effective diameter ranges from 0.34 m to 0.59 m, for the 1:1 and 3:1 burner aspect ratios, respectively. However, Beyler (1999) points out that the validation for this model was carried out using pools of diameter ranging from 1 to 80 m; significantly larger than what was used in this research. Counter-intuitively, according to Equation 18, as the fire diameter increases, the emissive power actually decreases. Mudan (1984) outlines that this effect has been reported numerous times in the literature. Furthermore, most of the fires used for Mudan's validation were liquid pool fires; likely to have different emissive properties than propane gas. Therefore, perhaps the recommended values for the equivalent black body emissive power, E_{max}, extinction coefficient, s, and emissive power of smoke, E_s, are not valid for propane flames, especially of the order of magnitude observed in this research.

5.6.6 Distance convention

In keeping with the convention used in the radiation models, the distance between the fire and the target was always taken from the centre of the fire. It is of interest to determine what effect changing this convention has on the predictions. As the rectangular planar model is an original method developed by the author, it is most appropriate to modify this

model, rather than the more established ones. An investigation was carried out whereby the rectangular planar model was reprogrammed so that the two radiation-emitting planes were located at the edges of the burner, as opposed to the centre. This resulted in a significant change to the predictions made by the model, as shown by Figure 70. This figure compares the average percentage errors at each heat release rate during Test 11 for the standard convention (centre) and the new convention (edge). At low heat release rates, the edge convention is far less accurate (has higher percentage errors) than the centre convention. As the heat release rate rises, so too does the accuracy of the edge convention, until it surpasses that of the centre convention. With the original setup, the percentage error is a lot more uniform across the heat release rate range. It can be seen that the average percentage error for the standard convention is less than when the emitting plane is located at the burner edge. What Figure 70 does not show is that when the edge convention is used, the results increase significantly; such that the model over-predicts the measured data rather than under-predicts as with the centre convention.

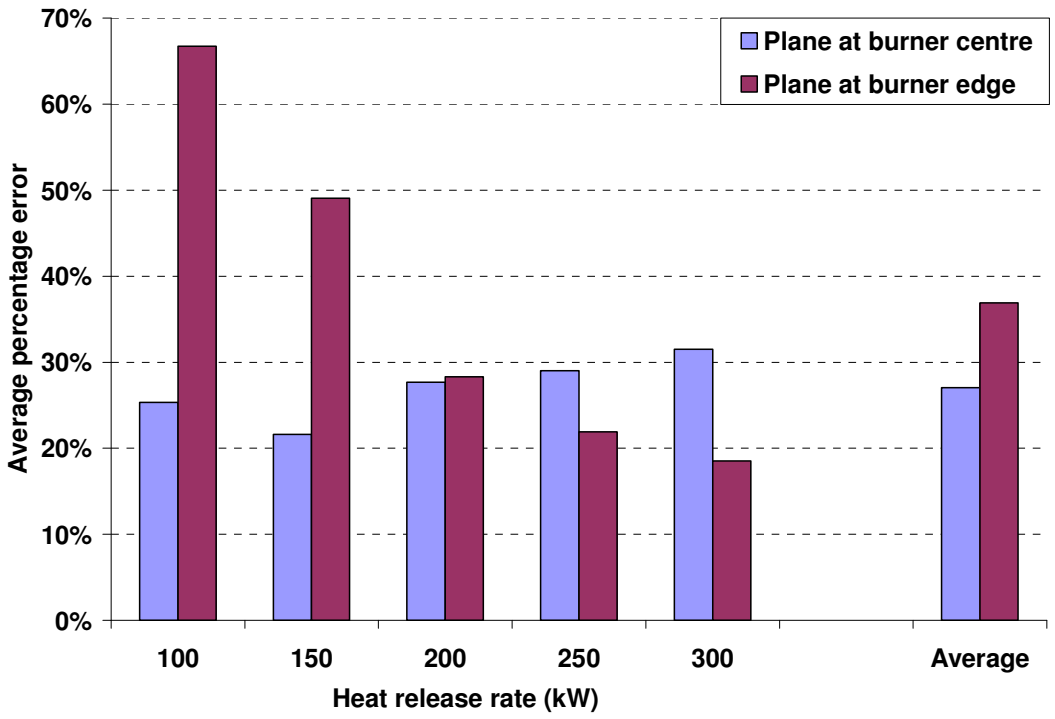

Figure 70: Comparison of average percentage errors from experimental results at different heat release rates for different conventions of measuring distance between target and fire. From rectangular planar model, Test 11, front and side gauges, height above flame base = 0.5 m

5.7 Summary of Models

Table 9 displays the average percentage errors from the experimental results for each of the thermal radiation models through each of the 16 experiments. Refer to Table 1 for a description of the conditions under which each test was conducted. The table below shows that under the same fire conditions, the predictions made by the different radiation models varies considerably. In any one test, the average percentage error of the model predictions from the experimental results ranges from 16 % to as high as 259 %.

Table 9: Summary of average absolute percentage errors from experimental results for all theoretical models

	Average % error from experimental results					
Test #	**Shokri & Beyler**	**Point Source**	**Shokri & Beyler Detailed**	**Mudan**	**Dayan & Tien**	**Rectangular Planar**
1	92%	16%	52%	236%	29%	23%
2	90%	17%	58%	248%	28%	25%
3	152%	17%	62%	245%	20%	38%
4	157%	18%	64%	252%	19%	43%
5	45%	17%	33%	202%	54%	40%
6	45%	20%	41%	223%	50%	36%
7	47%	19%	30%	186%	56%	52%
8	49%	19%	31%	186%	56%	52%
9	163%	19%	60%	231%	20%	44%
10	171%	21%	63%	239%	21%	55%
11	90%	18%	53%	228%	32%	32%
12	89%	19%	48%	217%	33%	35%
13	152%	20%	61%	232%	21%	48%
14	N/A	81%	118%	259%	66%	81%
15	N/A	70%	59%	139%	79%	77%
16	N/A	77%	91%	216%	68%	70%
AVERAGE	**103%**	**29%**	**58%**	**221%**	**41%**	**47%**

To get a better understanding of which models perform best under different conditions, it is useful to further investigate the results presented in Table 9. In the following series of tables, the percentage errors of the models from the experimental results are broken down into different categories to be compared. The best performing model within each category is highlighted.

Table 10 provides the average percentage errors from the experimental results for each model in terms of the target orientation. The point source model is confirmed as the best performing method for vertically oriented targets, whereas the Dayan and Tien method performed the best for horizontal targets. With the exception of the Shokri and Beyler

correlation, which cannot predict the radiation heat flux to horizontal targets, and the Mudan method, all other models were considerably more accurate for vertically oriented targets.

Table 10: Summary of results for different target orientations

	Average % error from experimental results					
Target orientation	**Shokri & Beyler**	**Point Source**	**Shokri & Beyler Detailed**	**Mudan**	**Dayan & Tien**	**Rectangular Planar**
Vertical	103%	18%	50%	224%	35%	40%
Horizontal	N/A	76%	89%	205%	71%	76%

A comparison of average percentage errors with varying burner aspect ratio is given in Table 11. Not only is the point source model the most accurate for all three burner aspect ratios tested, the model is also essentially equally accurate for each of the geometries. Other models, such as the Shokri and Beyler correlation and the Dayan and Tien method, exhibit significant change in the percentage errors for the different burner aspect ratios.

Table 11: Summary of results for different burner aspect ratios

	Average % error from experimental results					
Aspect ratio	**Shokri & Beyler**	**Point Source**	**Shokri & Beyler Detailed**	**Mudan**	**Dayan & Tien**	**Rectangular Planar**
1:1	46%	19%	34%	199%	54%	45%
2:1	90%	18%	53%	232%	31%	29%
3:1	159%	19%	62%	240%	20%	45%

As shown by Table 12, the point source model was found to be the most accurate model when the measured radiant heat flux was less than 10 kW/m². Above 10 kW/m², the Shokri and Beyler correlation was marginally better and was surprisingly the best performing model for higher heat fluxes. The Dayan and Tien method and rectangular planar model were most able to deal with a wide range of heat fluxes, in that their percentage errors were very similar within each heat flux bracket.

Table 12: Summary of results for different radiant heat flux ranges. From Tests 9, 11 and 13

	Average % error from experimental results					
Radiant heat flux	**Shokri & Beyler**	**Point Source**	**Shokri & Beyler Detailed**	**Mudan**	**Dayan & Tien**	**Rectangular Planar**
$\dot{q}'' < 5$ kW/m²	126%	17%	46%	205%	36%	44%
$5 \leq \dot{q}'' < 10$ kW/m²	48%	17%	54%	240%	35%	40%
$\dot{q}'' \geq 10$ kW/m²	29%	31%	49%	238%	36%	41%

Table 13 summarises the average percentage errors for when targets are located centrally and offset in relation to the centreline of the burner. In general, all models seemed to be reasonably unaffected by the lateral change in target position, as can be seen by the fact that the percentage errors are very similar for the central and offset positions. This is somewhat expected, as the different lateral positions can easily be dealt with by the models by way of distances and angles, without any new assumptions required. As with many of the other results, the point source model was found to be the best performing model under different lateral target positions.

Table 13: Summary of results for different target positions

	Average % error from experimental results					
Target position	**Shokri & Beyler**	**Point Source**	**Shokri & Beyler Detailed**	**Mudan**	**Dayan & Tien**	**Rectangular Planar**
Central	101%	19%	48%	215%	36%	45%
Offset	97%	17%	52%	234%	33%	34%

Similarly, all of the models seemed very capable at dealing with different burner angles, as shown in Table 14. It follows, therefore, that the point source model was again the most accurate for both burner angles.

Table 14: Summary of results for different burner angles

	Average % error from experimental results					
Burner angle	**Shokri & Beyler**	**Point Source**	**Shokri & Beyler Detailed**	**Mudan**	**Dayan & Tien**	**Rectangular Planar**
0°	98%	18%	48%	221%	35%	38%
45°	100%	19%	51%	227%	35%	41%

Under the conditions tested in this work, the Shokri and Beyler correlation struggled to accurately predict the radiant heat flux to targets located at many different positions. Due to its simplistic nature, the model is unable to predict changes in radiant heat flux with

varying heat release rate or height above the burner surface. Furthermore, it cannot be used when the target is horizontally oriented. The Shokri and Beyler correlation was best suited to low burner aspect ratios and high heat fluxes. The shortcomings of this correlation arise from the fact that the correlation was formed based on heat flux measurements conducted around large, circular, liquid pool fires. Also, only two inputs are required for the model; none of which relate to the fire's energy release rate or emissive power. All of this resulted in an average percentage error of around 100 % from the experimental results.

The point source model was seen to perform surprisingly well for predicting the radiant heat flux around a propane burner. In fact, it was the best performing method overall out of the six different models investigated. Taking into account all of the experimental data, the point source model resulted in an average percentage error of 29 %, as shown in Table 9. However, this was reduced to 18 % when the predictions to horizontal targets were excluded. The point source model proved to be the most capable model at dealing with varying fire source geometries, with essentially no difference in percentage errors for the three burner aspect ratios tested. The rather common advice of restricting the use of the point source model to applications where the radiant heat flux is 5 kW/m² or less was found to be irrelevant in this application.

The Shokri and Beyler detailed method was found to be the fourth most accurate model, with an average percentage error of 58 %. The model was largely let down by its performance in dealing with horizontal targets and high burner aspect ratios. The performance of this model was made considerably worse when the flame height was determined using Heskestad's correlation, rather than *ImageStream*. This suggests that the model is too reliant on the mean flame height value, which can be a significant issue if the correlation is unable to accurately predict the flame height.

The Mudan method proved to be incapable of producing results that were remotely close to the measured data. The effective emissive power calculation appeared to be inappropriate for the propane gas burner used in the experiments, resulting in an average over-prediction of 221 %. Other researches have found the Mudan method performs much better than what was found in this work, when significantly larger fire diameters are used.

The Dayan and Tien method was the second most accurate model, having an average percentage error of 41 % from the measured data. This was the best performing cylindrical model and the most accurate method for predicting the radiant heat flux to horizontal targets. The percentage errors of this model were only slightly affected by the use of the flame height correlation rather than the *ImageStream* flame height and the model was able to deal with a wide range of heat fluxes with no consequence to its accuracy. The Dayan and Tien method was found to be rather sensitive to two inputs; namely the effective absorption coefficient and the flame temperature.

Finally, the rectangular planar model was found to be the third most accurate; however, was not as robust as some of the other models at coping with changing conditions. This model strangely performed best for the 2:1 burner aspect ratio and the offset targets rather than the central ones. The predictions were quite sensitive to the effective absorption coefficient and the flame temperature; however, the standard values used in the calculations were very near the optimal values for minimising the percentage error from the experimental data.

5.8 Limitations to Results

Although this work has attempted to simulate a range of conditions and scenarios, there are still many limitations to the results. The aim of this research is to evaluate the performance of a number of thermal radiation models with the outcome being recommendations to BRANZ Ltd on the most appropriate method for implementation into their zone model software. This means that the main scenario of interest is item-to-item fire spread within compartments. Accordingly, the experimental programme was set up to emulate likely single-object fires within a compartment. The findings therefore may only be applicable to fires of this scale and not to other fire scenarios, such as large, open fires.

Ideally, when investigating single-item fires it would be most useful to burn real objects, such as items of furniture, and measure their radiative properties. However, it was not economically or practically viable to do this for the amount of data that was desired. The propane gas burner provided a very controlled, repeatable fire from which extensive radiative heat flux measurements could be taken. Although it was intended to represent a compartment fire, the propane fuel would have different radiative properties than the

solids that are the likely fuel source in compartment fires. Clearly, this presents a limitation to the findings.

Other limitations were naturally imposed by the equipment and the laboratory in which the experiments were carried out. The tendency for the propane gas bottles to freeze limited the heat release rate that could be sustained for 15 minutes to 300 kW. This was not too much of an issue, however, because heat release rates above 300 kW from the 1:1 burner resulted in flames that entered the collection hood, meaning that the full flame height could not be captured by the video camera.

Much of the experimental work carried out by other researchers for thermal radiation modelling has been using liquid pool fires. Commonly, these pool fires have had diameters at least 10 m in diameter. This is in stark contrast to the magnitude of the fires used in this work and there are likely to be differences in the radiation emitted. This highlights another limitation to the work.

In the interest of time, radiative heat flux measurements were taken for 3 minutes at each distance setting. To allow for relative steady state conditions to be reached, only 2 minutes of this period was selected for averaging, to then be used in the analysis. Similarly, 2 minute segments of video were used to determine the mean flame height by *ImageStream*. It was assumed that these 2 minute segments were representative of the fire behaviour over any longer period of time.

Overall, it cannot be said with certainty that the findings of this work extend to any application outside the conditions of the experimental programme. One can, however, make reasonable assumptions to extend the results to fires of a similar fuel and order of magnitude as those tested in this work.

5.9 Recommendation for BRANZFIRE Radiation Sub-Model

When recommending one of the models for use in the radiation sub-model within BRANZFIRE, one must consider two main factors. Firstly, the accuracy of the model must be considered. Obviously, as the function of the model will be to predict the radiant heat flux from a fire at given locations around the room, one wishes the predictions to be

as close an approximation of the real scenario as possible. Section 5.7 of this work determined that the point source model was, on average, the most accurate model under the conditions tested. In addition, when selecting a model for BRANZFIRE, it is important that the model is accurate over a wide range of conditions. The point source model satisfies this, as it was found to be not only the most accurate model, but also the most robust. For example, the model was shown to be essentially equally accurate for each of the three burner geometries tested. Also, the model was relatively insensitive to changes in the input variables of radiative fraction and mean flame height.

The second consideration of importance when selecting the most appropriate model is the ease of implementation into BRANZFIRE. Coupled with this is the ease of application by the end-user. A model that is very complex, such as the rectangular planar model, would be somewhat difficult to program into the software so that it could applied in a user-friendly manner by the operator. Use of this model requires a high level of detail about the fire, target position and target orientation relative to the fire. Often, zone models such as BRANZFIRE are used for design purposes, where the exact locations and orientations of objects within rooms are unknown. This introduces the need for a great number of assumptions to be made by the operator. Amateur users of the model could unknowingly specify an arrangement that results in a radiative heat flux that is far from the maximum experienced at another location. A simpler model, like the point source model, is not orientation-specific and therefore always assumes the maximum heat flux at a given location. This is of great importance in design purposes and necessarily takes some responsibility away from the user.

Considering again the main equation used to calculate the radiant heat flux by the two best performing models, the difference in ease of use is evident. Firstly, the point source model uses Equation 5 to calculate the radiant heat flux from the fire to a target.

$$\dot{q}'' = \frac{\dot{Q}_r \cos\theta}{4\pi R^2} \tag{5}$$

The required inputs are reasonably straightforward. $\dot{Q}_r$ is determined from the heat release rate of the fire (required BRANZFIRE input anyway) and the radiative fraction (can be sourced from the literature). The angle θ and the distance R require the mean

flame height (can be determined from the Heskestad correlation) and the distance between the target and the fire (fundamental to any thermal radiation model).

Now considering the second most accurate model, the Dayan and Tien method, the radiative heat flux is calculated by Equation 24.

$$\dot{q}'' = \sigma \varepsilon T_f^4 \left(F_1 + F_2 + F_3 \right) \tag{24}$$

The inputs to this equation are far more complex than the point source model. The emissivity term, ε, is very sensitive to the effective absorption coefficient value used (as shown in section 5.6) and also requires the fire diameter, flame height and distance from the fire to the target. The flame temperature, T_f, was found to have a large effect on the accuracy of the model, therefore care is needed in the selection of this value. Furthermore, the configuration factor terms, $F_{1\text{-}3}$, require detailed information about the target location and orientation. With every additional input required by the user, the probability of misusing the model increases. Therefore, in this regard simpler is better, providing that accuracy is not overly compromised.

The point source model satisfies both of the important considerations discussed above: it was found to be the most accurate model and apart from the Shokri and Beyler correlation, would be the simplest model to program into the BRANZFIRE software. It follows, therefore, that the recommended thermal radiation model for use in a radiation sub-model within BRANZFIRE is the point source model.

Chapter 6

CONCLUSIONS

This work aimed to evaluate the performance of a number of thermal radiation models with respect to item-to-item fire spread within a compartment. The intent was to provide recommendations to BRANZ Ltd on which model would be most appropriate for implementation into the BRANZFIRE software as part of a radiation sub-model. The six methods that were investigated are as follows:

- Shokri and Beyler correlation (Shokri & Beyler, 1989)
- Point source model (Modak, 1977)
- Shokri and Beyler detailed method (Shokri & Beyler, 1989)
- Mudan method (Mudan, 1984)
- Dayan and Tien method (Dayan & Tien, 1974)
- Rectangular planar model (original by the author)

In order to evaluate the performance of these models, a large amount of real radiant heat flux data was required. An experimental programme was carried out, whereby measurements of radiant heat flux were taken around a propane gas burner. The geometry, position and heat release rate of the burner were altered, in addition to a variety of heat flux gauge locations and orientations. In all, over 3000 independent measurements of radiant heat flux were taken; each one averaged over a 2 minute logging period. Video recordings taken of the fires during experimentation were analysed using the *ImageStream* software to determine the mean flame height.

6.1 Experimental Results

6.1.1 Radiant heat flux

The radiant heat flux measurements were somewhat as expected. For example, the heat flux was seen to decrease with distance away from the fire and also with decreasing heat release rate. Measurements taken 0.5 m above the base of the fire were greater than at the other three heights (0.0, 1.0 and 1.5 m). This can be explained by configuration factor

theory. Heat fluxes measured to the side of the burner usually varied from those at the front due to the burner geometry – the heat release rate of the fire, and therefore the flame height, appeared to govern which was higher. Gauges positioned inline with the burner centreline received greater heat flux than those positioned offset. Similarly, vertically oriented gauges had higher readings than horizontal ones, again due to configuration factor theory. Of the three burner aspect ratios tested, the 3:1 burner generally resulted in the highest heat fluxes to the same location. The angle of the burner relative to the gauges appeared to have insignificant effect on the heat flux measured.

6.1.2 Flame height

The *ImageStream* software produced probability contour plots of flame shape over the 2 minute periods of video capture. From these, the mean flame height was determined for each burner aspect ratio at each heat release rate setting. These flame heights were used as inputs to the thermal radiation models. As expected, the 1:1 burner produced the tallest flames at any given heat release rate, due to the same amount of gaseous propane flowing through a smaller cross-sectional area. Predictions of mean flame height from Heskestad's and Thomas' correlations were approximately 10-70 % greater than those determined from *ImageStream*.

6.2 Performance of Models

Each of the six radiation models were then set up to replicate the conditions of the experimental programme. All of the 3000+ heat flux measurements taken in the experiments were compared with the predictions made by the radiation models. It was found that the six models varied significantly in their predictions.

The most accurate model was found to be the point source model, with an average absolute percentage error from the measured data of 29 %. This was an unexpected result based on the simplicity of the model. The point source model also proved to be the most robust of all those investigated, showing good accuracy over the wide range of conditions tested.

The second most accurate model was the Dayan and Tien method. This had an average error of 41 % and was the best performing cylindrical model. Two of the required inputs, the effective absorption coefficient and the flame temperature, had a significant effect on the predictions when varied.

The rectangular planar model was by far the most complex of the six models investigated. It was the third best performing model and had an average error of 47 % from the experimental results. Its complexity and the large number of inputs required mean that the rectangular planar model would be inappropriate for use in the proposed radiation sub-model.

Next, the Shokri and Beyler detailed method resulted in an average error of 58 %. This model had reasonable accuracy in some situations but performed poorly in others. It was found to be very dependent on the flame height input, as when the Heskestad correlation was used instead of the *ImageStream* result, the average percentage error more than doubled.

The Shokri and Beyler correlation was the most rudimentary of the radiation models. With only two inputs required, it is very quick and easy to use; however, in this work the trade-off was accuracy. The average error for this model was 103 %. Also, its simplicity meant that it was unable to predict the heat flux to horizontal targets and the predictions did not vary with heat release rate or height.

Finally, the Mudan method was found to over-predict the measured data by a considerable margin. The expression used to calculate the effective emissive power of the flame seemed entirely inappropriate for the magnitude of fires used in this work. This resulted in an average percentage error of 221 % from the experimental data. This model is only recommended for use with fires at least 1 m in diameter.

6.2.1 Recommendation

In terms of implementing one of these models into a radiation sub-model within BRANZFIRE, the two most important factors are the model's accuracy and its ease of use. The point source model was found to satisfy both of these criteria in that fact that it was

the most accurate model under the conditions tested and also one of the simplest. Programming the point source model into BRANZFIRE should be relatively straightforward for the software's developer, as should applying the model by an end user. Therefore, the point source model is being put forward as the recommended model for a radiation sub-model within BRANZFIRE.

6.3 Further Research

In addition to the planned programming of a thermal radiation sub-model within BRANZFIRE, there is scope for further related work in this field. This may entail an extension of the work presented in this thesis or merely draw on certain aspects for a different purpose altogether.

Although the experimental programme aimed to cover a wide range of potential fire scenarios by varying many different factors, it would be useful to broaden the scope of the experiments even more. This could be done in the following ways (among others):

- Investigate more burner geometries by increasing the dimensions, changing the aspect ratio and using circular burners
- Vary the fuel source. Different flammable gases could be trialled through burners of the same dimensions. Liquid pool fires would be a useful comparison to the gaseous fuels. Burning solids, such as upholstered furniture, would provide a more realistic application to test the radiation models
- Take heat flux measurements closer to the edge of the flame. This would provide more data with high heat fluxes
- Further investigate the distribution of radiant heat flux with lateral position relative to the face of the fire

By collecting experimental data from a wider range of scenarios, the potential limitations of the theoretical models would be further highlighted. The point source model has been shown to work effectively for the propane burner within the bounds of the experimental programme of this work; however, there may be fuels or locations in which it is not as accurate. Similarly, some of the less accurate models in this work may prove to be better performing in other situations, such as the Mudan method for large liquid pool fires.

There is potential for a lot more fire-related work using *ImageStream*. Rather than just analysing flame heights, the software could be used to analyse flame shapes, volumes and pulsation frequencies. With respect to flame heights, a more in-depth analysis could be carried out and compared with numerous other flame height determination methods. A sensitivity study on the duration of video capture would be useful. From this, an optimal length of video input could be found that yields the same mean flame height as for longer durations.

Chapter 7

REFERENCES

Adobe Systems Incorporated (2007). Adobe Premier Pro CS3 (Version 3.0.0): Adobe Systems Incorporated.

Beyler, C. L. (1986). Fire plumes and ceiling jets. *Fire Safety Journal, 11*(1-2), 53-75. DOI:10.1016/0379-7112(86)90052-4

Beyler, C. L. (1999). *Engineering Guide: Assessing Flame Radiation to External Targets from Pool Fires*. Bethesda, MD: Society of Fire Protection Engineers.

Beyler, C. L. (2002). Fire hazard calculations for large, open hydrocarbon fires. In P. J. DiNenno, et al. (Ed.), *SFPE Handbook of Fire Protection Engineering* (3rd ed.). Quincy, MA: National Fire Protection Association.

Beyler, C. L., DiNenno, P. J., Carpenter, D. J., & Watts Jr., J. M. (2008). Introduction to fire modeling. In A. E. Cote, J. R. Hall, P. Powell, C. C. Grant & R. E. Solomon (Eds.), *Fire protection handbook* (20th ed., Vol. 1). Quincy, MA: National Fire Protection Association.

BRANZ Ltd (2007). *Building safety design-fire tool for use in a risk-informed regulatory environment: proposal application.* Wellington: BRANZ Ltd.

Cox, G., & Chitty, R. (1985). Some source-dependent effects of unbounded fires. *Combustion and Flame, 60*(3), 219-232. DOI:10.1016/0010-2180(85)90027-6

Cox, G., & Kumar, S. (2002). Modelling enclosure fires using CFD. In P. J. DiNenno, et al. (Ed.), *SFPE Handbook of Fire Protection Engineering* (3rd ed.). Quincy, MA: National Fire Protection Association.

Crocker, W. P., & Napier, D. H. (1986). *Thermal radiation hazards of liquid pool fires and tank fires.* Paper presented at the Institution of Chemical Engineers Symposium Series (97), Manchester, England.

Davis, B. C., & Bagster, D. F. (1989). The computation of view factors of fire models : 1. Differential targets. *Journal of Loss Prevention in the Process Industries, 2*(4), 224-234. DOI:10.1016/0950-4230(89)80037-3

Dayan, A., & Tien, C. L. (1974). Radiant Heating from a Cylindrical Fire Column. *Combustion Science and Technology, 9*(1-2), 41-47. DOI:10.1080/00102207408960335

Drysdale, D. (1999). *An Introduction to Fire Dynmaics* (2nd ed.). Chichester: John Wiley and Sons.

Drysdale, D. (2002). Thermochemistry. In P. J. DiNenno, et al. (Ed.), *SFPE Handbook of Fire Protection Engineering* (3rd ed.). Quincy, MA: National Fire Protection Association.

Goble, K. (2007). *Height of flames projecting from compartment openings : a thesis submitted in partial fulfilment of the requirements for the degree of Master of Engineering in Fire Engineering.* Department of Civil Engineering, University of Canterbury, Christchurch, New Zealand.

He, Y. (2001). Evaluation of the Maximum Configuration Factor for Cylindrical Flame Hazard Calculation. *Journal of Fire Sciences, 19*(2), 121-136. DOI:10.1106/j5ta-d9cu-6mf6-5vmj

Heskestad, G. (2002). Fire plumes, flame height, and air entrainment. In P. J. DiNenno, et al. (Ed.), *SFPE Handbook of Fire Protection Engineering* (3rd ed.). Quincy, MA: National Fire Protection Association.

Howell, J. R. (2008). A catalog of radiation heat transfer configuration factors (2nd ed.) 2. Retrieved 26 Mar, 2009, from http://www.me.utexas.edu/~howell/

Iqbal, N., & Salley, M. H. (2004). *Fire Dynamics Tools (FDT^s): Quantitative Fire Hazard Analysis Methods for the U.S. Nuclear Regulatory Commission Fire Protection Inspection Program.* Washington, DC: U.S. Nuclear Regulatory Commission.

Janssens, M. (2002). Calorimetry. In P. J. DiNenno, et al. (Ed.), *SFPE Handbook of Fire Protection Engineering* (3rd ed.). Quincy, MA: National Fire Protection Association.

Karlsson, B., & Quintiere, J. G. (2000). *Enclosure fire dynamics*. Boca Raton, FL: CRC Press.

Lohninger, H. (2009). Fundamentals of Statistics Retrieved 19 October, 2009, from http://www.statistics4u.info/fundstat_eng/index.html

Markstein, G. H. (1976). Radiative energy transfer from turbulent diffusion flames. *Combustion and Flame, 27*, 51-63. DOI:10.1016/0010-2180(76)90005-5

Mason, P. (2003). *Estimating thermal radiation fields from 3D flame reconstruction: A thesis submitted in partial fulfilment of the requirements for the degree of Master of Applied Computing.* Lincoln University, Christchurch.

Mason, P. S., Fleischmann, C. M., Rogers, C. B., McKinnon, A. E., Unsworth, K., & Spearpoint, M. (2009). Estimating thermal radiation fields from 3D flame reconstruction. *Fire Technology, 45*(1), 1-22. DOI:10.1007/s10694-008-0041-0

Modak, A. T. (1977). Thermal radiation from pool fires. *Combustion and Flame, 29*, 177-192. DOI:10.1016/0010-2180(77)90106-7

Mudan, K. S. (1984). Thermal radiation hazards from hydrocarbon pool fires. *Progress in Energy and Combustion Science, 10*(1), 59-80. DOI:10.1016/0360-1285(84)90119-9

NIST (2008). NIST Chemistry WebBook Retrieved 21 Jul, 2009, from http://webbook.nist.gov/chemistry/

Nokes, R. (2008a). ImageStream (Version 7.00): Department of Civil and Natural Resources Engineering, University of Canterbury.

Nokes, R. (2008b). *ImageStream Version 7.00 User's Guide*. Christchurch, N.Z.: Department of Civil and Natural Resources Engineering, University of Canterbury.

NRC, ICC, DBH, & ABCB (2005). *International fire engineering guidelines* (2005 ed.). Canberra: Australian Building Codes Board.

Oenbring, P. R., & Sifferman, T. R. (1980). Flare Design - Are Current Methods Too Conservative? *Hydrocarbon Processing, 59*(5), 124-129.

Quintiere, J. G. (2002). Compartment fire modelling. In P. J. DiNenno, et al. (Ed.), *SFPE Handbook of Fire Protection Engineering* (3rd ed.). Quincy, MA: National Fire Protection Association.

Rasbash, D., Ramachandran, G., Kandola, B., Watts, J., & Law, M. (2004). *Evaluation of fire safety*. Hoboken, NJ: John Wiley & Sons Ltd.

Rew, P. J., Hulbert, W. G., & Deaves, D. M. (1997). Modelling of Thermal Radiation From External Hydrocarbon Pool Fires. *Process Safety and Environmental Protection, 75*(2), 81-89. DOI:10.1205/095758297528841

Robertson, R. B. (1976). *Spacing in chemical plant design against loss by fire.* Paper presented at the Institution of Chemical Engineers Symposium Series (47), Livingston, Scotland.

Seeger, P. G. (1974). Heat transfer by radiation from fires of liquid fuels in tanks. In N. H. Afgan & J. M. Beer (Eds.), *Heat transfer in flames* (pp. 431-439). Washington, D.C.: Scripta Book Company.

Shokri, M., & Beyler, C. L. (1989). Radiation from Large Pool Fires. *Journal of Fire Protection Engineering, 1*(4), 141-149. DOI:10.1177/104239158900100404

Siegel, R., & Howell, J. R. (1992). *Thermal radiation heat transfer* (3rd ed.). Washington, D.C: Hemisphere Pub. Corp.

Sivathanu, Y. R., & Faeth, G. M. (1990). Soot volume fractions in the overfire region of turbulent diffusion flames. *Combustion and Flame, 81*(2), 133-149. DOI:10.1016/0010-2180(90)90060-5

Society of Fire Protection Engineers (2005). *SFPE engineering guide to application of risk assessment in fire protection design. Review draft.* Bethesda, MD: Society of Fire Protection Engineers.

Thomas, P. H. (1963). The size of flames from natural fires. *Symposium (International) on Combustion, 9*, 844-859. DOI:10.1016/S0082-0784(63)80091-0

Thomas, P. H. (1986). Design guide: Structure fire safety CIB W14 Workshop report. *Fire Safety Journal, 10*(2), 77-137. DOI:10.1016/0379-7112(86)90041-X

Thornton, W. (1917). The relation of oxygen to the heat of combustion of organic compounds. *Philosophical Magazine and Journal of Science, 33*, 196-203.

Wade, C. A. (2004). *Study Report No. 92 (rev.), BRANZFIRE Technical Reference Guide*. Wellington: BRANZ Ltd.

Wade, C. A. (2008). BRANZFIRE (Version 2008.2): Building Research Association of New Zealand Incorporated.

Zukoski, E. E., Cetegen, B. M., & Kubota, T. (1985). Visible structure of buoyant diffusion flames. *Symposium (International) on Combustion, 20*(1), 361-366. DOI:10.1016/S0082-0784(85)80522-1

Zukoski, E. E., Kubota, T., & Cetegen, B. (1981). Entrainment in fire plumes. *Fire Safety Journal, 3*(3), 107-121. DOI:10.1016/0379-7112(81)90037-0

APPENDIX A – EMISSIVITY PLOTS

The following plots are required by the Mudan model (see section 2.3.4) if the atmospheric transmissivity, τ, is being calculated.

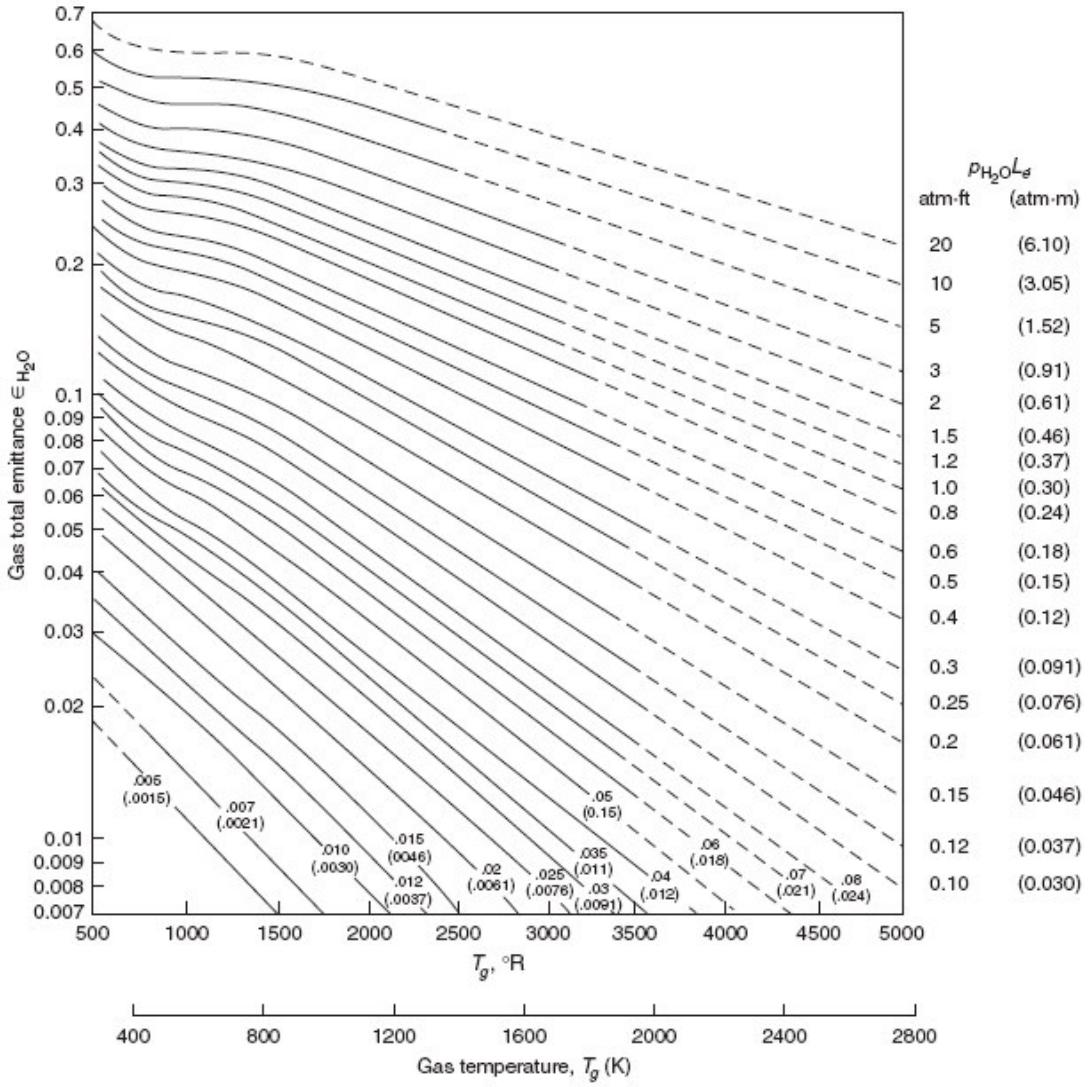

Figure A 1: Total emissivity of water-vapour in a mixture of total pressure of 1 atm (Beyler, 2002)

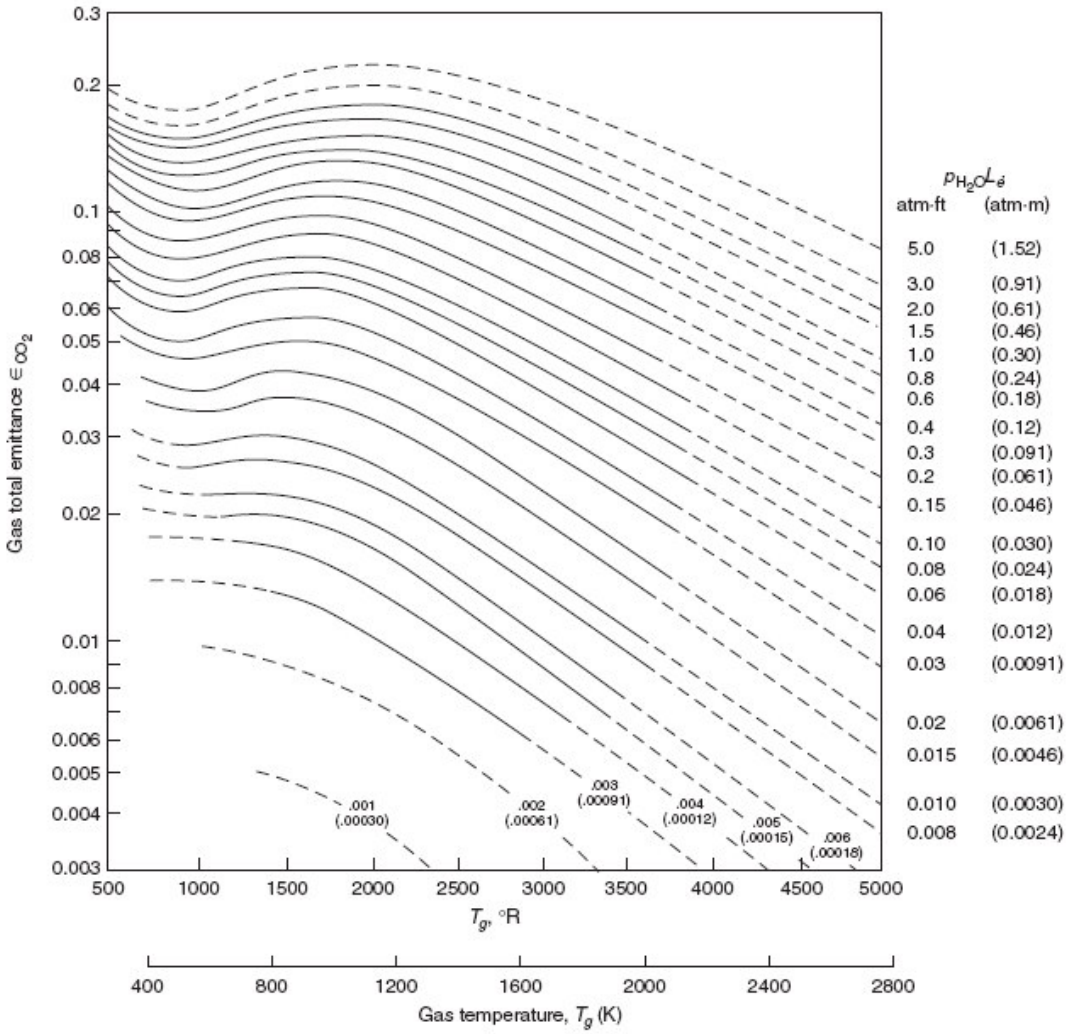

Figure A 2: Total emissivity of carbon dioxide in a mixture of total pressure of 1 atm (Beyler, 2002)

APPENDIX B – CONTOUR PLOTS

In order to determine the contour plots of flame probability within *ImageStream*, the following steps were carried out.

1. Convert the raw video to individual frame-by-frame images using *Adobe Premier Pro*. Output the images as Windows Bitmap files (.bmp file extension). Repeat for each heat release rate of each burner
2. Open *ImageStream* and create an *Image Sequence* using all Bitmap files for each run.
3. Select *Create Transformed Image Sequence*. Go to *Transformations* tab. Select *Trim* and enter number of pixels to trim off each side. Browse for filename, select first in sequence. Change file type from .bmp to .png. This reduces files size but loses very little resolution
4. Open *Details View*. Change *x* and *y scales* based on known real measurements taken during experimentation.
5. Open *Filter View*. Add following *Filters*, modifying parameters to suit:
    - *Extract Filter*, extracting the *Red* colour intensity
    - *Threshold Filter*, removing *Red* colours below threshold of 200
    - *Amplify Filter*, amplifying *Red* to value of 255
    - *Amplify Filter*, normalising *Red* to value of 1 by amplifying *Red* gun by factor of 1/255
    - *Convert Type Filter*, converting from *RGB* image to *Real Values*

    Note: do not apply filters here. Also, these filters can be saved (individually) so that they can be called upon in subsequent analyses.
6. Select *Create Intensity Field*. Go to *Fields* tab, ensuring *Apply Filters* is checked. Specify desired grid parameters in *Grid* tab (i.e. 40 mm, with enough grid cells to cover width and height of image). Click *OK*.
7. Double click *Intensity Field* to open *Calculator View*. Double click *I* calculator at top of list.
8. Set *t axis* to *Averaged*, but leave *x* and *y axis* as *Variable*. Click *Calculate Field*. Double click on new calculated field.

9. Unselect *Cells* and select *Contour*. Can change image properties, such as background colour. Save image and intensity field.

The following figures provide the contour plots generated by *ImageStream* from which the experimental mean flame heights were determined.

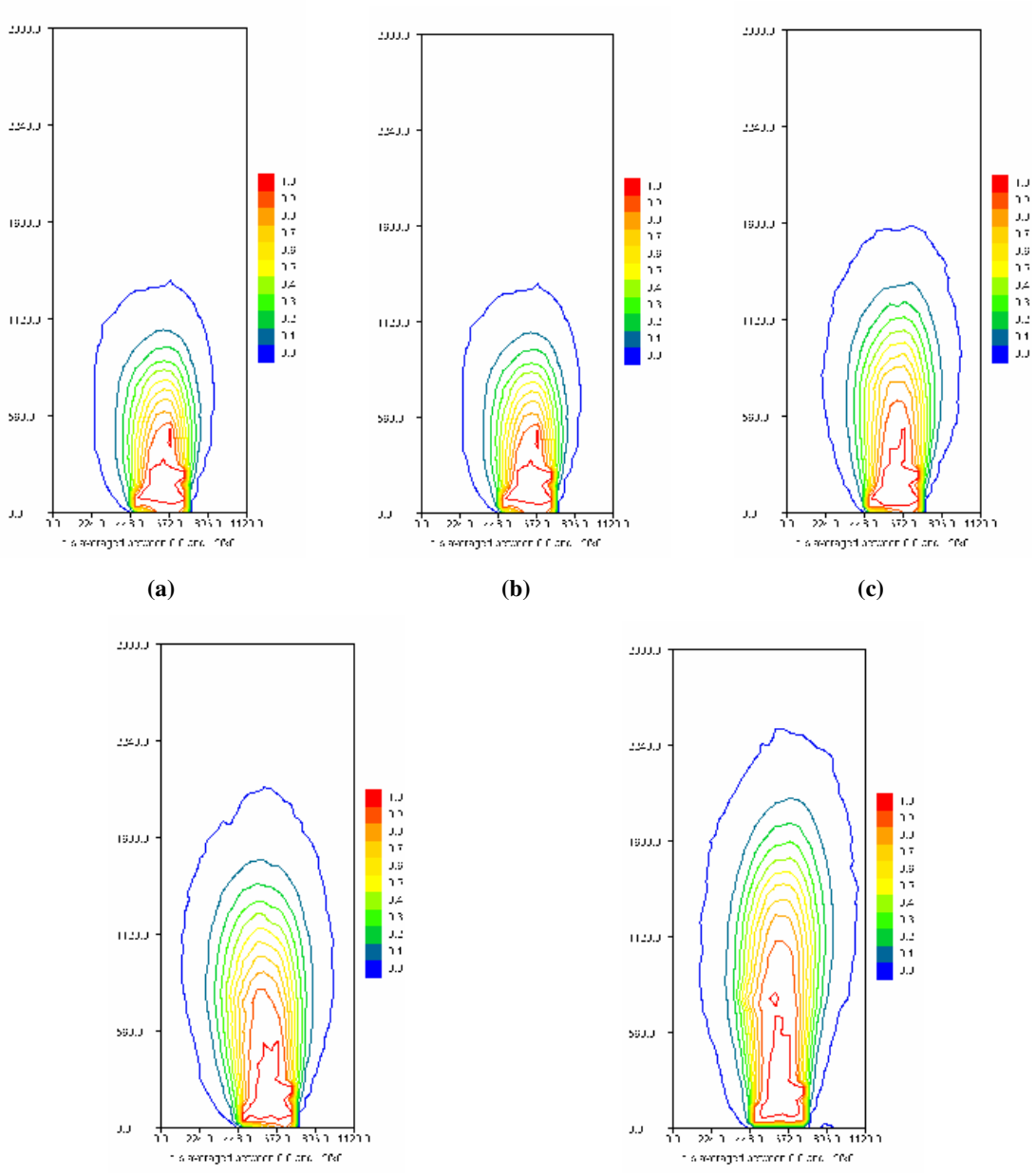

(a) **(b)** **(c)**

(d) **(e)**

Figure B 1: *ImageStream* contour plots to determine flame height for 1:1 burner at (a) 100 kW, (b) 150 kW, (c) 200 kW, (d) 250 kW and (e) 300 kW

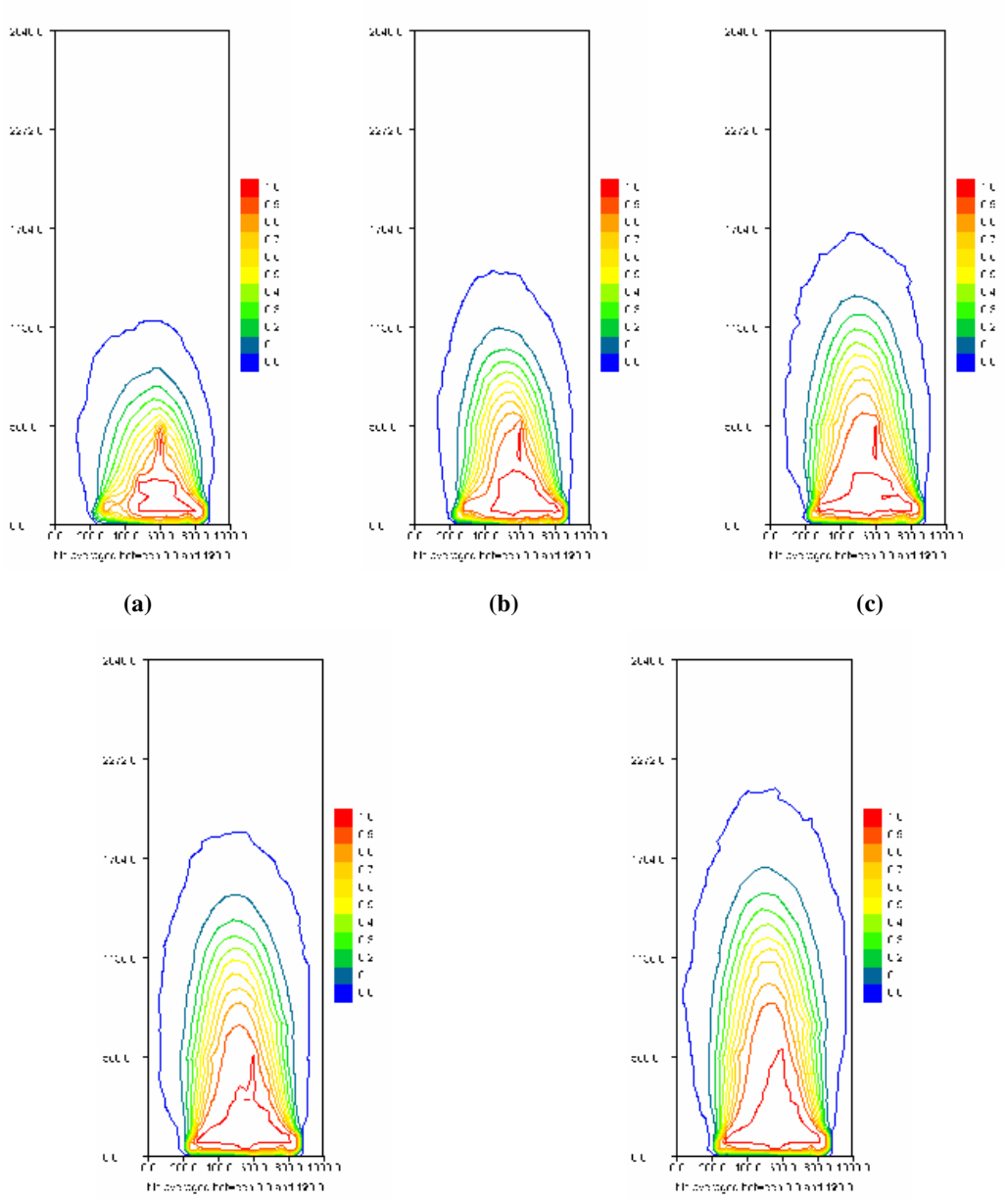

(a) **(b)** **(c)**

(d) **(e)**

Figure B 2: ImageStream contour plots to determine flame height for 2:1 burner at (a) 100 kW, (b) 150 kW, (c) 200 kW, (d) 250 kW and (e) 300 kW

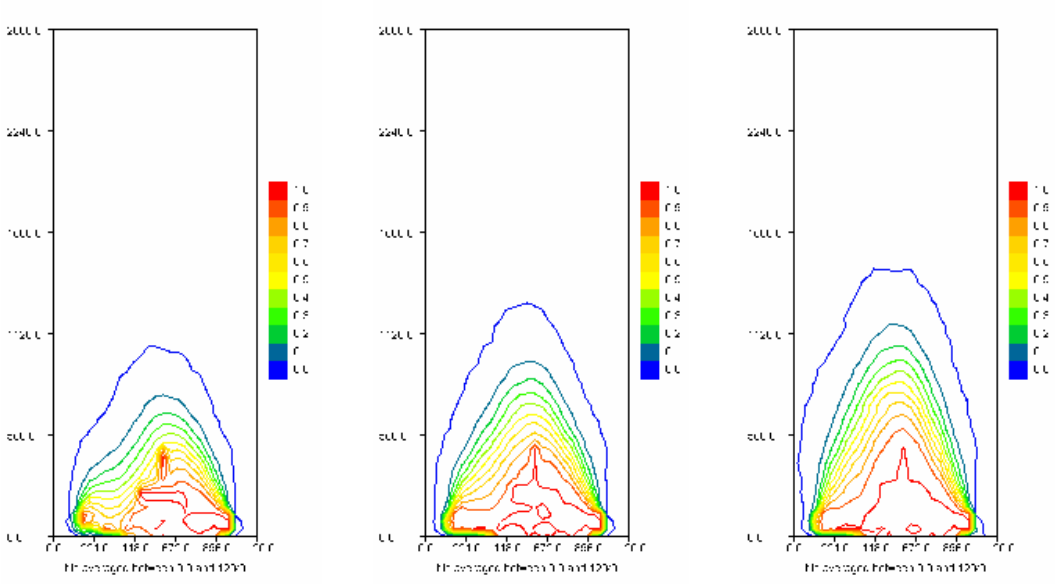

(a) **(b)** **(c)**

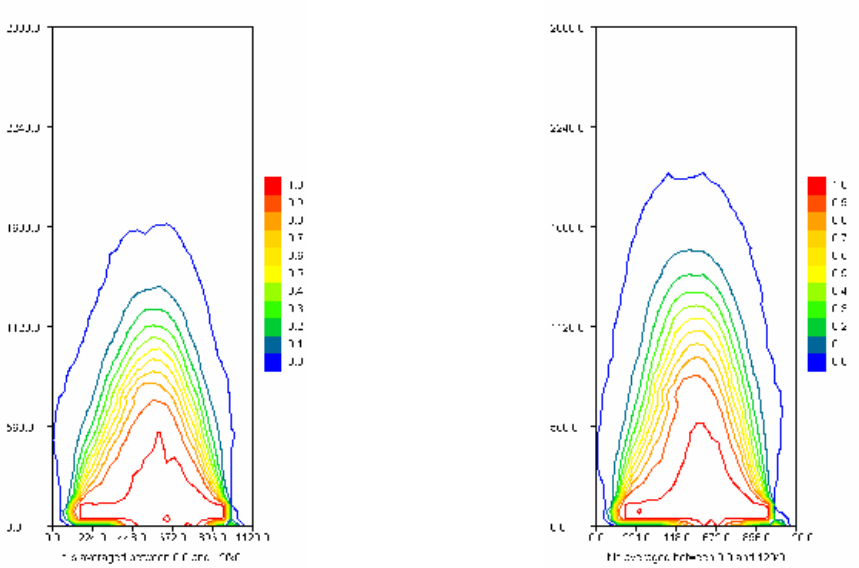

(d) **(e)**

Figure B 3: ImageStream contour plots to determine flame height for 3:1 burner at (a) 100 kW, (b) 150 kW, (c) 200 kW, (d) 250 kW and (e) 300 kW

APPENDIX C – HORIZONTAL RESULTS

Figure C 1 compares the measured data with the predicted results of each model for horizontal targets. These plots take into account all of the data collected in Tests 14-16.

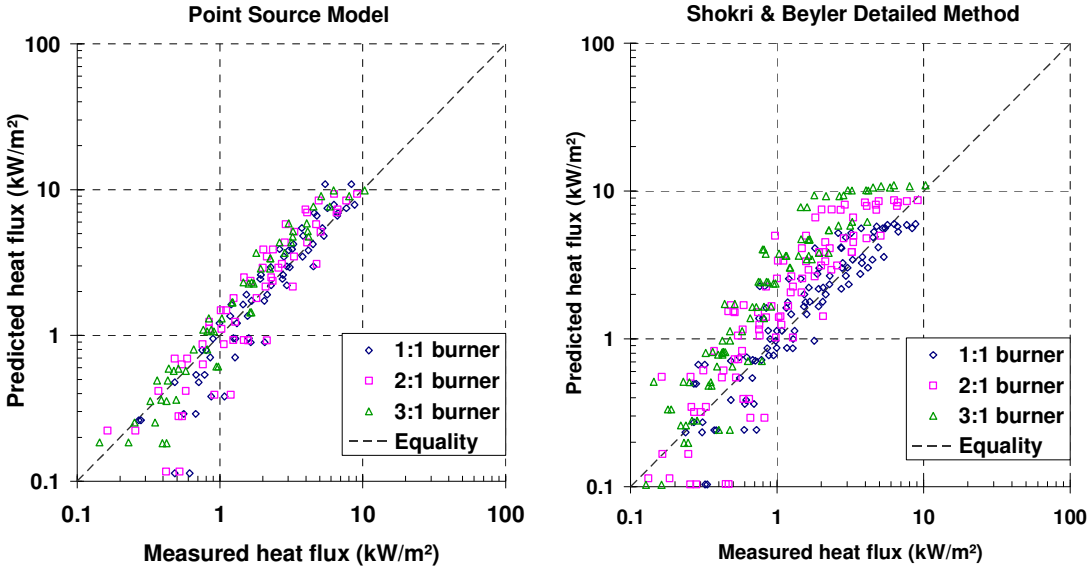

(a)

(b)

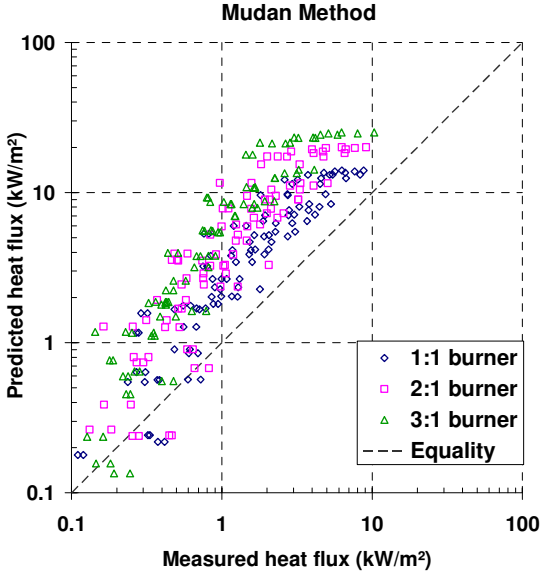

(c)

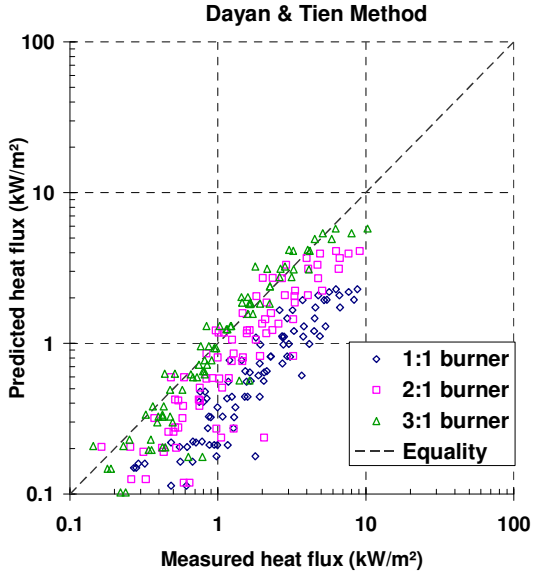

(d)

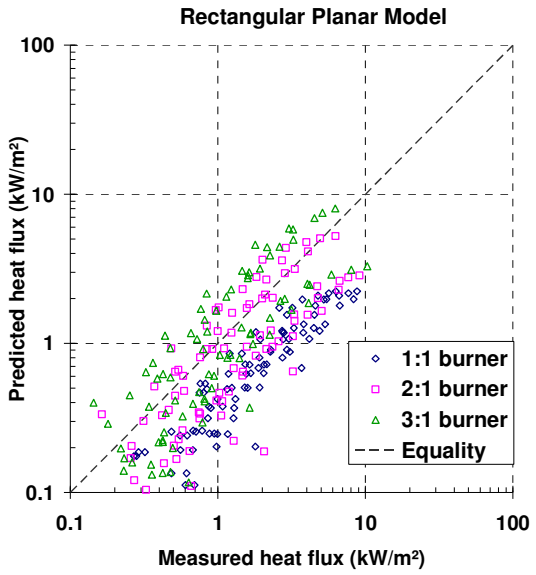

(e)

Figure C 1: Measured vs predicted heat fluxes for horizontal targets for (a) point source model, (b) Shokri & Beyler detailed method, (c) Mudan method, (d) Dayan & Tien method and (e) rectangular planar model